

***In vitro* susceptibility of *Staphylococcus aureus* to porphyrin-silver mediated photodynamic antimicrobial chemotherapy**

A thesis submitted in fulfilment of the requirements for the degree of

Master of Science

By

Samuel Malewa Shabangu



RHODES UNIVERSITY
Where leaders learn

February 2020

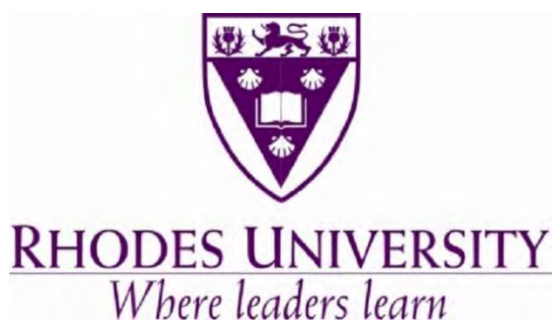
Acknowledgements

My humble gratitude goes towards my research advisor Prof. Tebello Nyokong, your unwavering support and guidance was of paramount importance in this work, thank you very much!

My gratitude also goes towards Prof. John Mack, Dr Jonathan Britton, Dr Balaji Babu, Dada Rodah “shangazi”, Dr Muthumuni Managa and Miss Gail Cobus, your support has not gone down unnoticed. To Dr Edith Amuhaya and all my colleagues in Nairobi, Kenya thank you very much for giving me a memorable experience, “asante sana”.

To my family, you have been my rock of Gibraltar, thank you so much for your undivided attention and support, and lastly to my labmates, thank you so much, S22 shall rule!

“The most authentic thing about us is our capacity to create, to overcome, to transform and be greater than our suffering.” - Ben Okri



Abstract

This work reports on the syntheses and characterization of symmetrical and unsymmetrical porphyrin complexes namely, 5,10,15,20-tetra(4-pyridyl)-porphyrinato zinc(II) (**1**), 5,10,15,20-tetrathienyl porphyrinato zinc(II) (**2**), 5-(4-hydroxyphenyl)-10,15,20-tris(2-thienyl) porphyrinato zinc(II) (**3**), 5-(4-carboxyphenyl)-10,15,20-tris(pentafluorophenyl)- porphyrinato zinc(II) (**4**), 5-(4-carboxyphenyl)-10,15,20-triphenyl-porphyrinato zinc(II) (**5**) and 5-(4-carboxyphenyl)-10,15,20-tris(2-thienyl)-porphyrinato zinc(II) (**6**). The synthesis of silver nanoparticles (AgNPs) was also undertaken in this research work. Complexes **1**, **2**, **3** and **6** were linked to oleic acid/oleylamine functionalized nanoparticles via self-assembly and **4-6** were linked via covalent interaction through an amide bond to glutathione capped AgNPs. The effect of nature of bond along with symmetry were investigated, of interest were the five membered thienyl substituents. The photophysical and photochemical behaviour of the complexes and their conjugates with AgNPs were investigated in dimethylformamide. The porphyrin and AgNPs conjugates afforded an increase in singlet oxygen quantum yield. Complexes **1-6** and their conjugates were used for photodynamic antimicrobial chemotherapy of *Staphylococcus aureus*. The antimicrobial studies were done in two different concentrations of 0.36 and 2.0 µg/mL. The thienyl substituted porphyrin complexes and their conjugates gave better photodynamic activity as compared to phenyl analogues.

Table of contents

Acknowledgements	li
Abstract	iii
List of abbreviations	vii
List of symbols	viii
Preamble	ix

CHAPTER 1

Introduction	1
1.1 Photodynamic antimicrobial chemotherapy	2
1.1.1 The problem of bacterial infection	2
1.1.2 Background and working principle	2
1.1.3. Target micro-organisms	3
1.2. Porphyrins	5
1.2.1. Brief history and structure	5
1.2.2. Methods for porphyrin synthesis	6
1.2.3. Electronic absorption spectroscopy	8
1.2.4. Examples of selected <i>meso</i> -substituted porphyrins applied for PACT	10
1.2.5. Porphyrins synthesized in this work	14
1.2.6. Rationale	17
1.3 Introduction to nanomaterials	18
1.3.1 General background and synthesis of silver nanoparticles (AgNPs)	18
1.3.2 Porphyrin-nanoparticle reported before	21
1.4 Photophysical and photochemical Parameters	24
1.4.1 Jablonski diagram	24
1.4.2 Fluorescence quantum yield and lifetime	24
1.4.3 Singlet oxygen quantum yield	25
1.5 Summary of aims in point form	26

CHAPTER 2

Experimental	27
2.1. Materials	28
2.1.1 General reagents and solvents	28
2.1.2 Reagents for the synthesis of porphyrin synthesis	28
2.1.3 Reagents for nanoparticle synthesis and linking to porphyrins	28
2.1.4 Reagents for determination of singlet oxygen	28
2.1.5 Reagents for bacterial work	29
2.2. Instrumentation	29
2.3. Syntheses of AgNPs	32
2.3.1 Synthesis of OA/OLA capped AgNPs	32
2.3.2 Synthesis of GSH capped AgNPs	32
2.4 Synthesis of porphyrins	32
2.4.1 Synthesis of 5,10,15,20-tetra(4-pyridyl) porphyrinato zinc(II) (complex 1)	32

2.4.2 Synthesis of 5,10,15,20-tetrathieryl porphyrinato zinc(II) (complex 2)	33
2.4.3 Synthesis of 5-(4-hydroxyphenyl)-10,15, 20-tris(2-thienyl)-porphyrinato zinc(II) (complex 3)	33
2.4.4 Synthesis of 5-(4-carboxyphenyl)-10,15,20-tris(pentafluorophenyl)-porphyrinato zinc(II) (complex 4)	34
2.4.5 Synthesis of 5-(4-carboxyphenyl)-10,15,20-triphenyl-porphyrinato zinc(II) (complex 5)	34
2.4.6 Synthesis of 5-(4-carboxyphenyl)-10,15, 20-tris(2-thienyl)-porphyrinato zinc(II) (complex 6)	35
2.4.7 Self-assembly formation conditions	35
2.4.8 Amide bond formation conditions	36
2.5 PACT conditions	36

CHAPTER 3

Attempted syntheses	37
3.1 Synthesis of complex 7	38
3.2 Synthesis of complex 8	39
3.3 Rationale behind synthesis	42

Results and discussion

43

Publications

44

CHAPTER 4

Synthesis, characterization and photophysical properties	45
4.1 Synthesis and characterization of complexes 1-6	46
4.1.1 UV-vis spectroscopy	48
4.1.2 Nuclear Magnetic Resonance Spectra	49
4.2 Formation of conjugates	50
4.2.1 SA for complexes 1, 2, 3 and 5	50
4.2.2 Amide for complexes 4-6	50
4.3 Characterization of conjugates	52
4.3.1 UV-vis spectroscopy	52
4.3.2 Transmission electron microscopy (TEM) and energy dispersive spectroscopy (EDS)	55
4.3.3 Surface charge (zeta potential)	56
4.3.4 X-ray diffraction (XRD)	57
4.3.5 FT-IR	58
4.3.6 X-ray photoelectron spectroscopy (XPS)	59
4.4 Photophysical and photochemical parameters	62
4.4.1 Fluorescence quantum yields and lifetimes	62
4.4.2 Singlet oxygen quantum yields	63
4.5 Summary of chapter	64

CHAPTER 5

Antimicrobial experiments	66
5.1 PACT studies with <i>S. aureus</i>	67
Table 5.1A: Log reduction values for photoinactivation effect on <i>S. aureus</i> at 0.36 µg/mL at 75 min irradiation	74
Table 5.1B: Log reduction values for photoinactivation effect on <i>S. aureus</i> at 2.0 µg/mL at 75 min irradiation	75
5.2 Synergy studies	75
5.3 Summary of chapter	76

CHAPTER 6

General conclusions and Recommendations	77
6.1 Conclusions	78
6.2 Recommendations	78

References	80
-------------------	----

Appendix	87
-----------------	----

List of abbreviation

Abbreviation	Description
DMF	Dimethylformamide
DCM	Dichloromethane
DMA	9,10 Dimethylantracene
DIPA	Diisopropylamine
DPE	Diphenyl ether
DDQ	2,3-Dichloro-5,6-dicyano-1,4-benzoquinone
EtOAc	Ethyl acetate
EDS	Energy dispersive spectroscopy
EDC	1-Ethyl-3-dimethylaminopropyl carbodiimide
TFA	Trifluoroacetic acid
FT-IR	Fourier transform-infrared
GSH	L-glutathione reduced
HUMO	Highest occupied molecular orbital
ISC	Intersystem crossing
LUMO	Lowest unoccupied molecular orbital
MALDI	Matrix-assisted Laser desorption/ionization
NPs	Nanoparticles
NHS	N-hydroxysuccinimide
OA	Oleic acid
OLM	Oleylamine
PACT	Photodynamic antimicrobial chemotherapy
PDT	Photodynamic therapy
¹H NMR	Proton nuclear magnetic resonance
ROS	Reactive oxygen Species
RB	Rose Bengal
AgNPs	Silver nanoparticles
TEM	Transmission electron microscope
THF	Tetrahydrofuran
TCSPC	Time correlated single photon counting
UV/vis	Ultraviolet/visible
XRD	X-ray diffractometer
ZnTPP	Tetrakis-5,10,15,20-(4-phenyl) porphyrinato zinc (II)

List of symbols

Symbol	Description
Φ_F	Fluorescence quantum yield
τ_F	Fluorescence lifetime
ϵ	Molar extinction coefficient
3O_2	Molecular oxygen
α	Non-peripheral position
β	Peripheral position
Φ_Δ	Singlet oxygen quantum yield
1O_2	Singlet oxygen
S_0	Singlet ground state
S_1	Singlet excited state
λ	Wavelength

Preamble

This thesis covers the biological activity of porphyrin-silver nanoconjugates for *in vitro* photoinactivation of *Staphylococcus aureus* using photodynamic antimicrobial chemotherapy as the mode of action. The effect of self-assembly in comparison to covalent linkage in the nanoconjugates as well as the effect of varying substituents on the *meso*-position of the porphyrins are explored.

Chapter 1

Introduction

This chapter provides a brief account of the literature pertaining to problems associated with antimicrobial drug resistance, history of porphyrins, silver nanoparticles and photodynamic antimicrobial chemotherapy.

1.1 Photodynamic antimicrobial chemotherapy (PACT)

1.1.1 The problem of bacterial infection

Internationally, there is a growing concern over antimicrobial drug resistance which is currently estimated to account for more than 700,000 deaths per year worldwide [1]. In contrast to some other health issues, antimicrobial drug resistance is a problem that concerns every country irrespective of its level of income and development, as resistant pathogens do not respect borders or partitions [1, 2]. The gap in public health capacity is also an issue given the changing resistance mechanisms and the emergence of multidrug-resistant bacteria that can only be detected through systematic screening in quality assured microbiology laboratories [3, 4].

1.1.2 Background and working principle

The phenomenon of PACT was first described by Raab in 1890 [5]. It was reported for the first time by Raab and others that the toxicity of acridine orange against *Paramecia caudatum* was dependent on the amount of light introduced to the cells [5-7]. Later on, Raab's teacher van Tappeiner reported that the toxic effects in the presence of light were not due to heat [8]. In 1904 Tappeiner introduced the term "Photodynamic reaction" [8].

The understanding of the scientific basis of PACT is still in its initial stages, but it follows a similar principle to that of photodynamic therapy (PDT) of cancer [9]. PACT is based on the administration of a non-toxic photosensitizer to the pathogenic cells followed by inactivation by light of appropriate wavelength. The photoexcited photosensitizer produces reactive oxygen species (ROS) such as singlet oxygen that are cytotoxic to the pathogens [9, 10]. With an increase in the number of drug resistant bacteria such as methicillin resistant *Staphylococcus aureus* (MRSA) [11], a new generation of drugs are needed. There are various photosensitizers (drugs) that have been used for PACT, *meso*-substituted porphyrins are used in this work for photoinactivation of *Staphylococcus aureus* (*S. aureus*).

The photoinactivation mechanism involves **Type I** and **Type II** mechanisms (**Fig. 1.1**). **Type I** process involves an electron transfer from the photosensitizer in the triplet state to an oxygen molecule which results in the formation of ROS. In **Type II** the excited photosensitizer in the triplet state transfers energy to the ground state

molecular oxygen to produce cytotoxic singlet oxygen. **Type II** mechanism is generally assumed for PACT.

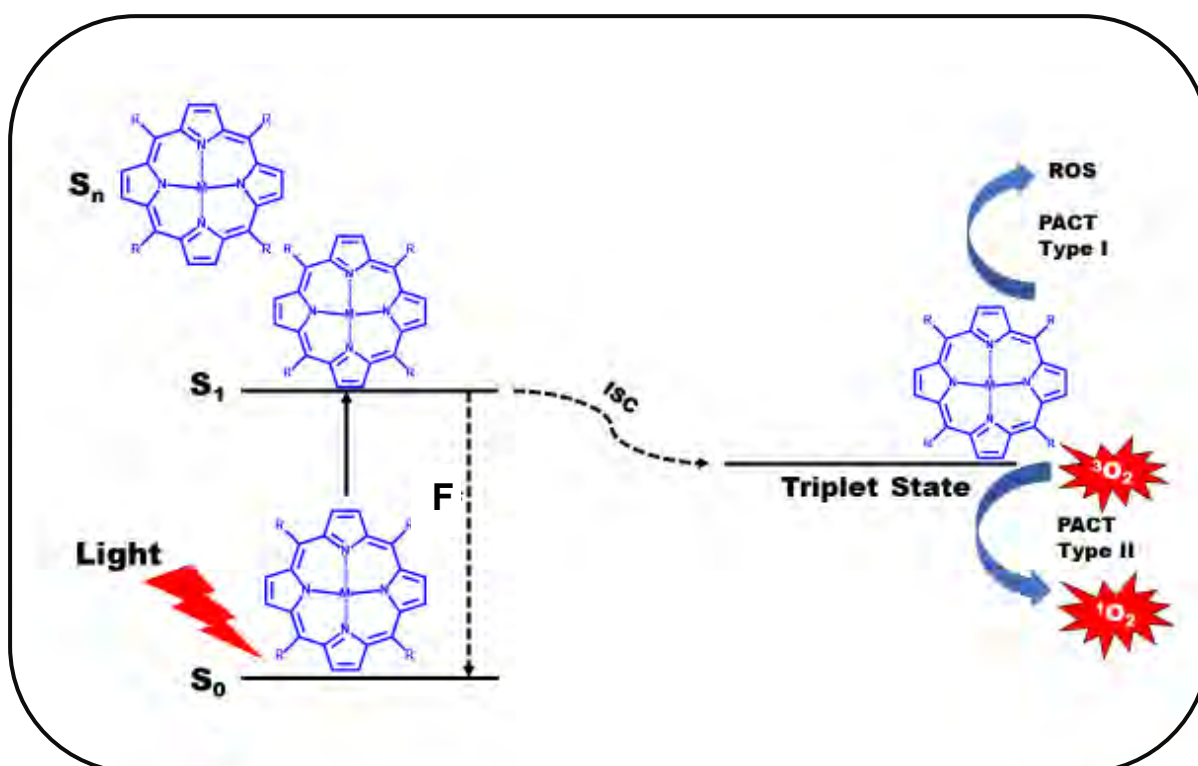


Figure 1.1: A schematic representation of **Type I** and **Type II** photochemical mechanism for photoinactivation of bacteria illustrating the transition between the ground singlet state (S_0), electronic excited state (S_1), n^{th} excited singlet state (S_n), intersystem crossing (ISC) to the triplet state, fluorescence (F). ROS = reactive oxygen species.

1.1.3 Target micro-organisms

Bacteria fall into two categories, Gram (+ve) and Gram (-ve) bacteria. Gram (+ve) strain such as *S. aureus* has 15-80 nm thick cell wall that is composed of a thick peptidoglycan layer, while Gram (-ve) strain is characterized by a thin peptidoglycan cell wall sandwiched between an inner cytoplasmic cell membrane and a bacterial outer membrane. The significant difference between the two bacterial strains is illustrated in **Fig. 1.2**. The Gram (+ve) strain is more susceptible to photoinactivation than the Gram (-ve) strain such as *Escherichia coli* (*E. coli*) due to absence of an

outer membrane in the former as compared to the latter [12]. Hence Gram (+ve) bacteria is employed in this work.

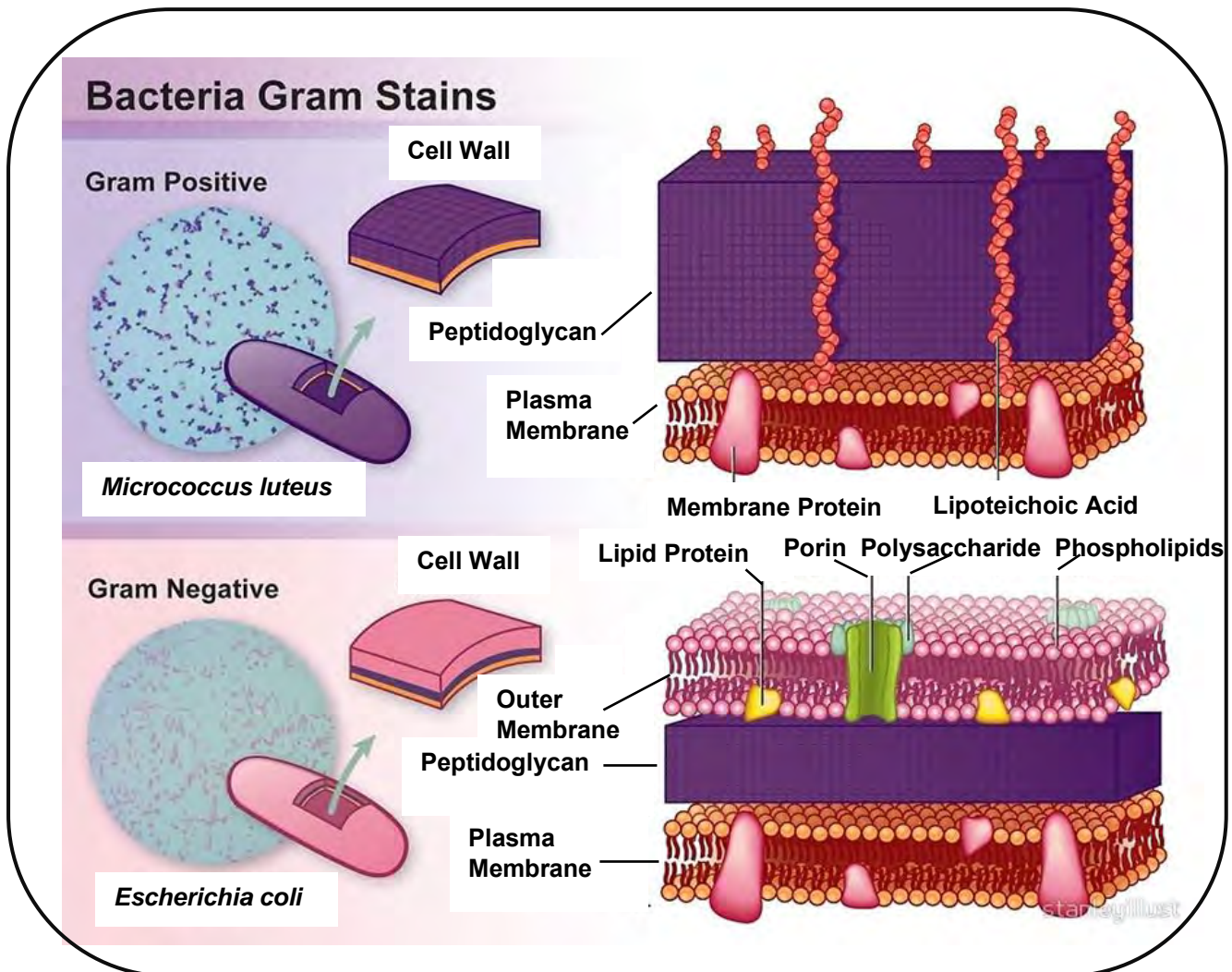


Figure 1.2: Gram (+ve) and Gram (-ve) structures [12].

1.2 Porphyrins

1.2.1 Brief history and structure

Porphyrins are biochemically important, medically useful, and synthetically interesting compounds. Porphyrins that occur naturally play a major role in the life sustaining biochemical reactions. These biologically important porphyrins include (hemes, chlorophylls, myoglobins, cytochromes, catalases, peroxidases, and several others). Used by nature in the most important processes of photosynthesis and solving transport and other problems in living systems, these compounds have been described as “pigments of life” [13, 14]. Porphyrins and their metal complexes have also stirred interdisciplinary interest due to a multitude of their intriguing physical, chemical and biological properties [15].

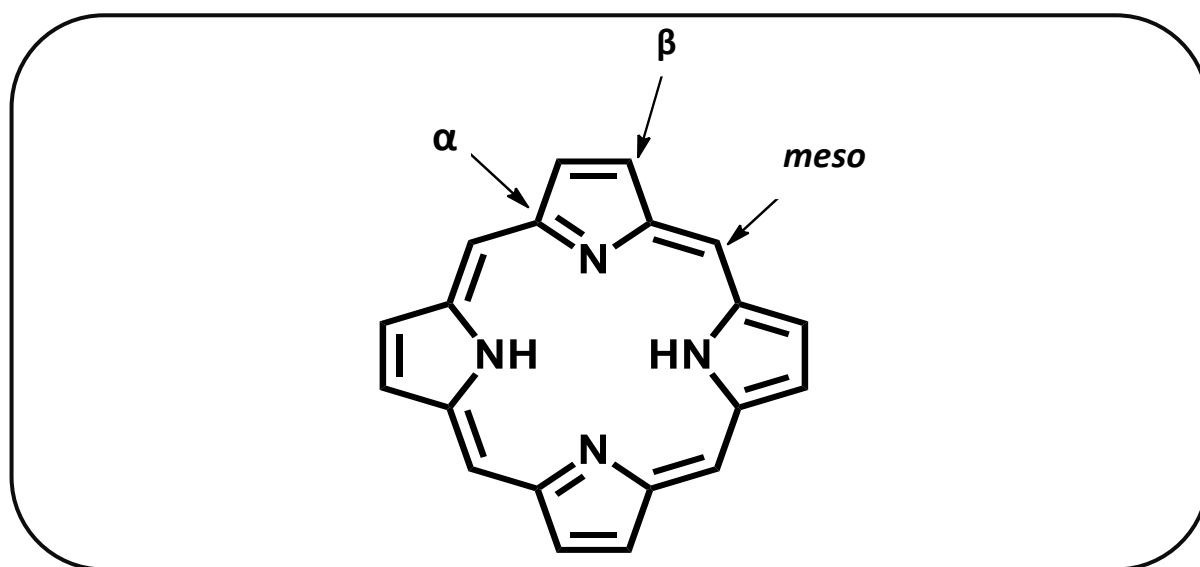


Figure 1.3: A typical general macrocycle structure of porphyrins.

The porphyrin macrocycle, **Fig. 1.3** consists of four pyrrole rings joined by four interpyrrolic methine bridges to give a highly conjugated aromatic 18 π -electron macrocycle.

There are two distinct types of substituents at the porphyrin periphery, the β and *meso*-substituted porphyrins, with the former having a close resemblance to naturally occurring porphyrins, **Fig. 1.4**. *Meso-substituted* porphyrins have gained popularity due to their ease of synthesis, as well as the ability to add highly sophisticated

groups at the *meso* position, hence *meso*-substituted porphyrins are employed in this work.

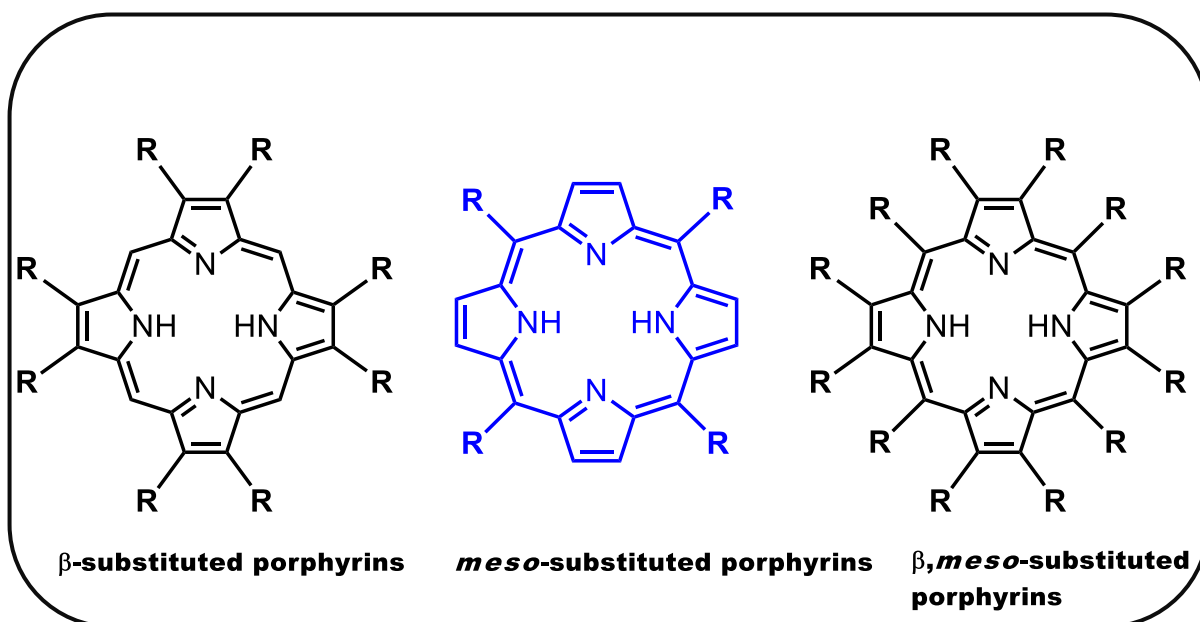
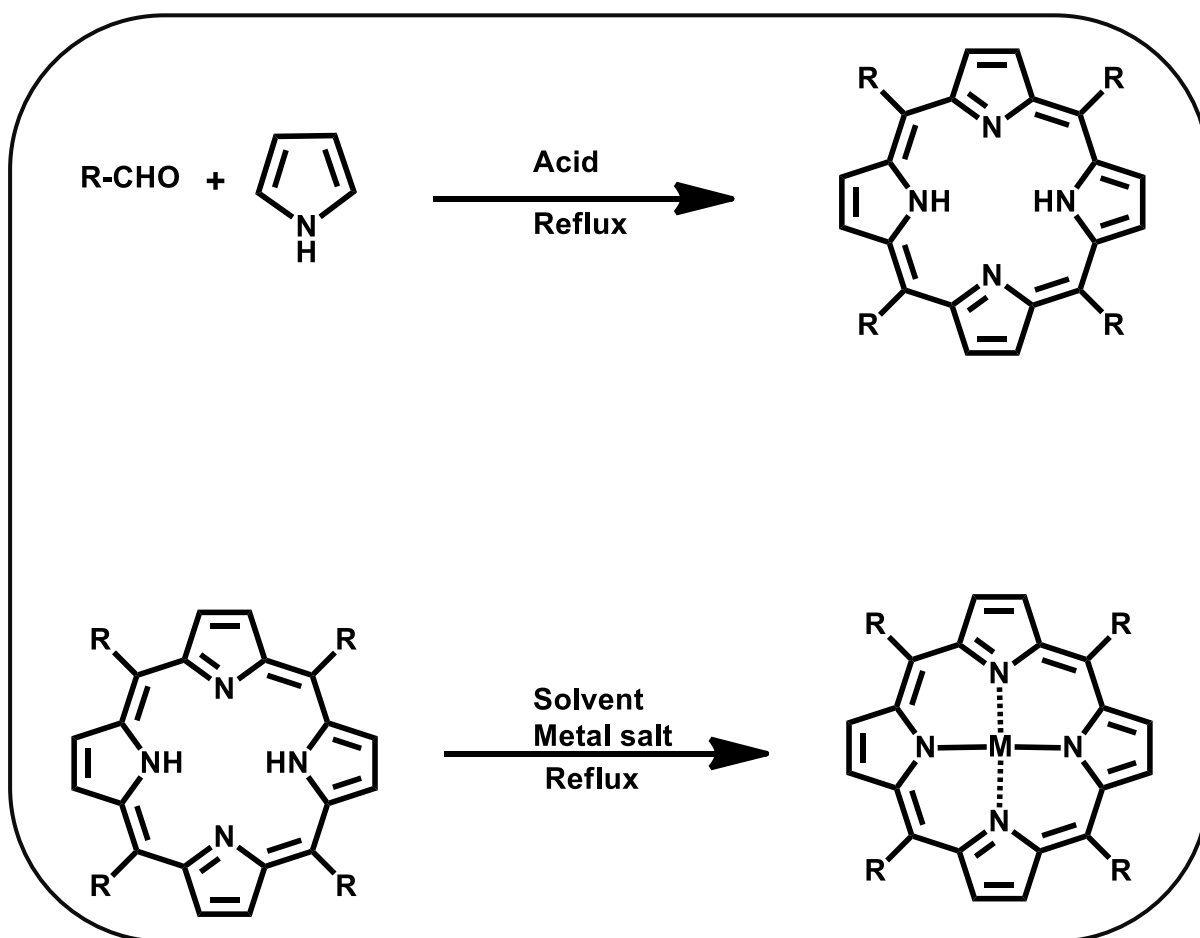


Figure 1.4: Three types of porphyrins.

1.2.2 Methods for Porphyrin Synthesis

Synthesis of *meso*-substituted porphyrins was initiated by Rothmund in 1935 [16, 17]. He carried out the syntheses by reacting different aldehydes with pyrroles at very high temperatures. Despite several variations by different research groups [18], this method has not been employed extensively. This is largely due to the low overall yields obtained. The Adler method was developed by Adler and co-workers in the mid-1960s [19, 20]. This method basically requires the use of acidic solvents at reflux conditions in an open atmosphere resulting in high yields, **Scheme 1.1**. This is obviously better than the Rothmund method. In addition to the high yields, another attractive feature of this method is the fact that the porphyrin product can often crystallize out of the cooled acidic solvent. A major drawback, however, is the limit in the types of aldehydes that can be used in this synthesis. Many aldehydes with substituents that are sensitive to acids cannot be used to prepare porphyrins using this method, and as a result, extra steps of protection and deprotection of the substituents must be employed [21, 22]. In the early 1980s, Lindsey and co-workers developed the Lindsey protocol which facilitated the synthesis of porphyrins under mild conditions [23]. This method takes advantage of the highly reactive aldehyde

and pyrrole starting materials, which do not require harsh conditions to react. The mild conditions include condensation of the aldehyde and pyrrole in the presence of an acid catalyst, normally trifluoroacetic acid (TFA) or boron trifluoride etherate ($\text{BF}_3 \cdot \text{OEt}_2$) at room temperature to form a porphyrinogen intermediate. This step is followed by the addition of an oxidant, usually *p*-chloranil or 2,3-dichloro-5,6-dicyano-1,4-benzoquinone (DDQ), to afford the more stable aromatic porphyrin [24]. The major disadvantage here is that dilute concentrations of aldehyde and pyrrole are required to minimize the competition between oligomerization of pyrromethanes and cyclization to give the porphyrinogen [25]. This means that when running large scale synthesis of porphyrins, one must handle large amounts of solvents. In this thesis, Adler method was employed since it does not require extra steps and large amounts of solvents as compared to the much-favoured Lindsey method. The latter was attempted in this work but was unsuccessful.



Scheme 1.1: A general synthetic pathway for *meso*-substituted porphyrins (Adler method).

1.2.3 Electronic absorption spectroscopy

The electronic absorption spectra of macrocycles such as porphyrins and phthalocyanines has long been understood in terms of the Gouterman's four-orbital model [26-30]. In this model the two highest occupied molecular orbitals (HOMO) and lowest unoccupied molecular orbitals (LUMO) are considered [30]. The absorption bands in porphyrin systems arise from transitions between two HOMOs and a LUMO, **Fig. 1.5**. The HOMOs are a_{1u} and a_{2u} orbital, while the LUMO is a degenerate set of e_g orbitals [31].

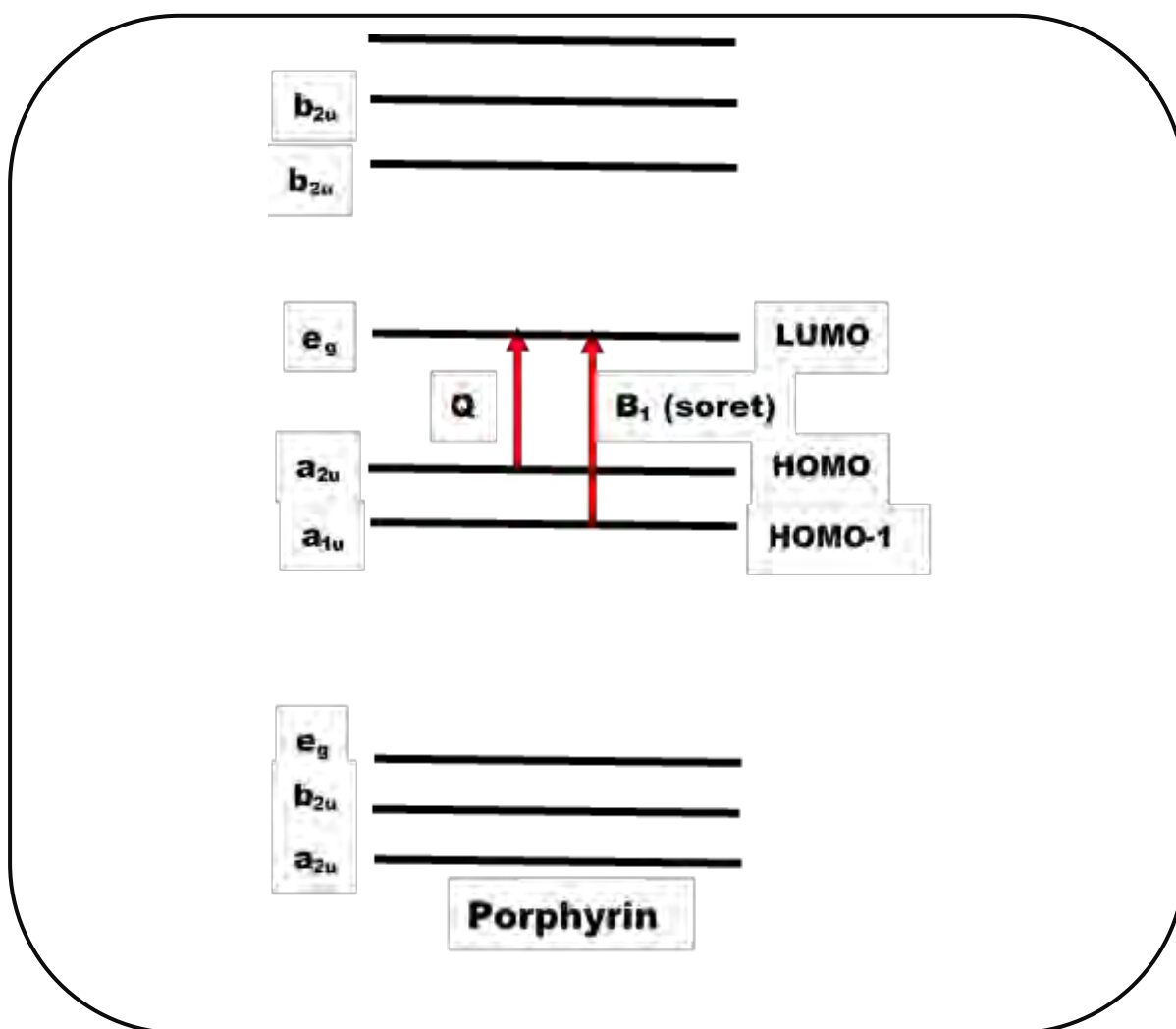


Figure 1.5: Electronic transitions in porphyrins showing the origin of Q and B (Soret) absorption bands.

Generally, porphyrins are characterized by an intense band called the Soret or B band at about 400 nm, named after the biochemist who first observed it in haemoglobin [32]. The Q bands are observed between 500-600 nm [31, 33, 34], and four are observed for metal free porphyrin, **Fig. 1.6**. In the presence of a central metal, the Q bands collapse to two, **Fig. 1.6** [34, 35].

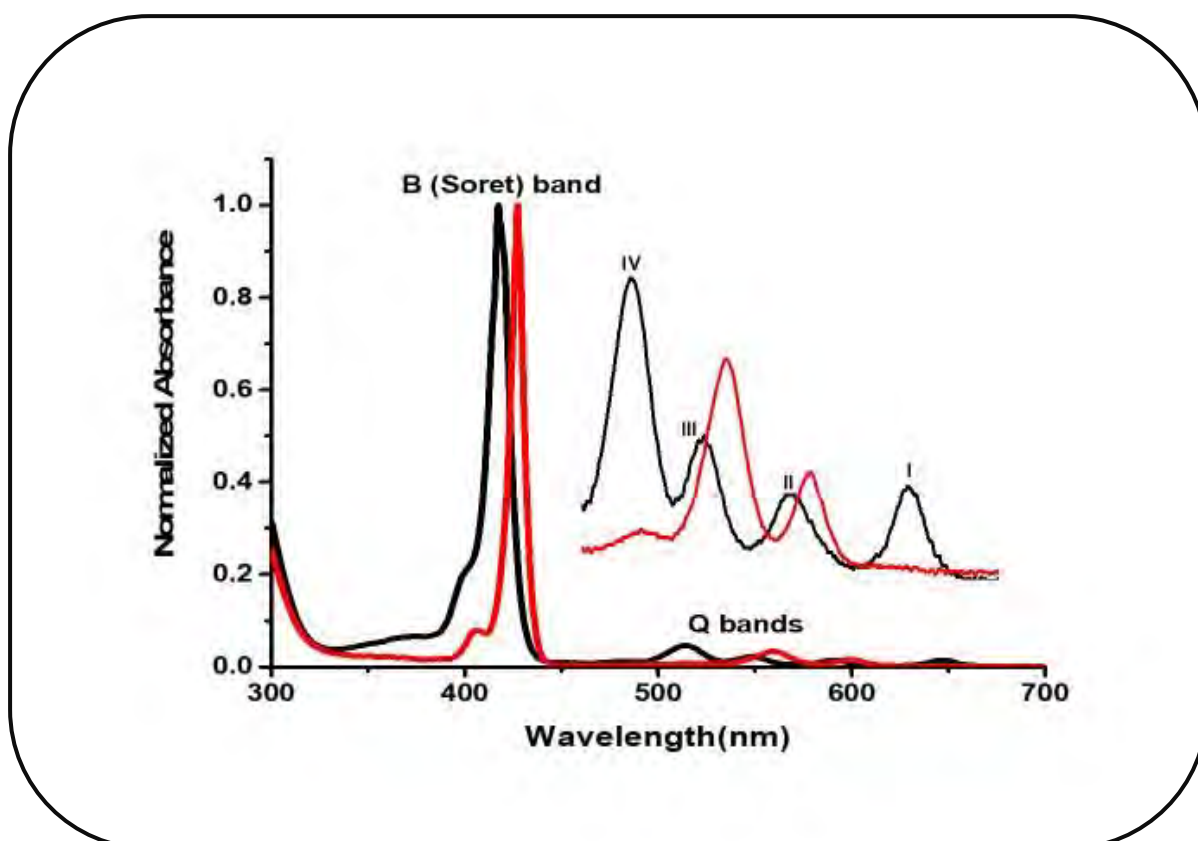
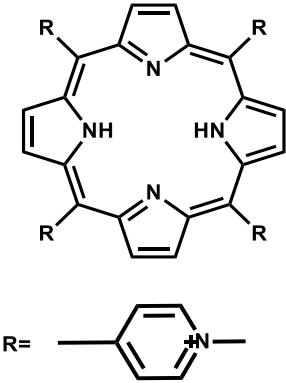
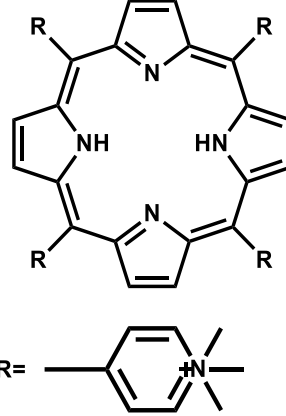
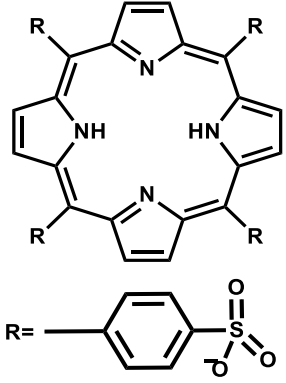


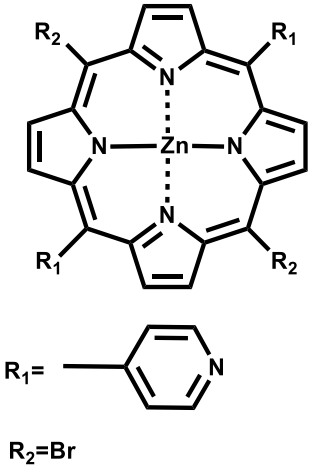
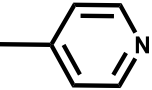
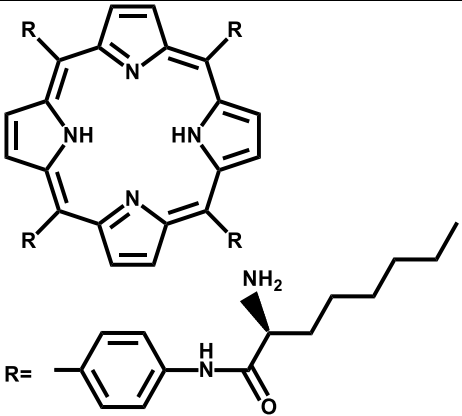
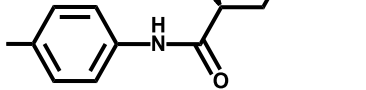
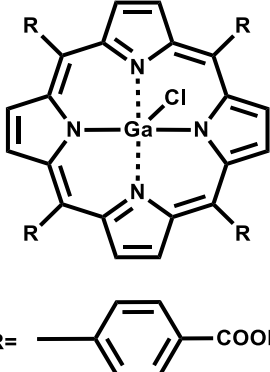
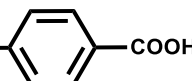
Figure 1.6: Ground state absorption spectra of typical free base (black) and metallated porphyrin (red).

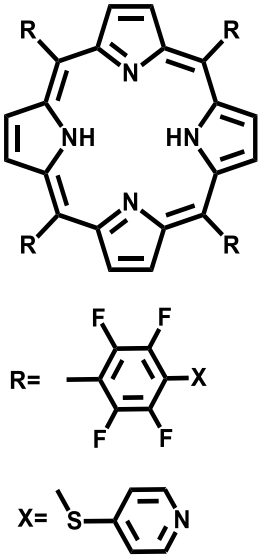
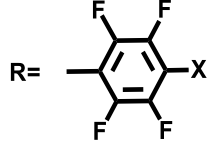
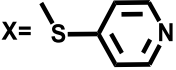
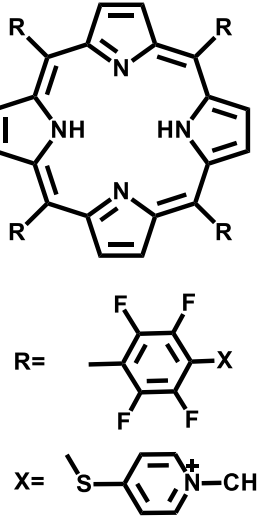
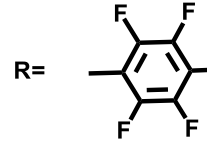
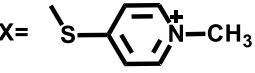
1.2.4 Examples of selected *meso*-substituted porphyrins previously applied for PACT

Table 1.1 lists *meso*-porphyrins that have been previously applied for PACT [36-44]. In this work photoinactivation of *S. aureus* was the prime objective.

Table 1.1 Selected porphyrins which have been applied for PACT before.

Structure of complex	Microorganism	Ref
 <p>The structure shows a central porphyrin ring with four meso-substituents labeled 'R'. Below the main structure, the R group is defined as a 4-pyridyl ring (a benzene ring fused to a pyridine ring).</p>	<i>E. coli</i> , <i>Acinetobacter baumannii</i> , <i>Enterococcus seriolicid</i> and <i>Vibrio anguillarum</i>	[36,37]
 <p>The structure shows a central porphyrin ring with four meso-substituents labeled 'R'. Below the main structure, the R group is defined as a 4-pyridyl ring with a methyl group on the nitrogen atom.</p>	<i>Dinococcus radiodurans</i> , <i>E. coli</i> <i>Enterococcus seriolicida</i> and <i>Vibrio anguillarum</i>	[37,38]
 <p>The structure shows a central porphyrin ring with four meso-substituents labeled 'R'. Below the main structure, the R group is defined as a 4-pyridyl ring with a sulfonate group (-SO₃⁻) at the para position.</p>		

 <p>$R_1 =$ </p> <p>$R_2 = \text{Br}$</p>	<p><i>S. aureus</i>, <i>E. coli</i>, <i>Enterococcus faecalis</i>, <i>Bacillus anthracis</i> and <i>Saccharomyces cerevisiae</i></p>	<p>[39]</p>
 <p>$R =$ </p>	<p><i>MRSA</i>, <i>E. coli</i> and <i>P. aeruginosa</i></p>	<p>[40]</p>
 <p>$R =$ </p>	<p><i>S. aureus</i></p>	<p>[41]</p>

 <p>R = </p> <p>X = </p>	<p><i>Penicillium chrysogenum</i> conidia</p>	<p>[42]</p>
 <p>R = </p> <p>X = </p>	<p><i>Candida albicans</i></p>	<p>[43]</p>

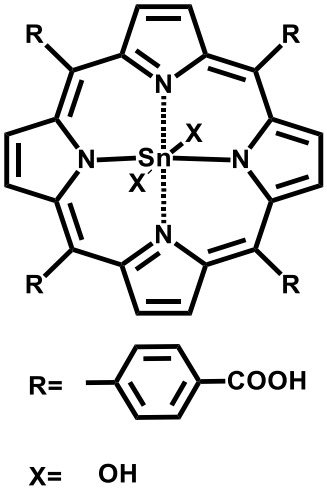
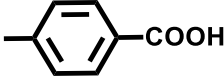
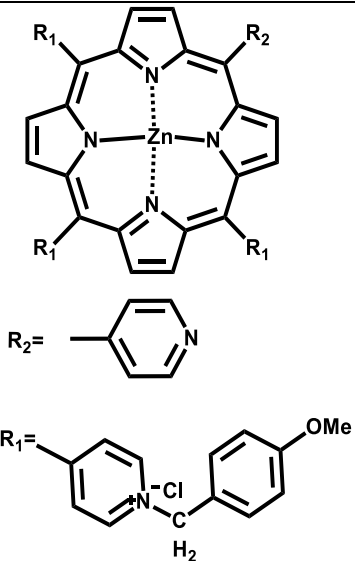
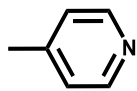
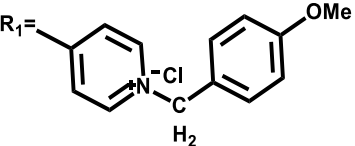
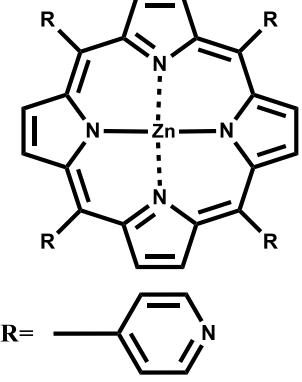
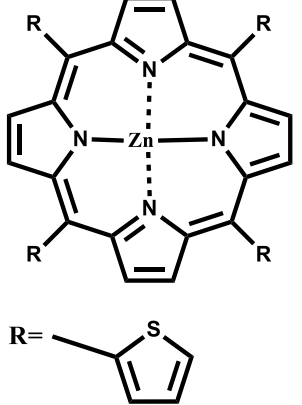
 <p>R = </p> <p>X = OH</p>		
 <p>R₂ = </p> <p>R₁ = </p>	<i>E. coli</i> , <i>S. aureus</i> and <i>P. aeruginosa</i>	[44]

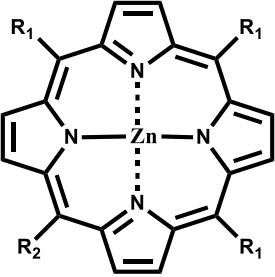
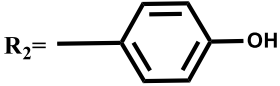
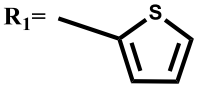
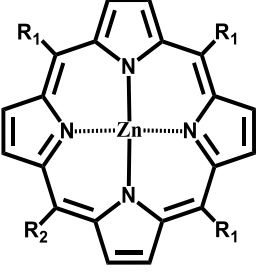
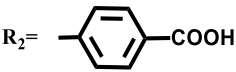
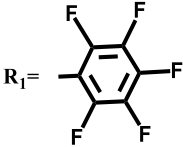
Table 1.1 shows that there are very few asymmetrical zinc porphyrins that have been applied for PACT, hence are the subject of this thesis. Asymmetry is also known to improve triplet state parameters such as singlet oxygen generation in porphyrins [45]. In addition, insertion of heavy atoms into the porphyrin core such as zinc as the case in this thesis enhances efficiency in intersystem crossing to long-lived triplet state of the porphyrin, leading to high singlet oxygen quantum yield [46, 47].

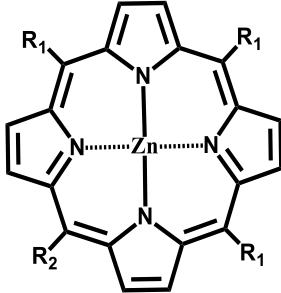
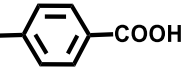
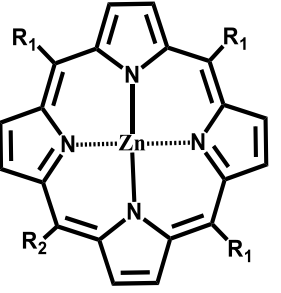
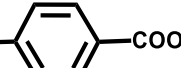
1.2.5 Porphyrins synthesized in this work

Investigation of the effect of *meso*-substituted porphyrins bearing different substituents are yet to be exploited extensively for PACT. The search for new photosensitizers with good properties such as efficient singlet oxygen, intense light absorption and improved attachment to the pathogenic cell wall is on the rise [48-50]. The properties of porphyrins can further be tailored to suit for PACT use, for example, by introducing asymmetry which results in favourable alteration of triplet state parameters as stated above [45]. In this thesis various asymmetric and symmetric porphyrin complexes bearing different substituents are reported, of interest were the five membered rings of thienyl substituents. Compared to phenyl substituents, thienyls show red shifted absorption bands [51], a property which allows them to be applied in reality for deep seated infections. The thienyl groups also offer a striking advantage in that they can form self-assembled structures with silver nanoparticles (AgNPs) through silver-sulfur (Ag-S) interaction via self-assembly (SA). All the porphyrins in this thesis have been synthesized before [52-57] (**Table 1.2**) and their characterization will be provided in the ensuing chapter. Interaction of the porphyrins with silver nanoparticles via SA and amide bond is reported here for the first time.

Table 1.2 Summary of different porphyrin complexes used for PACT in this work against *S. aureus*.

Structures of complexes	Type of bond
<div style="text-align: center;">  <p>[52]</p> <p>(1-AgNPs-SA)</p> <p>5,10,15, 20-tetra (4-pyridyl) porphyrinato zinc(II) (1)</p> </div>	SA
<div style="text-align: center;">  <p>[53]</p> <p>(2-AgNPs-SA)</p> <p>5,10,15, 20-tetrathienyl porphyrinato zinc(II) (2)</p> </div>	SA
	SA

 <p>[54]</p>   <p>(3-AgNPs-SA) 5-(4-hydroxyphenyl)-10, 15, 20-tris (2-thienyl)-porphyrinato zinc(II) (3)</p>	
 <p>[55]</p>   <p>(4-AgNPs-amide) 5-(4-carboxyphenyl)-10, 15, 20-tris (pentafluorophenyl) -porphyrinato zinc(II) (4)</p>	amide

 <p style="text-align: center;">[56]</p> <p style="text-align: center;"> $R_2 =$  </p> <p style="text-align: center;"> $R_1 =$  </p> <p style="text-align: center;">(5-AgNPs-amide)</p> <p style="text-align: center;">5-(4-carboxyphenyl)-10, 15, 20-triphenyl-porphyrinato zinc(II) (5)</p>	amide
 <p style="text-align: center;">[57]</p> <p style="text-align: center;"> $R_2 =$  </p> <p style="text-align: center;"> $R_1 =$  </p> <p style="text-align: center;">(6-AgNPs-amide)</p> <p style="text-align: center;">(6-AgNPs-SA)</p> <p style="text-align: center;">5-(4-carboxyphenyl)-10, 20-tris (2-thienyl)-porphyrinato zinc(II) (6)</p>	amide and SA

1.2.6 Rationale

1. Complex **1** was compared to **2** for pyridyl vs thienyl both by SA.
2. Complex **3** was compared to **2** for asymmetry.
3. Complex **3** was compared to **6** for effect of COOH vs OH substituent.
4. Effect of bulky substituent in complex **4** was compared to **5** and **6**.

1.3 Introduction to nanomaterials

Nanomaterials may be defined as objects with sizes that range between 1 to 100 nm [58]. They have attracted a lot of interest in recent years due to their extraordinary size and shape dependent properties [59] which make them useful in many areas of science such as in sensing, catalysis, imaging, non-linear optics and lastly drug delivery [60-64].

This work focuses entirely on the development of porphyrin-AgNPs (silver nanoparticles) dyad for enhanced photoinactivation of *S. aureus*. The nanomaterials were functionalized accordingly to allow for covalent or non-covalent linkage as shown in **Table 1.2**.

1.3.1 General background and synthesis of silver nanoparticles (AgNPs)

AgNPs have been used for several applications, including as antibacterial agents, in industrial, household and healthcare-related products [65].

In general, AgNPs can be obtained by two methods, classified as “top-down” and “bottom-up”, **Fig. 1.7** [66].

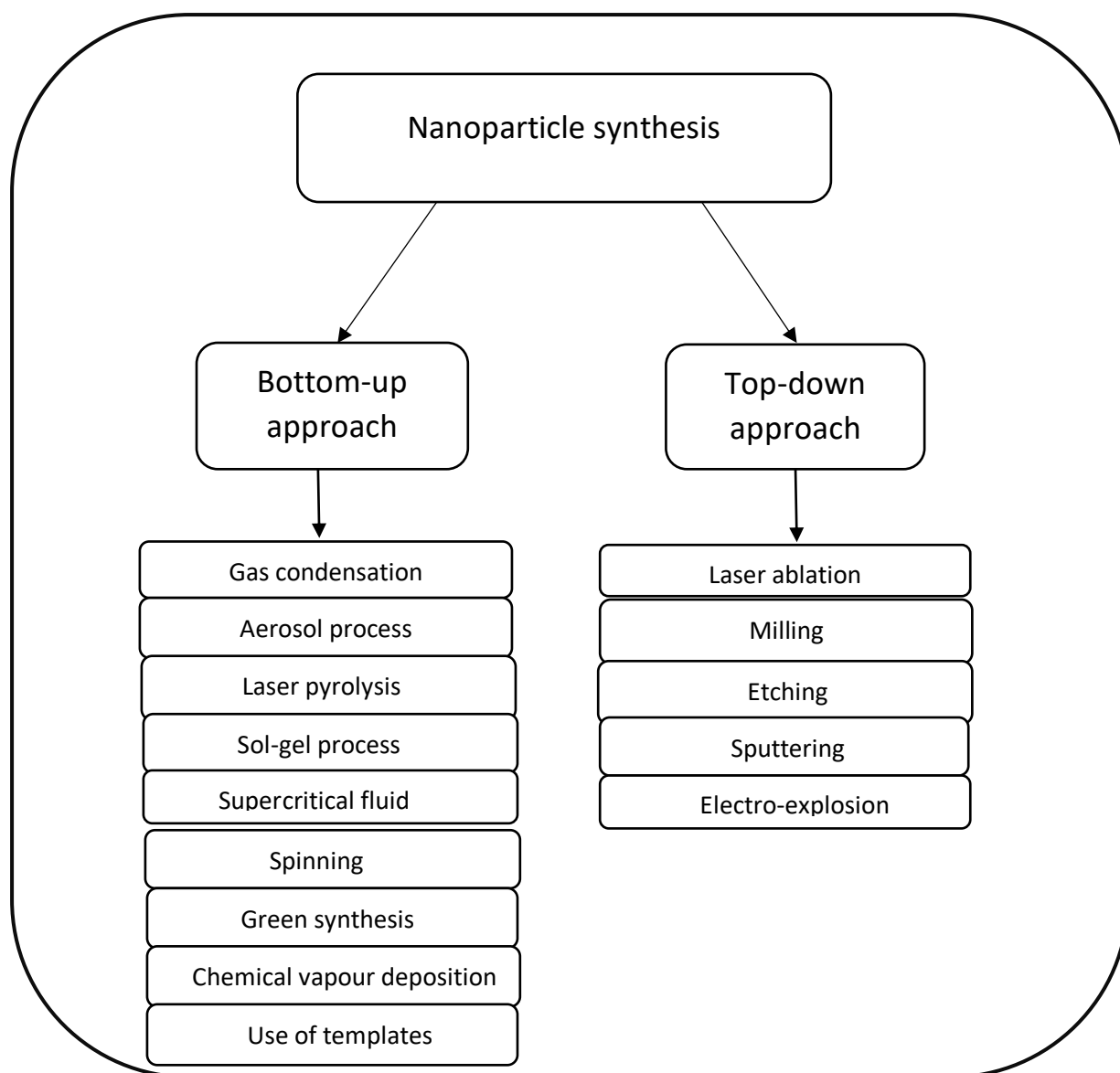
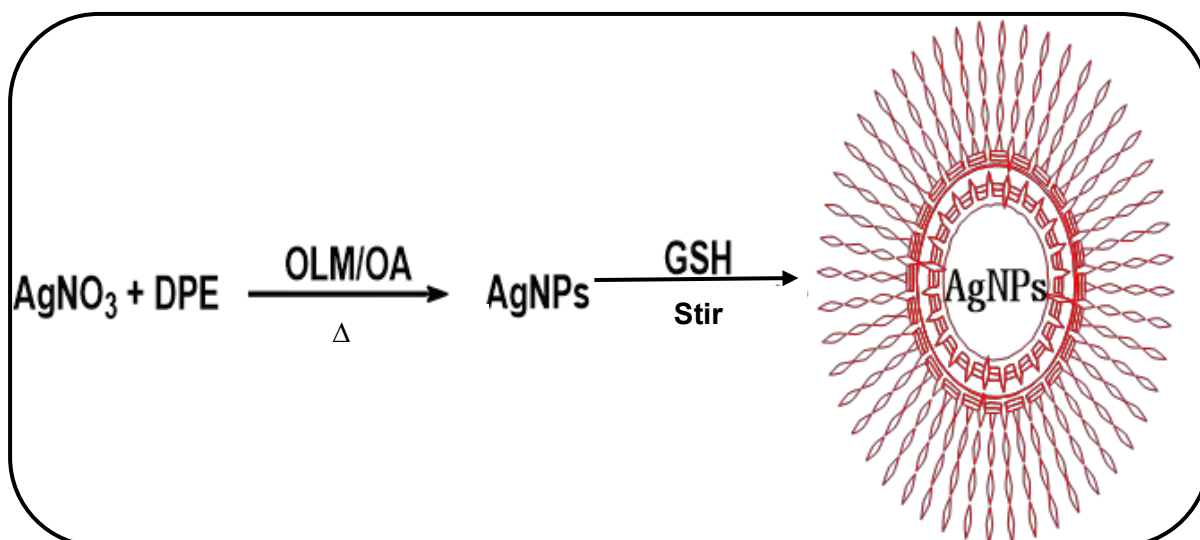


Figure 1.7: Some nanoparticle preparation methods.

The “top-down” method is the mechanical grinding of bulk metals with subsequent stabilization using colloidal protecting agents [67, 68]. The “bottom-up” methods include chemical reduction, electrochemical methods, and sono-decomposition. Chemical reduction method was used in this thesis (**Scheme 1.2**) for bottom up approach. The major advantage of chemical methods is high yield, contrary to physical methods, which have low yield.

Functionality is provided by introducing different capping agents such as surfactants, biomolecules, small molecules and polymers [69-73]. The functionalization makes it possible for covalent and non-covalent conjugation or interaction with a variety of compounds for enhanced activity [74]. **Scheme 1.2** provides a general pathway for

the synthesis of oleylamine/oleic acid (OLM/OA) and glutathione (GSH) capped AgNPs [75, 76], employed in this work.

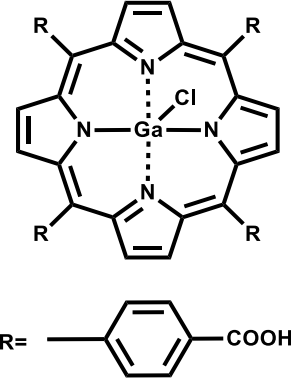
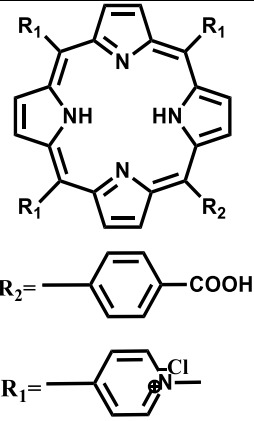


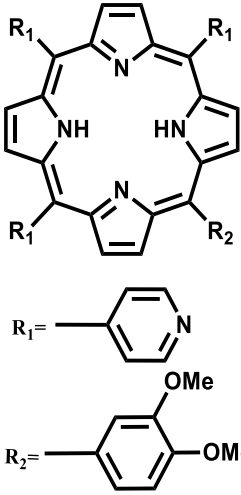
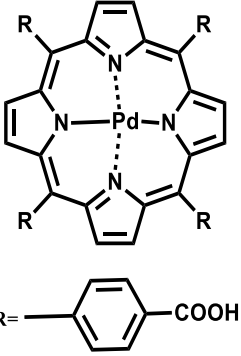
Scheme 1.2: General pathway for glutathione capped AgNPs with oleylamine (OLM), oleic acid (OA), diphenyl ether (DPE) and glutathione (GSH) as reagents.

1.3.2 Porphyrin-nanoparticle reported before.

Table 1.3 shows selected porphyrin-nanoconjugates [41, 77-79] that have been reported before for PACT or PDT. Photosensitizers have been conjugated to nanoparticles before mostly through covalent linkage (**Table 1.3**). Porphyrins containing thienyl rings for application in PACT are very scarce, not only do these molecules enhance production of singlet oxygen, which is a key element for PACT, they also result in red-shifted porphyrins as stated above. Photosensitizers can activate AgNPs into silver ions under light illumination, at the same time, AgNPs can enhance the generation of ROS by the photosensitizer [80]. Together the two components activate each other leading to remarkable antimicrobial efficacy against Gram (+ve) bacteria [80]. Effect of covalent and non-covalent linkage, latter through self-assembly for biological studies has not been exploited in detail. This thesis reports here for the first time on the effect of thienyl substituents and some phenyl derived groups along with effect of the nature of bonding through covalent and non-covalent linkage by self-assembly in the presence of silver nanoparticles for PACT.

Table 1.3. Porphyrins that have been conjugated to nanoparticles.

Structures of complexes	Type of nanoparticle	Type of bonding	Ref for conjugates	Application
	Platinum nanoparticle	Covalent (amide bond)	[41]	PACT of <i>S.aureus</i>
	Polyacrylamide nanoparticles	Covalent (amide bond)	[77]	PDT of human Caucasian colon adenocarcinoma cells

 <p>The structure shows a porphyrin ring with four nitrogen atoms. Two of the nitrogen atoms are labeled 'NH'. The porphyrin ring is substituted with R₁ and R₂ groups. R₁ is a pyridine ring, and R₂ is a 3,5-dimethoxyphenyl ring.</p>	Disk shaped porphyrin-silver colloid hybrid nanoparticles	Covalent (ester bond)	[78]	PACT of <i>E. coli</i> , <i>M. smegmatis</i> and <i>S. aureus</i>
 <p>The structure shows a porphyrin ring with four nitrogen atoms coordinated to a central Pd atom. The porphyrin ring is substituted with R groups. R is a 4-carboxyphenyl ring.</p>	Mesoporous silica nanoparticles	Covalent (amide bond)	[79]	PDT of MDA-MB-231 breast cancer

As **Table 1.3** shows, there are very few porphyrin-AgNPs nanoconjugates and only one has been used for PACT, hence the importance of this work.

1.4 Photophysical and Photochemical Parameters

1.4.1 Jablonski diagram

When light of a specific wavelength is taken up by a photosensitizer (porphyrin), physical changes can be made and can be merely described by use of modified Jablonski diagram as described above in **Fig. 1.1**.

When a porphyrin absorbs a photon of a specific wavelength, it is first excited from the ground state (S_0) to the first excited state (S_1) which is short lived due to collisions that occur. The excited porphyrin can either dissipate energy by emitting light through fluorescence or by undergoing intersystem crossing (**ISC**) to the triplet state. The triplet state is long lived hence it allows for porphyrins to interact with molecular oxygen to generate ROS.

1.4.2 Fluorescence quantum yield and lifetime

Fluorescence quantum yield (Φ_F) is a measure of the efficiency of an emission process. It may be defined as the ratio of the number of photons emitted, to the number of photons absorbed.

In this work, a comparative method described by eq. **(1.1)** was used to determine the fluorescence quantum yields of the porphyrin derivatives using zinc tetraphenyl porphyrin (ZnTPP) in dimethylformamide (DMF) as the standard ($\Phi_F = 0.033$) [81].

$$\Phi_F = \Phi_F^{(std)} = \frac{F A_{Std} n^2}{F_{Std} A n_{Std}^2} \quad (1.1)$$

where F and F_{Std} are the areas under the fluorescence curves of the sample and standard, respectively. A and A_{Std} represent the absorbance of the sample and standard at the excitation wavelength, respectively. The n and n_{Std} are the refractive indices of the solvent used for the sample and standard, respectively.

Fluorescence intensity varies significantly in a linear way that is synonymous with the absorbed light intensity but non-linearly with the concentration of the porphyrin. A linear dependence can however be assumed for the porphyrin concentration if the absorbance at the wavelength of excitation is ≤ 0.05 . This is vital in order to prevent

the inner-filter effect [82], which may result in self-quenching of the fluorescence and a decrease in the quantum yield values.

Fluorescence lifetime may be defined as the time it takes the population of the molecule in the excited state to decay to 1/e or 37% of its original value in that state. It can be determined using the wavelength of time domain by a pulsed laser of picosecond (ps) time duration with techniques such as the steady-state fluorescence and time-correlated single-photon counting (TCSPC).

Fluorescence lifetimes of porphyrins molecules are of the order of few nanosecond (<10 ns) [83, 84] and are strongly dependent on the nature of the central metal ion, the types of substituents and the presence of other species that are capable of interacting with the molecules such as nanoparticles.

1.4.3 Singlet oxygen quantum yield (Φ_{Δ})

The principal target for studies that assess the suitability of photosensitizers for PACT is singlet oxygen. This cytotoxic agent is responsible for initiating a cascade of biochemical reactions that ultimately lead to the destruction of infected cells [85]. In this work, a chemical method for Φ_{Δ} determination was employed using 9,10-dimethylanthracene (DMA) as the quencher and Rose Bengal as the standard in an organic media. A comparative method (**eq. 1.2**) was used to determine the singlet oxygen quantum yield of the complexes. The chemical method (DMA in this case) requires a suitable singlet oxygen sensitive quencher that can react quickly with the singlet oxygen, as soon as it is produced in an oxygenated solution. The decomposition product of the quencher should not react with the generated singlet oxygen and thus it is not expected to interfere with the Soret or Q bands of the porphyrins, hence the porphyrin must remain intact. The experiment is usually carried out by irradiating a sample solution containing the porphyrin and the quencher.

$$\Phi_{\Delta} = \Phi_{\Delta(\text{std})} \cdot \frac{R.I(\text{std})}{R(\text{std}).I(\text{abs})} \quad (1.2)$$

where $\Phi_{\Delta(\text{std})}$ is the singlet oxygen quantum yield using Rose Bengal (RB) as the standard (0.37) [86] in DMF. In equation (1.2), R and $R(\text{std})$ are the rates at which the

quencher (DMA) is photobleached in the presence of porphyrin and $I_{(\text{std})}$ and $I_{(\text{abs})}$ are the rates of light absorbance of the standard and samples, respectively. Spectroscopic methods are then used to monitor production of singlet oxygen through decay of the quencher.

1.5 Summary of aims in point form

The aims of this thesis can be summarized as follows:

- Characterization of metalloporphyrins bearing different substituents for covalent or self-assembly linkage to AgNPs
- Synthesis and characterization of spherical AgNPs
- Synthesis and characterization of porphyrin-silver nanoconjugates
- Photophysical (fluorescence quantum yields and lifetimes) and photochemical properties (singlet oxygen quantum yields) of the porphyrins alone and in the presence of AgNPs
- Effect of asymmetry on PACT
- Investigation of the effect of self-assembly or covalent linking of porphyrins to AgNPs on PACT

Chapter 2

Experimental

This chapter provides an outline on the synthetic procedures applied and lists the materials and equipment used.

2.1 Materials

2.1.1 General reagents and solvents

Ethyl acetate (EtOAc), chloroform, cyclohexane, hexane, toluene, ethanol, methanol (MeOH), isopropanol, tetrahydrofuran (THF), acetonitrile, diethyl ether and dichloromethane (DCM) were purchased from Saarchem. Ultra-pure water was prepared by using the Milli-Q Water system from Millipore Corp, Bedford, MA, USA or ultra-pure Type II water obtained from Elga PURELAB chorus 2 (RO/DI) system. Dimethylformamide (DMF) was obtained from Associated Chemical Enterprises.

2.1.2 Reagents for porphyrin synthesis

Propionic acid, pyrrole, benzaldehyde, 4-formylbenzoic acid, 2-thiophenecarboxyaldehyde, 4-pyridinecarboxyaldehyde, 2,3,4,5,6-pentafluorobenzaldehyde, 4-hydroxybenzaldehyde, 5-bromothiophene-2-carbaldehyde, palladium(II)bis(triphenylphosphine) dichloride, copper iodide, ethynyltrimethylsilane, diisopropylamine (DIPA), trifluoroacetic acid (TFA), zinc acetate dehydrate [Zn(OAc)₂], boron trifluoride etherate (BF₃.OEt₂), sodium bicarbonate, sodium sulfate, 2,3-dichloro-5,6-dicyano-1,4-benzoquinone (DDQ), sodium hydroxide were all obtained from Sigma-Aldrich.

2.1.3 Reagents for nanoparticle synthesis and linking to porphyrins

Oleic acid (OA), oleylamine (OLM), silver nitrate, diphenyl ether (DPE), L-glutathione reduced (GSH), N-hydroxysuccinimide (NHS), 1-ethyl-3-dimethylaminopropyl carbodiimide (EDC), and potassium hydroxide were obtained from Sigma-Aldrich.

2.1.4 Reagents for determination of singlet oxygen

9, 10-Dimethylanthracene (DMA), Zn-5,10,15,20 tetraphenylporphyrin (ZnTPP), rose bengal (RB) were obtained from Sigma-Aldrich.

2.1.5 Reagents for bacterial work

Phosphate-buffered saline (PBS) solution pH 7.4 was prepared using appropriate amounts of Na₂HPO₄ and NaOH in ultra-pure Type II water obtained from Elga PURELAB chorus 2 (RO/DI) system. Nutrient agar and agar bacteriological BBL Muller Hinton broth were purchased from Merck Chemical Ltd and *S. aureus* (ATCC 25923) from Microbiologics.

2.2 Instrumentation

1. Ground state UV-visible absorption spectra were measured on a Shimadzu UV-2550 spectrophotometer using a 1 cm pathlength quartz cuvette for studies in solution.
2. $^1\text{H-NMR}$ spectra were recorded in deuterated solvents (CDCl_3 or DMSO-d_6) at room temperature on Bruker AMX 600 and 400 instruments operating at 600 and 400 MHz respectively.
3. Fluorescence emission and excitation spectra were obtained using a Varian Cary Eclipse spectrofluorimeter.
4. Photo-irradiations for singlet oxygen were done using the spectra-physics^R primoScan OPO series, which is pumped by Spectra-Physics Quanta Ray INDI Lab with maximum pump energy of 750 mJ and output energy of 27 mJ with $\lambda=485$.
5. Elemental compositions of the NPs and the conjugates were qualitatively determined using energy dispersive X-ray spectroscopy (EDS), INCA PENTA FET coupled with the VAGA TESCAMEM operated at 20 kV accelerating voltage.
6. Mass spectral data were collected with a Bruker AutoFLEX III Smartbeam TOF/TOF Mass spectrometer. The instrument was operated in positive ion mode using an m/z range of 400–3000 amu. The voltages of the ion sources were set at 19 and 16.7 kV for ion sources 1 and 2, respectively, while the lens was set at 8.50 kV and the reflector 1 and 2 voltages were set at 21 and 9.7 kV, respectively. α -Cyano-4-hydroxycinnamic acid was used as the MALDI matrix with a 337 nm nitrogen laser selected as the ionising source.
7. Fourier transform-infrared (FT-IR) spectra were recorded on a Perkin Elmer Spectrum 100 FT-IR spectrometer.
8. Fluorescence lifetime values were measured using a time-correlated single photon counting (TCSPC) setup (FluoTime 300, Picoquant GmbH) (**Fig. 2.1**). The excitation source was a diode laser (LDH-P-670 driven by PDL 800-B, 420 nm, 20 MHz repetition rate, 44 ps pulse width, Picoquant GmbH). Fluorescence was detected under the magic angle with a Peltier cooled photomultiplier tube (PMT) (PMA-C 192N-M, Picoquant) and integrated electronics (PicoHarp 300E, Picoquant GmbH).

A monochromator with a spectral width of 8 nm was used to select the required emission wavelength band. The response function of the system, which was measured with a scattering Ludox solution (DuPont), had a full width at half-maximum (FWHM) of about 300 ps. The ratio of stop to start pulses was kept low (below 0.05) to ensure good statistics. All luminescence decay curves were measured at the maximum of the emission peak. The data were analysed using the FluoFit program (Picoquant, GmbH).

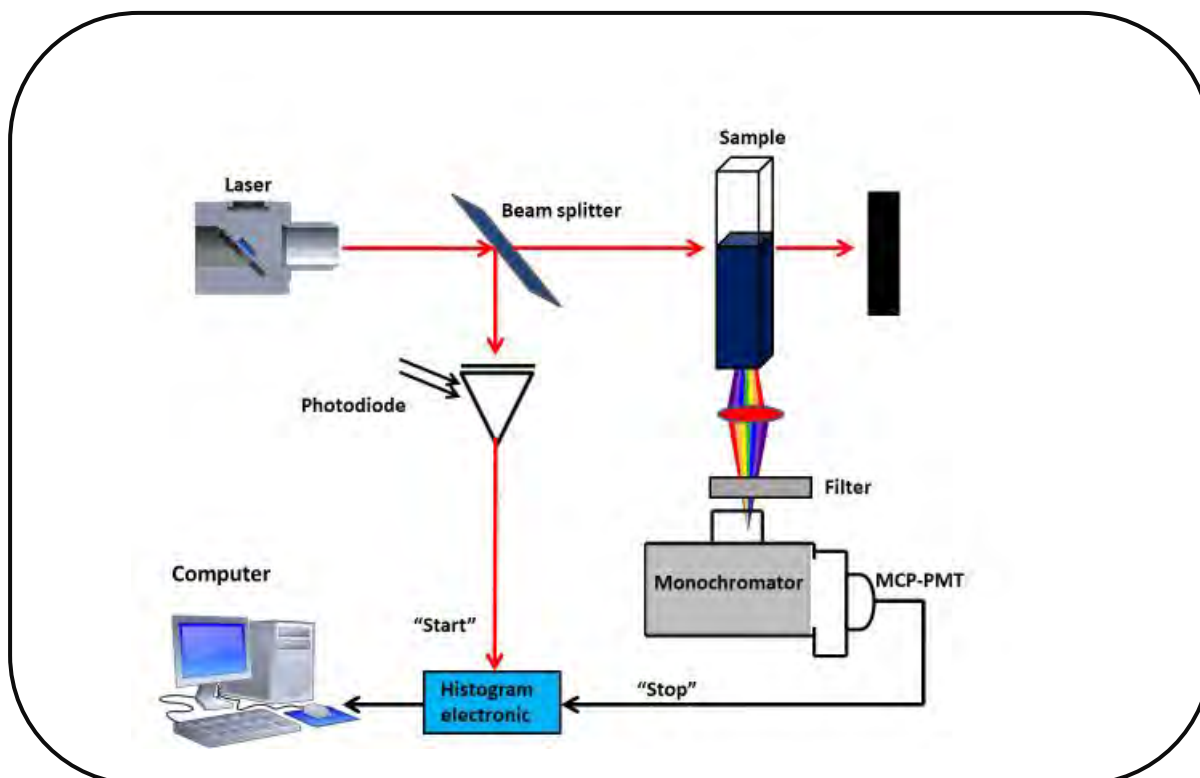


Figure 2.1: Diagram reflecting working principle of TCSPC.

9. X-ray photoelectron spectroscopy (XPS) analysis was measured using an AXIS UltraDLD (supplied by Kratos Analytical) with an Al (monochromatic) anode equipped with a charge neutralizer. The following parameters were used: the emission was 10 mA, the anode (HT) was set at 15 kV, and the operating pressure was kept below 5×10^{-9} torr. A hybrid lens was used, and the resolution to acquire scans was set at 160 eV pass energy in slot mode. The centre used for the scans was set at 520 eV (width of 1205 eV) with steps of 1 eV and a dwell time of 100 ms. High-resolution scans were acquired using 80 eV pass energy in slot mode. The chemically distinct species were resolved using a nonlinear least squares curve fitting procedure.

10. The morphologies of AgNPs and their conjugates with porphyrins were assessed using a transmission electron microscope (TEM), ZEISS LIBRA model 120 operated at 90 kV and iTEM software was used for TEM micrographs processing.

11. X-ray powder diffraction (XRD) patterns were recorded on a Bruker D8, discover instrument equipped with a Lynx Eye Detector, using Cu K α radiation ($\lambda = 1.5405 \text{ \AA}$, Ni filter). Data were collected over the $2\theta = 5\text{--}100^\circ$ range, scanning at 1° min^{-1} with a filter time-constant of 2.5 s per step and a slit width of 6.0 mm. Samples were placed on a zero-background silicon wafer slide. The X-ray diffraction data were retreated using Eva (evaluation curve fitting) software. A baseline correction was performed on each diffraction pattern by subtracting a spine fitted to the curved background and the full width at half maximum values reported in this study were obtained from the fitted curves.

12. Autoclave RAU-530D was used for the sterilization and autoclaving of nutrient broth, nutrient agar and phosphate buffer and other various apparatus for PACT studies.

13. The optical density of the bacteria culture was monitored using the LEDETECT 96 from LABXIM PRODUCTS.

14. HERMLE Z233M-2 centrifuge was used for the harvesting of the bacteria cells by centrifugation process.

15. The homogenization of the bacteria suspension was done using PROVSM-3 Lab plus Vortex mixer.

16. The incubation processes for the photodynamic antimicrobial chemotherapy was done using the thermostatic oven.

17. Scan® 500 automatic color colony counter was utilized to determine the colony forming units (CFU)/mL of the bacteria.

18. The elemental analysis was conducted using a Vario-Elementar Microcube ELIII.

19. Zeta potential studies were done using a Malvern Zetasizer nanoseries, Nano-ZS90.

20. For biological photo-irradiation, samples were enclosed in a box is to ensure that no unwanted ambient light can reach the samples, thus invalidating the results. A

595 nm mounted LED (M420L3 purchased from Thorlabs) was employed. The LED is connected to a T-cube LED driver (LEDD1B purchased from Thorlabs), which is used to regulate the current it receives.

2.3 Syntheses of AgNPs

2.3.1 Syntheses of OLM/OA capped AgNPs (Scheme 1.2)

The synthesis of OLM/OA capped silver nanoparticles were synthesized using a previously reported method [75] as follows: silver nitrate (0.40 g, 2.35 mmol), diphenyl ether (7 g, 41.13 mmol) were weighed and added into a 250 mL round bottom flask followed by addition of OA (3 mL) and OLM (6 mL). The reaction mixture was refluxed in open air for 5 h and cooled overnight by stirring at room temperature. The solution was poured into a 30 mL centrifuge tube and topped up with 20 mL of isopropanol and centrifuged for 10 min at 5000 rpm three times. The supernatant was poured out and the sediment was air dried in an enclosed fumehood for 24 h to afford AgNPs-OLM/OA nanoparticles.

2.3.2 Syntheses of GSH capped AgNPs (Scheme 1.2)

Synthesis of GSH capped AgNPs was done following previously reported method [76]. AgNPs-OLM/OA (0.20 g) was transferred into 50 mL round bottom flask containing chloroform (5 mL). A solution containing MeOH (20 mL), GSH (0.25 g, 0.81 mmol) and KOH (1.50 g, 26.73 mmol) were added to the AgNPs mixture. The mixture was allowed to stir for 2 h at ambient temperature. Afterwards, the formed GSH capped AgNPs were precipitated out of solution using ethanol and purified using methanol. The obtained solid sediment was air dried in an enclosed fumehood to afford AgNPs-GSH.

2.4 Synthesis of porphyrins

2.4.1 Synthesis of 5,10,15,20-tetra (4-pyridyl) porphyrinato zinc(II) (complex 1), Schemes 4.1/4.2

Complex 1 was synthesized as follows [52] with slight modifications. A mixture of propionic acid (150 mL), 4-pyridinecarboxyaldehyde (500 mg, 4.6 mmol) and pyrrole (313 mg, 4.6 mmol) was allowed to reflux for 2 h. The reaction mixture was cooled in ice to obtain the crude precipitate, which was filtered and washed with Millipore water

(3 × 100 mL) and dried in vacuum. The crude product was then purified using silica gel column chromatography with chloroform as the eluent to yield free base porphyrin as a purple solid. Metalation of the free base porphyrin was carried out as follows: in a 25 mL round bottom flask containing chloroform (5 mL), free base porphyrin (0.0003 mg, 0.00048 mmol) was added followed by an excess amount of zinc acetate dihydrate (0.02 mg, 10.90 μmol) in MeOH (3 mL). The mixture was refluxed for 2 h. The metallated crude was poured into 100 mL of water and the organic layer collected, followed by purification with silica gel column chromatography with chloroform as the eluent to obtain a pure complex **1**. Yield: 86% (w/w); ¹H NMR (400 MHz, DMSO-d₆), δ_H (ppm): 8.82 (d, 8H, *J* = 5.36, pyridyl H), 7.74 (d, 8H, *J* = 4.88, pyridyl H), 6.93 (s, 8H, β-pyrrolic). UV/vis (DMF) λ_{max} nm (log ε): 421 (4.11), 551 (1.66), 600 (1.08). Anal. calc. for C₄₀H₂₄N₈Zn: C = 68.44, H = 3.55, N = 16.43, Found: C = 68.57, H = 2.87, N = 15.71 MALDI-TOF-MS m/z, calc: 680, found [M+H]⁺ = 681 amu.

2.4.2 Synthesis of 5,10,15,20-tetrathienyl porphyrinato zinc(II) (complex 2), Schemes 4.1/4.2

Complex **2** [53] was synthesized as in **1** except, 2-thiophenecarboxyaldehyde (500 mg, 4.5 mmol) was used instead of 4-pyridinecarboxyaldehyde. The reaction mixture was cooled in ice water containing NaHCO₃ to obtain the crude precipitate, which was filtered and washed with Millipore water (3 × 100 mL) and dried in vacuum. Metalation was carried out as in **1**. Yield: 82% (w/w); ¹H NMR (400 MHz, DMSO-d₆), δ_H ppm: 9.00 (s, 8H, β-pyrrolic), 8.12 (d, 4H, *J* = 5.04, thienyl-H), 7.95 (d, 4H, *J* = 2.72 Hz, thienyl-H), 7.57 (t, 4H, *J* = 4.32, thienyl-H). UV/vis (DMF) λ_{max} nm (log ε): 429 (4.30), 558 (2.01), 624 (1.02). Anal. calc. for C₃₆H₂₀N₄S₄Zn: C = 61.57, H = 2.87, N = 7.98, S = 18.27 Found: C = (62.72), H = (2.15), N = (7.10), S = (17.78). MALDI-TOF-MS m/z calc: 699, found [M+2H]⁺ = 701 amu.

2.4.3 Synthesis of 5-(4-hydroxyphenyl)-10,15,20-tris (2-thienyl)-porphyrinato zinc(II) (complex 3), Schemes 4.1/4.2

Complex **3** [54] was synthesized as in **1** except, 2-thiophenecarboxaldehyde (800 mg, 7.13 mmol) and 4-hydroxybenzaldehyde (290 mg, 2.37 mmol) were used instead of 4-pyridinecarboxyaldehyde. The reaction mixture was cooled in ice water containing NaHCO₃ to obtain the crude precipitate. The crude product was then

purified using silica gel column chromatography with chloroform/cyclohexane (8:2) as the eluent to yield free base porphyrin as a green-purple solid. Metalation was carried out as in **1**. Silica gel column chromatography with chloroform/cyclohexane (8:2) as the eluent was used to obtain a pure complex **3**. Yield: 78% (w/w); ^1H NMR (400 MHz, DMSO- d_6), δ_{H} , ppm: 9.02 (m, 6H, β -pyrrolic), 8.83 (s, 2H, β -pyrrolic), 8.41 (s, 2H phenyl-H), 8.27 (s, 2H, phenyl-H), 8.14 (t, 3H, $J = 3.16$, thienyl-H), 7.95 (s, 3H, thienyl-H), 7.56 (m, 3H, thienyl-H). UV/vis (DMF): λ_{max} nm (log ϵ) 430(4.32), 559 (2.05) 626 (1.03). Anal. calc for $\text{C}_{38}\text{H}_{22}\text{N}_4\text{OS}_3\text{Zn}$: C, 64.09; H, 3.11; N, 7.87; S, 13.51. Found: C, 63.21(; H, 3.05; N, 6.35; S, 14.16. MALDI-TOF m/z calc: 710 found $[\text{M} + 2\text{H}]^+ = 712$ amu.

2.4.4 Synthesis of 5-(4-carboxyphenyl)-10,15,20-tris (pentafluorophenyl) – porphyrinato zinc(II) (complex 4), Schemes 4.1/4.2

Complex **4** [55] was synthesized as in **1** except, 4-formylbenzoic acid (229 mg, 1.53 mmol), 2,3,4,5,6-pentafluorobenzaldehyde (900 mg, 4.59 mmol) and pyrrole (410 mg, 6.12 mmol) was used instead of 4-pyridinecarboxyaldehyde and different amount of pyrrole. The reaction mixture was cooled in ice water containing NaOH to obtain the crude precipitate, which was filtered and washed with Millipore water (3×100 mL). The free base crude product was purified as in **3**. Metalation was carried out as in **1**. Purification was followed as in **3**. Yield: 81% (w/w); ^1H NMR (600 MHz, CDCl_3), δ_{H} (ppm): 8.95 (m, 8H, β -pyrrolic), 8.34 (s, 2H, phenyl-H), 7.72 (s, 2H, phenyl-H), UV/vis (DMF) λ_{max} nm (log ϵ): 424 (4.15), 548 (1.77), 603 (1.01). Anal. calc. for $\text{C}_{45}\text{H}_{13}\text{F}_{15}\text{N}_4\text{O}_2\text{Zn}$: C = 54.49, H = 1.32, N = 5.65, Found: C 52.33, H= 1.73, N= 4.75. MALDI-TOF-MS m/z calc: 990, found $[\text{M}]^+ = 990$ amu.

2.4.5 Synthesis of 5-(4-carboxyphenyl)-10,15,20-triphenyl-porphyrinato zinc(II) (complex 5), Schemes 4.1/4.2

Complex **5** [56] was synthesized as in **1** except, 4-formylbenzoic acid (229 mg, 1.53 mmol), benzaldehyde (491 mg, 4.59 mmol) and pyrrole (410 mg, 6.12 mmol) was used instead of 4-pyridinecarboxyaldehyde and different amount of pyrrole. The free base crude product was purified as in **3**. Metalation of the free base porphyrin analogue was carried out as in **1**. Purification was followed as in **3**. Yield: 79% (w/w); ^1H NMR (600 MHz, CDCl_3), δ_{H} ppm: 8.78 (s, 8H, β -pyrrolic), 8.36 (s, 2H, phenyl-H), 8.18 (d, 6H, $J = 6.78$ Hz, phenyl-H), 7.95 (s, 2H, phenyl-H), 7.81 (s, 9H, phenyl-H),

UV/Vis (DMF) λ_{\max} nm (log ϵ): 426 (4.22), 548 (1.73), 612 (1.06). Anal. calc. for $C_{45}H_{28}N_4O_2Zn$: C = 73.84, H = 3.45, N = 7.63, Found: C = 74.21, H = 3.36, N = 6.85. MALDI-TOF-MS m/z calc: 720, found $[M+H]^+$ 721 amu.

2.4.6 Synthesis of 5-(4-carboxyphenyl)-10,15,20-tris (2-thienyl)-porphyrinato zinc(II) (complex 6), Schemes 4.1/4.2

Complex **6** [57] was synthesized as in **1** except, 4-formylbenzoic acid (229 mg, 1.53 mmol), 2-thiophenecarboxaldehyde (514.76 mg, 4.59 mmol) and pyrrole (410 mg, 6.12 mmol) were used instead of 4-pyridinecarboxyaldehyde and different amount of pyrrole. The reaction mixture was cooled in ice water containing $NaHCO_3$ to obtain the crude precipitate, which was filtered and washed with Millipore water (3×100 mL). The free base crude product was purified as in **3**. Metalation of the free base porphyrin was carried out as in **1**. Purification was followed as in **3**. Yield: 83% (w/w); 1H NMR (600 MHz, $CDCl_3$), δ_H ppm: 7.58 (m, 3H, thienyl-H), 7.97 (s, 3H, thienyl-H), 8.13 (t, 3H, $J = 4.74$ Hz, thienyl-H), 8.25 (s, 2H, thienyl-H), 8.42 (s, 2H, thienyl-H), 8.82 (s, 2H, β -pyrrolic), 9.01 (m, 6H, β -pyrrolic). UV/vis (DMF): λ_{\max} nm (log ϵ) 430(4.29), 557(2.01) 623(1.03). Anal. Calc for $C_{41}H_{28}N_4O_2S_3Zn$: C, 63.93; H, 3.66; N, 7.27; S, 12.49. Found: C, 63.75; H, 3.71; N, 7.21; S, 12.58. MALDI-TOF: calc: 739, found $[M + 2H]^+ = 741$ amu.

2.4.7 Self-assembly formation conditions, Scheme 4.3

For self-assembly [87] of **1**, **2**, **3** and **6** onto AgNPs, complexes **1** (0.010 g, 0.020 mmol), **2** (0.010 g, 0.040 mmol), **3** (0.010 g, 0.014 mmol) and **6** (0.015 g, 0.020 mmol) were each dissolved chloroform (5 mL), followed by addition of AgNPs-OA/OLM (0.004 g) in toluene (6 mL). The mixtures were heated under reflux for 1 h followed by stirring at room temperature for 24 h. The conjugates were then precipitated out of solution using methanol and centrifuged for 10 min at 5000 rpm. The solids were washed with methanol and ethanol 3 times to remove unreacted porphyrin. The products were then air dried in vacuum to afford **1**-AgNPs-SA, **2**-AgNPs-SA, **3**-AgNPs-SA and **6**-AgNPs-SA.

2.4.8 Amide bond formation conditions, Scheme 4.4

The amide linked conjugates: (**4**-AgNPs-amide, **5**-AgNPs-amide and **6**-AgNPs-amide) were synthesized in accordance with previously reported procedure [88]. To three separate round bottomed flasks, complexes **4** (0.03 g 0.03 mmol), **5** (0.03 g, 0.042 mmol) and **6** (0.03 g, 0.041 mmol) were added. Then EDC (0.004 g, 0.049 mmol) and NHS (0.003 g, 0.026 mmol) were added followed by DCM (2 mL) and acetonitrile (1 mL). The mixtures were stirred at room temperature for 48 h. After this time, GSH capped AgNPs (0.003 g) were added and the mixtures were stirred for another 48 h. The conjugates were collected and washed several times by centrifugation (10 min at 5000 rpm each time) in diethyl ether and methanol (50:50) to remove unbound porphyrin complexes and excess EDC and NHS. The nanocomposites were obtained by oven drying at 110 °C for 48 h to afford us **4**-AgNPs-amide, **5**-AgNPs-amide and **6**-AgNPs-amide.

2.5 PACT conditions

S. aureus (ATCC 6538) was grown on nutrient agar plates according to the manufacturer's specifications to obtain colonies. A colony was then inoculated into Luria nutrient broth and then placed overnight at 37°C on a rotary shaker (~200 rpm), to produce a bacteria culture. The optical density at 600 nm of the bacteria culture was adjusted to approximately 0.8 in nutrient broth. The inactivation of *S. aureus* was carried out by placing aliquots of 100 µL of the bacteria culture in a test-tube containing 50 µL of **1**, **2**, **3**, **4**, **5**, **6**, **1**-AgNPs-SA, **2**-AgNPs-SA, **3**-AgNPs-SA, **4**-AgNPs-amide, **5**-AgNPs-amide, **6**-AgNPs-amide, **6**-AgNPs-SA and AgNPs (fixed concentrations were 0.36 µg/mL and 2.0 µg/mL in 1% DMSO in 6 mL PBS (phosphate buffer saline)) and incubated for 30 min. An aliquot (100 µL) was transferred to 24 well plate and the plates were then illuminated with the setup described above at 15 min intervals for 75 min. Irradiation doses of 40 J/cm² were employed. Following irradiation, 10 µL was taken from the plates to determine colony forming unit (CFU), which was used to calculate the log reduction values and compared to that for the control containing no photosensitizer and before irradiation.

Chapter 3

Attempted syntheses

This chapter deals primarily with an attempt to synthesize novel porphyrin complexes.

3.1 Synthesis of complex 7, Scheme 3.1

An attempt to synthesize an asymmetric porphyrin (complex **7**) was as follows: 4-pyridinecarboxyaldehyde (0.3 g, 7.42 mmol) was added to freshly distilled pyrrole (0.18 g, 2.78 mmol) in a 250 mL round bottom flask, under nitrogen. To this mixture was added trifluoroacetic acid (TFA) (0.033 g, 0.288 mmol) and the mixture allowed to stir for 30 min at room temperature. The mixture was poured in water (5 mL) and extracted with dichloromethane (DCM) (3 x 5 mL). The organic layer was washed with saturated sodium bicarbonate (3 x 5 mL), followed by water (3 x 5 mL). The organic layers were dried over sodium sulfate and dried under vacuum to afford compound 5-(4-pyridyl)-2-dipyrromethane (**DP-pyridyl**). Synthesis of 5, 15-bis (5-bromothiophene-2-thienyl)-10, 20-tris (2-pyridyl) porphyrin (**7**) was carried out by following protocol as described in literature [89]. However, the cyclisation of **DP-pyridyl** and 5-bromo-2-thiophenecarboxyaldehyde to form complex **7** proved difficult, suggesting scrambling might have taken place. Scrambling is a well-known phenomenon that results in no product formation [90] thereby products that were obtained could not be assigned structures.

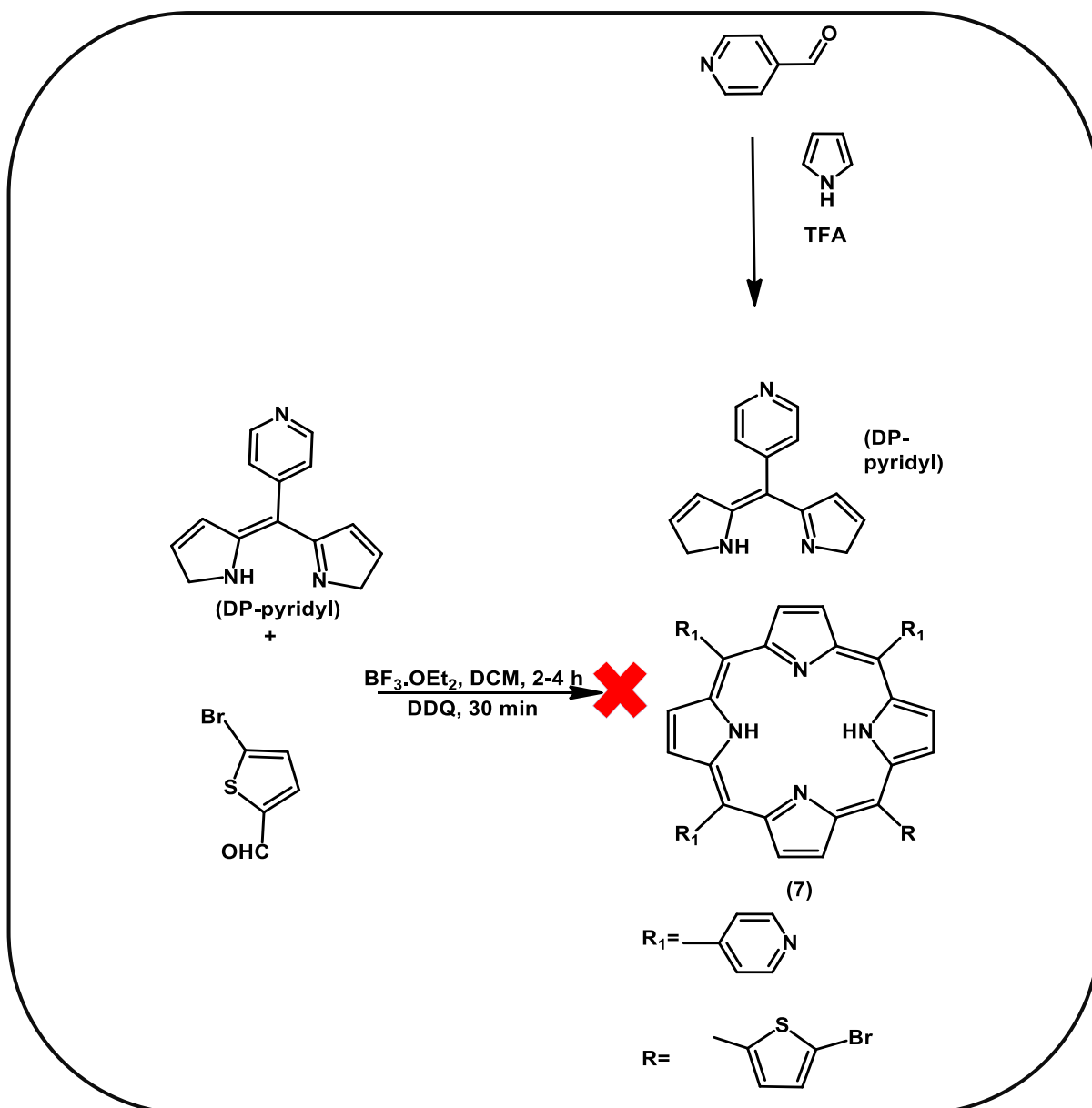


Figure 3.1: The figure represents an attempt to synthesize an asymmetric porphyrin (complex 7).

3.2 Synthesis of complex 8, Scheme 3.2

CA (coupled aldehyde)

The first attempt for synthesis of complex 8 followed a literature procedure [91] with modifications where 5-bromothiophene-2-carbaldehyde (1.67 g, 8.765 mmol), palladium(II) bis(triphenylphosphine) dichloride (0.154 g, 0.219 mmol), and copper iodide (0.0834 g, 0.438 mmol) were dissolved in tetrahydrofuran (THF) (30 mL). Ethynyltrimethylsilane (TMSA) (0.947 g, 9.64 mmol) was added to the reaction

mixture under argon followed by addition of diisopropylamine (DIPA) (36 mL) to the reaction mixture. The reaction was allowed to stir at room temperature for 24 h. The reaction mixture was then poured into water and extracted with ethyl acetate (EtOAc) and was supposedly meant to afford compound 5-((trimethylsilyl)ethynyl) thiophene-2-carbaldehyde (compound **CA**).

DP-1 (TMS)

Compound **CA** (0.3 g, 1.44 mmol) was added to freshly distilled pyrrole (1.93 g, 28.80 mmol) in a round bottom flask, under nitrogen. To this mixture, TFA (0.033 g, 0.288 mmol) was added and the mixture allowed to stir for 30 min at room temperature. The mixture was poured in water (5 mL) and extracted with DCM (3 x 5 mL). The organic layer was washed with saturated NaHCO₃ (3 x 5 mL), followed by water (3 x 5 mL). The organic layers were dried over Na₂SO₄ and dried under vacuum to afford compound 5-((trimethylsilyl)ethynyl) thiophene-2-dipyrrromethane (**DP-1**).

DP-2 (alkyne)

Trimethylsilane protecting group was removed by reacting **DP-1** (0.03 g, 0.092 mmol) with K₂CO₃ (0.038 g, 0.276 mmol) dissolved in a hexane/MeOH mixture (8:2) (5 mL) at room temperature for 2 h. The reaction was quenched by adding water. This was extracted with EtOAc, and the organic layer dried over Na₂SO₄ and dried under vacuum to afford compound 5-(ethynyl)-thiophene-2-dipyrrromethane (**DP-2**)

The synthesis of **8** was carried out by following previously reported protocol [89], where **DP-2** (0.0073 g, 0.023 mmol), **CA** (0.0067 g, 0.023 mmol) boron trifluoride etherate (BF₃.OEt₂) (0.00023 g, 0.0016 mmol) were stirred for 3-4 h at room temperature followed by addition of 2,3-dichloro-5,6-dicyano-1,4-benzoquinone (DDQ) (0.005 g, 0.024 mmol) and reaction was left for a further 30 min at room temperature. The cyclisation of the coupled aldehyde to form *meso*-5, 10, 15, 20-tetra-ethynylthienylporphyrin (**8**) proved difficult, suggesting Sonogashira reaction on the aldehyde was also unsuccessful. Separation of **CA**, **DP-1**, **DP-2** and **8** by silica gel chromatography proved to be difficult, and this led to low yields of the "product". Products that were obtained could not be assigned structures using the obtained

mass spectral data. A possible reason for this could be that there was “scrambling” during the reaction process as described above, and this led to the formation of polypyrroles for **CA**, **DP-1** and **DP-2**.

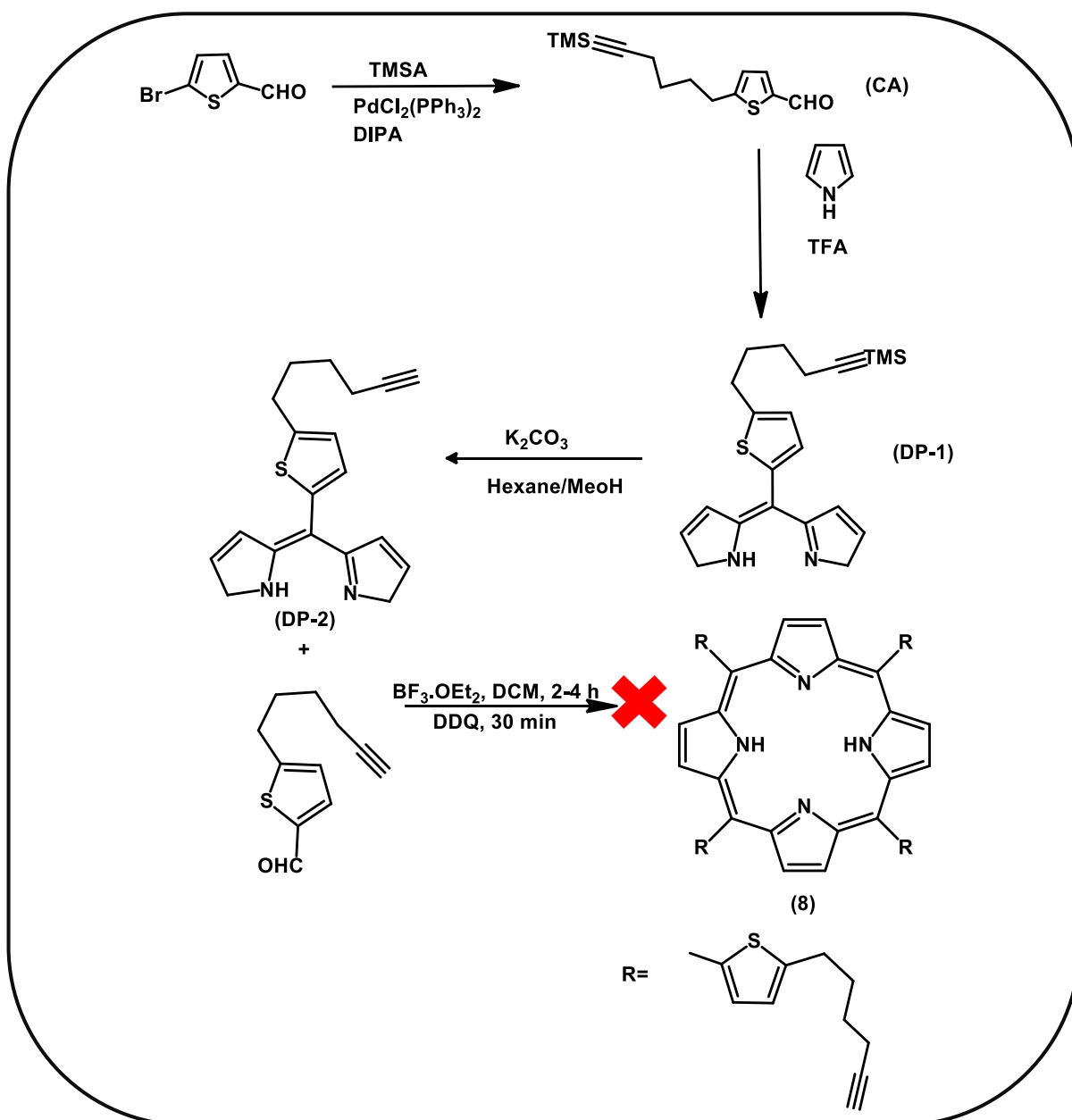


Figure 3.2: The figure represents an attempt to synthesize a sonogashira coupled tetrathienyl-ethyl-porphyrin (complex **8**).

3.3 Rationale behind synthesis.

The main rationale behind the synthesis of complex **7** and **8** was to perform a novel Sonogashira coupling on complex **8** by coupling with complex **7** to give a tetrasubstituted porphyrin for application in PACT of *S. aureus*, unfortunately a well-known phenomenon of scrambling described above might have possibly caused restrictions from obtaining the desired product.

Results and Discussion

This section has been split into two chapters

Chapter 4: Synthesis, characterization and photophysicochemical properties

Chapter 5: Antimicrobial experiments

The results discussed in the following chapters (4-5) have been published in peer-reviewed journals:

- **Samuel M. Shabangu**, Balaji Babu, Rodah C. Soy, Muthumuni Managa, Kutloano E. Sekhosana and Tebello Nyokong, Photodynamic antimicrobial chemotherapy of asymmetric porphyrin-silver conjugates towards photoinactivation of *Staphylococcus aureus*. [J. COORD. CHEM., 73 (2020) 593-608].
- **Samuel M. Shabangu**, Balaji Babu, Rodah C. Soy, James Oyim, Edith Amuhaya and Tebello Nyokong, Susceptibility of *Staphylococcus aureus* to porphyrin-silver mediated photodynamic antimicrobial chemotherapy. [J. Lumin, 22 (2020) 117158].

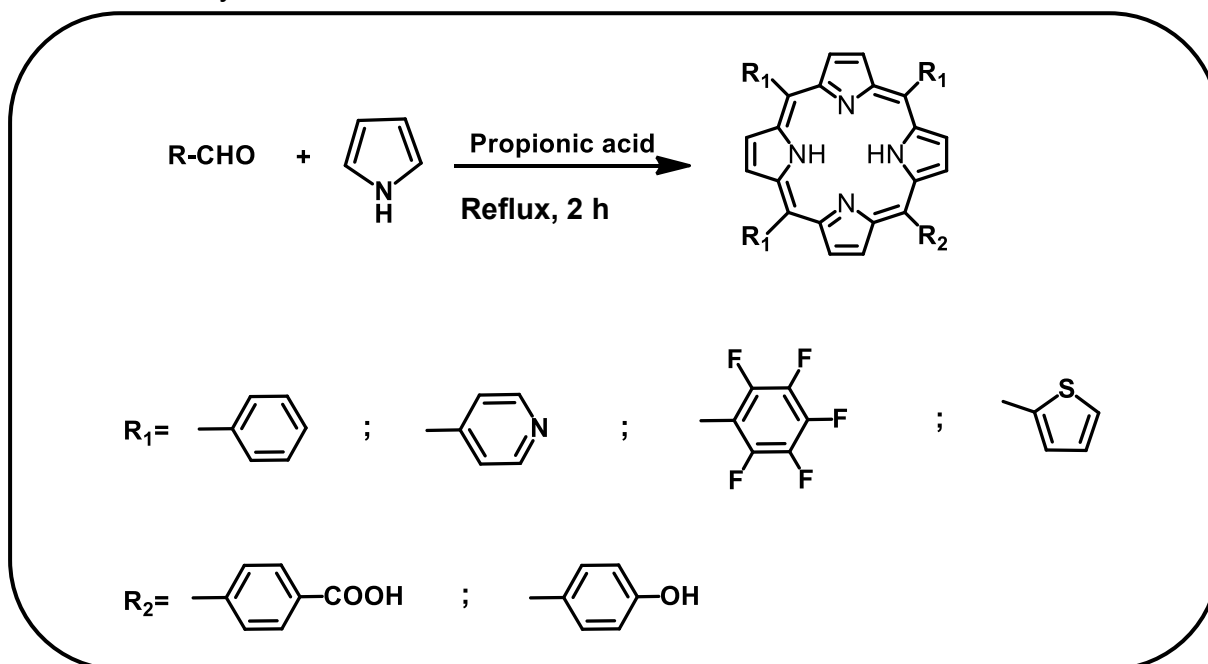
Chapter 4

Synthesis, characterization and photophysicochemical properties

Detailed discussions related to the synthesis and characterization of AgNPs, bare porphyrin complexes and their corresponding conjugates are carried out in this chapter.

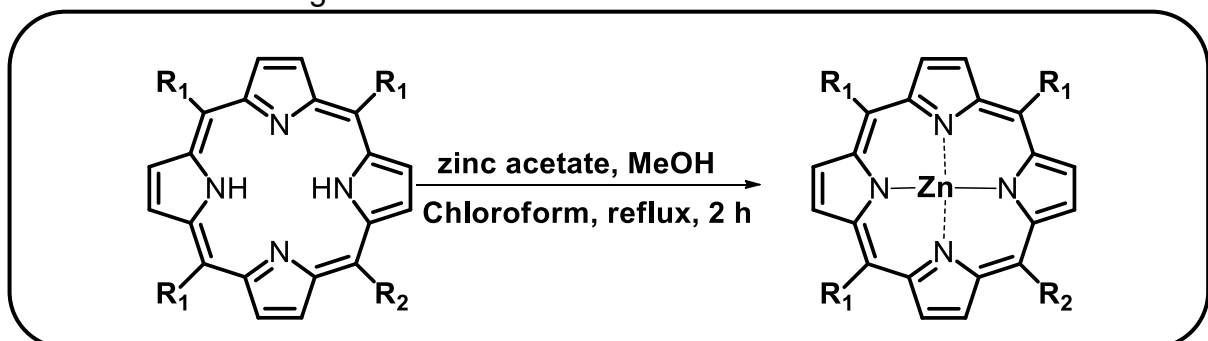
4.1 Synthesis and characterization of complexes 1-6

The syntheses of complexes **1-6** (**Scheme 4.1**) has been reported before [52-57] and their characterization is reported here. The syntheses of asymmetric and symmetric porphyrins in this thesis were achieved following the same method (Adler method). Characterization of the porphyrin complexes was achieved using MALDI-TOF mass spectrometer, nuclear magnetic resonance (^1H NMR) spectroscopies and elemental analysis.



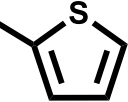
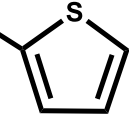
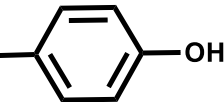
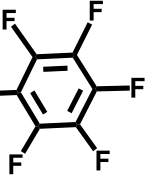
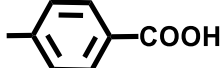
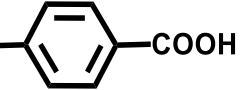
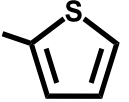
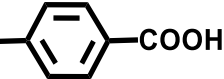
Scheme 4.1: Synthesis of asymmetric and symmetric porphyrins using Adler method (see **Table 4.1** for description of substituents)

The metalation of porphyrins was done by following previously reported methods [92] with slight modification. Normally, a free base porphyrin is dissolved in chloroform followed by addition of metal salt, in the case of this thesis zinc acetate was used, and the solution brought under reflux.



Scheme 4.2: Typical metalation of porphyrins using free base porphyrins.

Table 4.1 Structures of complexes discussed in this chapter and preceding ones.

Substituent	number of complex
$R_1=R_2=$ 	(1)
$R_1=R_2=$ 	(2)
$R_1=$  $R_2=$ 	(3)
$R_1=$  $R_2=$ 	(4)
$R_1=$  $R_2=$ 	(5)
$R_1=$  $R_2=$ 	(6)

4.1.1 UV-Vis spectroscopy

Porphyrins are characterized by an intense B (Soret) band that appears around 400 nm, and weak Q bands at lower energies. Two Q bands are observed for metallated porphyrins. **Fig 4.1** shows a typical UV/vis of porphyrins using complexes **1-3** as examples. The Soret bands for **1**, **2** and **3** are observed at 421, 429 and 430 nm respectively and for **4**, **5** and **6** are observed at 424, 426 and 430 nm respectively [**Table 4.2**]. Thus, the Soret band of **2**, **3** and **6** are red shifted compared to **1**, **4** and **5** due to the presence of sulfur atoms which are known to result in red-shifting of the porphyrin spectra [93, 94].

Table 4.2 Soret band absorbances of the complexes and their conjugates in DMF.

Complex/Conjugate	Soret band (λ) (nm)
1	421
2	429
3	430
4	424
5	426
6	430
1-AgNPs-SA	422
2-AgNPs-SA	428
3-AgNPs-SA	428
4-AgNPs-amide	425
5-AgNPs-amide	426
6-AgNPs-amide	430
6-AgNPs-SA	432
AgNPs	425 ^a

^aSPR band

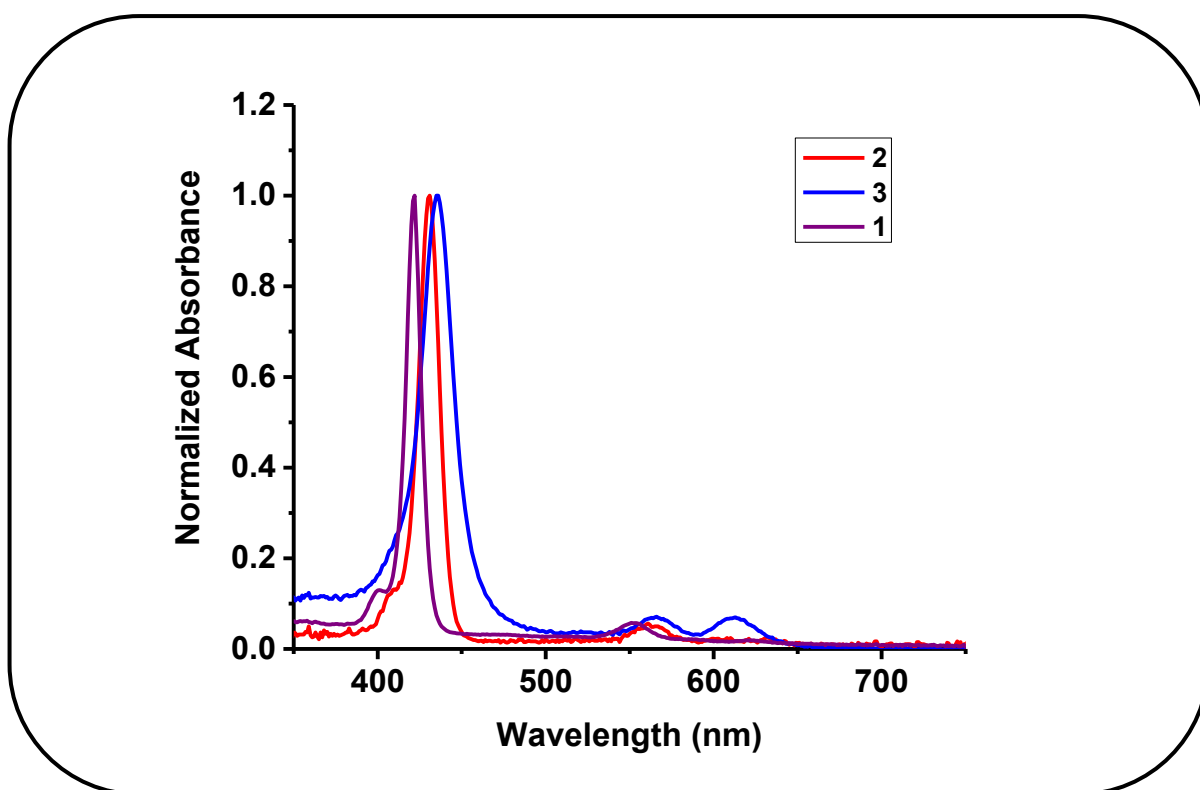


Figure 4.1: Normalized UV-visible absorption spectra using complex **1**, **2** and **3** as examples.

4.1.2 Nuclear Magnetic Resonance Spectra

Complex 1: ^1H NMR of complex **1** provided the characteristic chemical shifts for the structure as expected. It exhibited pyridyl protons at 8.82 ppm as a doublet along with β -pyrrolic protons at 7.74 ppm as a doublet and at 6.93 ppm as a singlet (See **Fig. A.1**).

Complex 2: β -pyrrolic protons were observed at 9.00 ppm as a singlet. Thienyl protons were observed at 8.12 ppm and 7.95 ppm both appearing as doublets and at 7.57 ppm appearing as a triplet (See **Fig. A.2**).

Complex 3: ^1H NMR spectrum for complex **3** indicates β -pyrrolic protons at 9.02 ppm as a multiplet and at 8.83 ppm as a singlet. Phenyl protons were observed at 8.41 ppm and 8.27 ppm both appearing as singlets. Thienyl protons were observed at 8.14 ppm as a triplet, at 7.95 ppm as a singlet and at 7.56 ppm as a multiplet (See **Fig. A.3**).

Complex 4: ^1H NMR spectrum for complex **4** indicates β -pyrrolic protons at 8.95 ppm as a multiplet followed by phenyl protons at 8.34 ppm and 7.72 ppm both appearing as singlets (See **Fig. A.4**).

Complex 5: Complex **5** showed presence of β -pyrrolic protons at 8.78 ppm as a singlet. Phenyl protons appeared at 8.36 ppm as singlet and at 8.18 ppm, 7.95 ppm and 7.81 ppm as doublets (See **Fig. A.5**).

Complex 6: ^1H NMR spectrum for complex **6** showed appearance of β -pyrrolic protons were observed at 9.01 ppm as a singlet and at 8.82 ppm as a multiplet. Thienyl protons were observed at 8.42 ppm and 8.25 ppm both appearing as singlets, 8.13 ppm as a triplet, 7.97 ppm as a singlet and at 7.58 ppm as a multiplet (See **Fig. A.6**).

4.2 Formation of conjugates

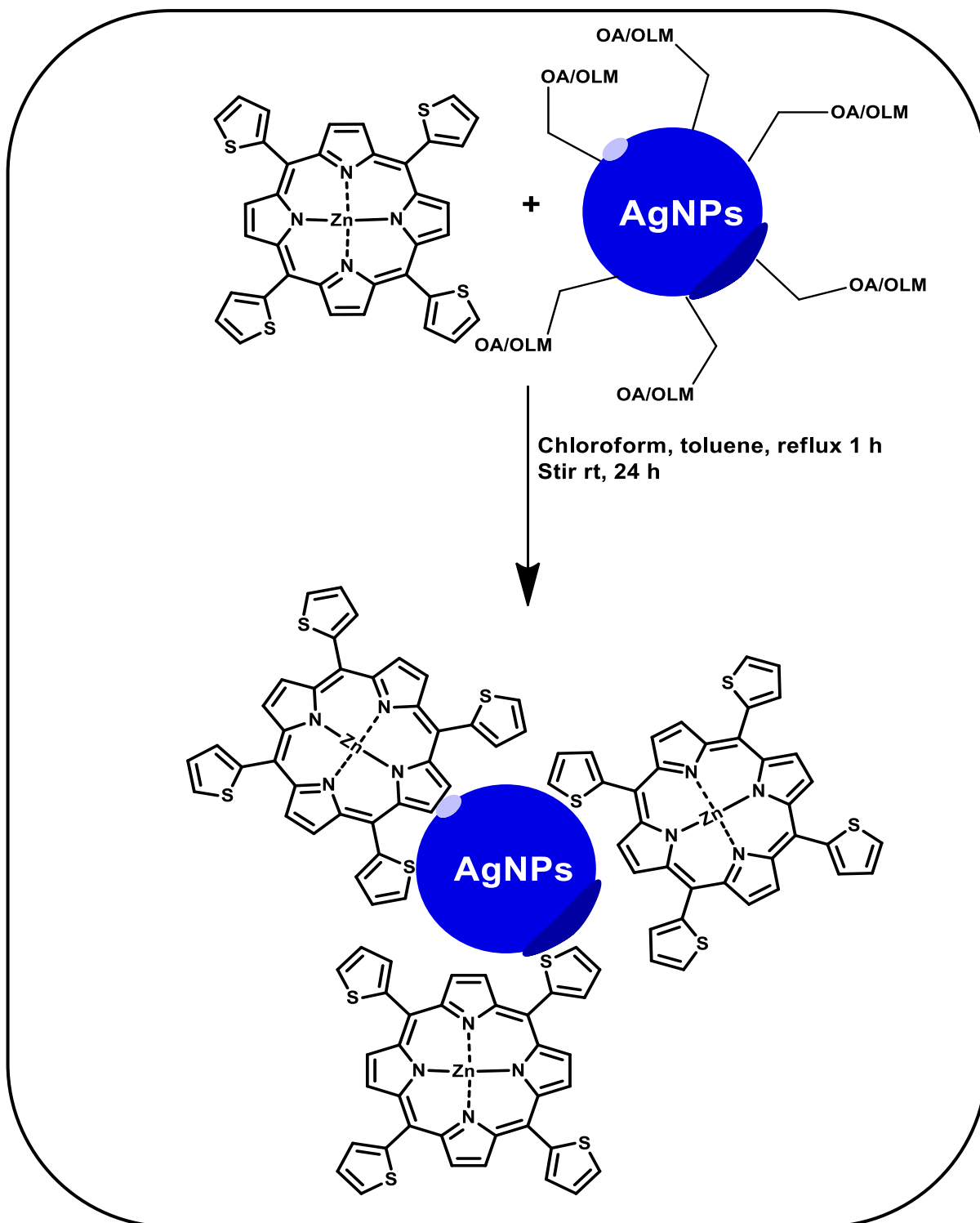
4.2.1 Self-assembly (SA) for complexes 1, 2, 3 and 6

The synthesis of OA/OLA and GSH capped AgNPs [75, 76], have been reported elsewhere. The presence of the loosely bound oleic acid and oleylamine on the surface of AgNPs allows for ligand exchange of these capping ligands with other molecules such as porphyrins bearing thiol or pyridyl moieties having stronger affinity for AgNPs surface. Synthesis of the conjugates via self-assembly was achieved using previously reported methods [87]. **Scheme 4.3** shows the synthetic route for porphyrin-AgNPs via SA using complex **2** as an example

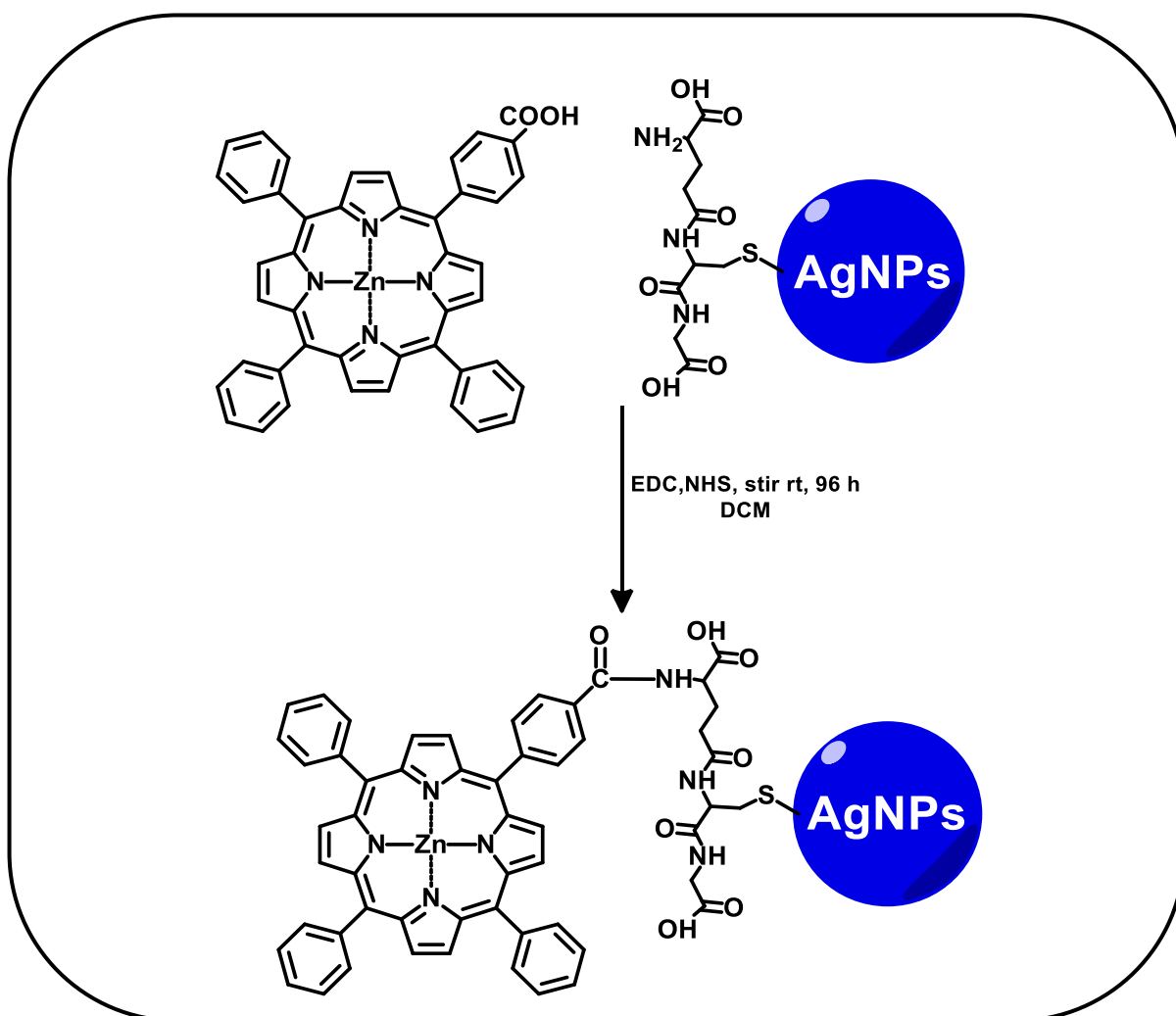
4.2.2 Amide bond for complexes 4-6

The syntheses of GSH capped AgNPs [76], have been reported elsewhere. Porphyrins bearing carboxylic moieties are more likely to undergo linkage with amino terminal of GSH. Synthesis of the conjugates via amide bond was achieved using previously reported methods [88]. **Scheme 4.4** shows the synthetic route for porphyrin-AgNPs via amide bond using complex **5** as an example. The complex **5** was firstly dissolved in DMF and then DCC and NHS were added to convert the carboxylic group (-COOH) of the porphyrin into an active carbodiimide ester group. The formation of the amide bond between the -COOH group of **5** (used as an

example as the process is the same for **4** and **6**) and the amino group of GSH in AgNPs-GSH was facilitated by EDC and NHS as a coupling agent, **Scheme 4.4**.



Scheme 4.3: The scheme for the synthesis of self-assembly of **2** onto AgNPs to form **2-AgNPs -SA** (via Ag-S interaction).



Scheme 4.4: The scheme for the synthesis of amide linkage of **5** onto AgNPs to form **5-AgNPs -amide**.

4.3 Characterization of conjugates

4.3.1 UV-vis spectroscopy

Fig. 4.2 shows UV/vis spectra of complex **2** and **2-AgNPs-SA** as examples. Upon conjugation of porphyrins to AgNPs, there were slight red shifts in the Soret band for **6** to conjugate **6-AgNPs-SA** and a slight blue shift for **3-AgNPs-SA** (**Table 4.2**). Blue or red shifts in the Soret band of porphyrin-AgNPs are associated with aggregation [95], there were no significant changes for **1-AgNPs-SA**, **2-AgNPs-SA**, **4-AgNPs-amide**, **5-AgNPs-amide** and **6-AgNPs-amide**. The surface plasmon resonance (SPR) band of AgNPs appears at 425 nm as seen in **Fig 4.2** and **Table 4.2**. This has been

reported to be a typical maxima for spherically shaped AgNPs [96]. The SPR band is not clearly observed after conjugation since it is at the same wavelength as the Soret band of the porphyrin, however there is slight broadening below 400 nm for the conjugates as shown in **Fig. 4.2** due to the presence of AgNPs. The loading of porphyrins onto the nanoparticles was estimated according to reported literature method [97], **Table 4.3** but using absorbance instead of fluorescence. This involves comparing the intensities of the Q bands of the conjugates with those of the bare porphyrin complexes [97]. Equal masses (mg) of porphyrins and porphyrin-AgNPs were separately weighed and dissolved in the same volume of the solvent. Conjugate **3-AgNPs-SA** had the highest loading.

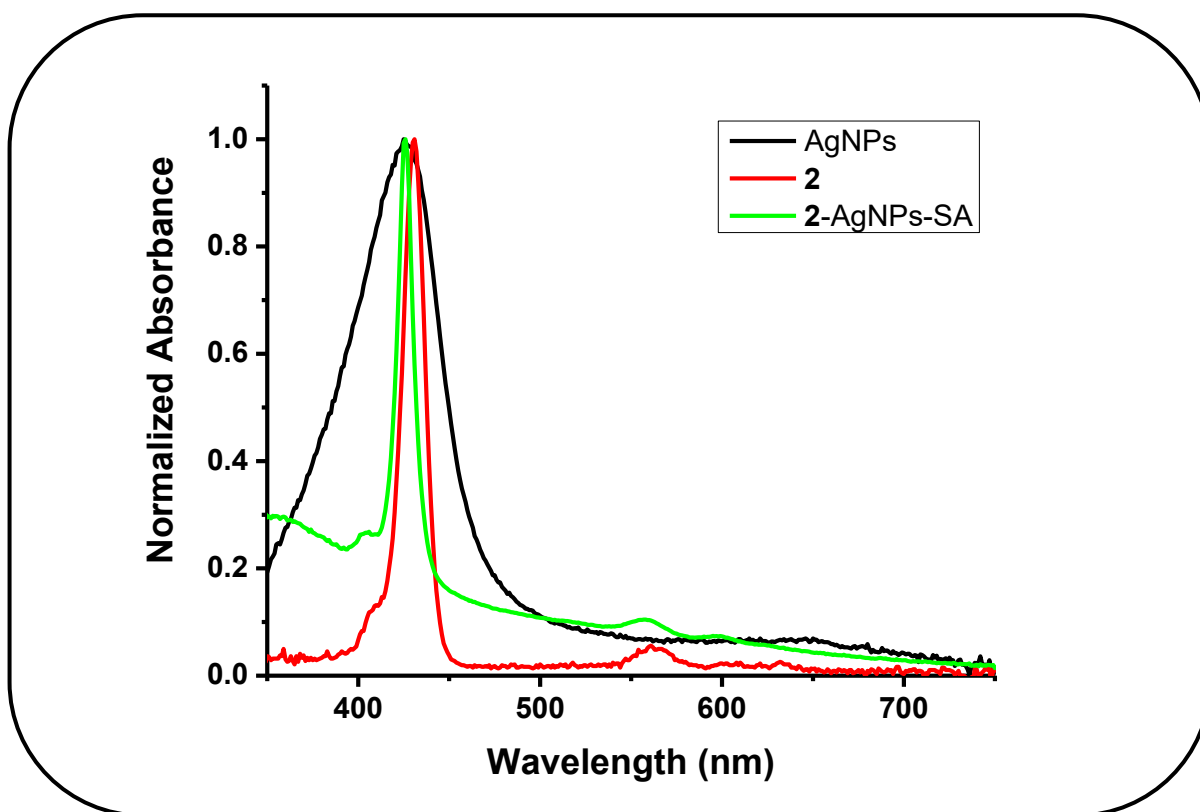


Figure 4.2: Normalized UV-visible absorption spectra using complex **2**, AgNPs and **2-AgNPs-SA** as examples.

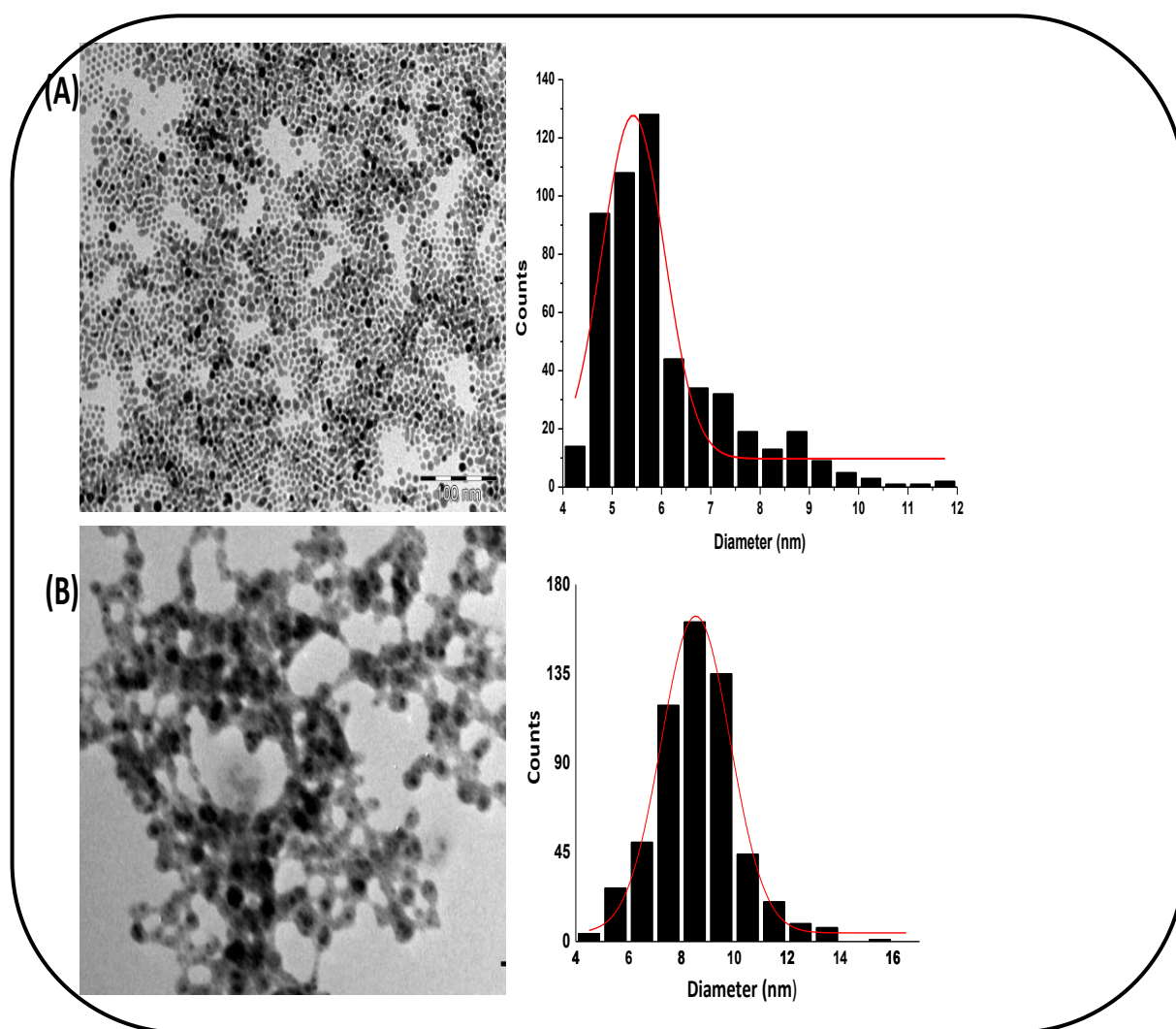
Table 4.3: Loading of conjugates.

Complex/Conjugate	loading ($\mu\text{g}/\text{mg}$)
1	-
2	-
3	-
4	-
5	-
6	-
1-AgNPs-SA	23
2-AgNPs-SA	19
3-AgNPs-SA	35
4-AgNPs-amide	27
5-AgNPs-amide	21
6-AgNPs-amide	25
6-AgNPs-SA	18
AgNPs	-

4.3.2 Transmission Electron Microscopy (TEM) and Energy dispersive spectra (EDS)

TEM micrograph of AgNPs (**Fig. 4.3A** using AgNPs and 2-AgNPs-SA as examples) show spherical monodispersed patterns with an average size of 5.56 nm. Upon conjugation, there is aggregation for all conjugates (**Fig. 4.3B**). Aggregation may occur by π - π interaction of porphyrins on adjacent AgNPs.

The elemental composition of the complexes and conjugates were qualitatively determined using an energy dispersive X-ray spectrometer (EDS) as shown in **Fig. 4.3C** using SA conjugates as examples. The EDS spectra of porphyrin-AgNPs conjugates showed the presence of N, S, C, O, Ag and Zn, which were the expected elements for all SA-conjugates except for 1-AgNPs-SA which had N instead of S.



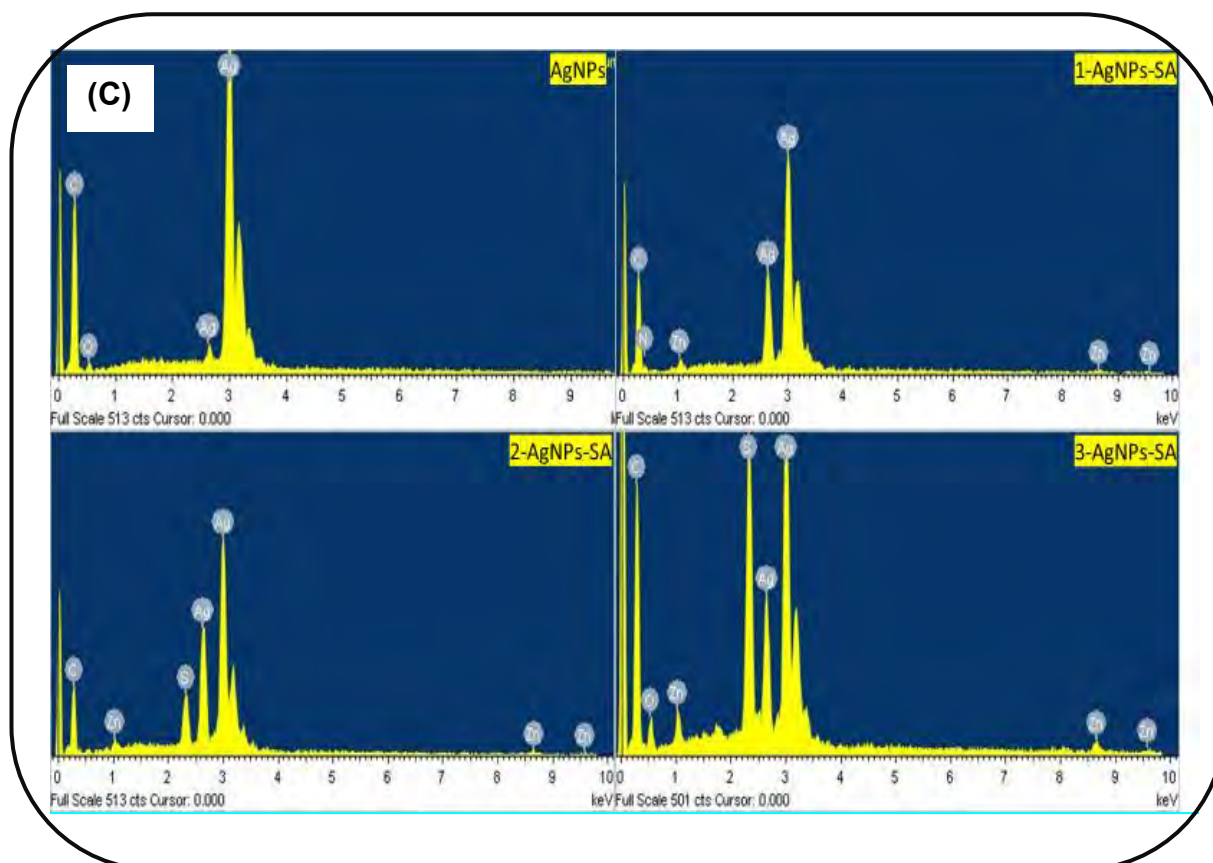


Figure 4.3: (A) TEM micrographs of AgNPs, (B) 2-AgNPs-SA and (C) EDS spectra of AgNPs, 1-AgNPs-SA, 2-AgNPs-SA and 3-AgNPs-SA.

4.3.3 Surface charge (zeta potential)

Zeta potential (ζ) is a measure of charges carried by particles suspended in a liquid. Zeta potential is important in that it indicates the stability of colloidal dispersions. The magnitude of the zeta potential shows the degree of electrostatic repulsion between adjacent particles. A high zeta potential will confer stability (the dispersion will resist aggregation) [98]. **Table 4.4** shows zeta potentials of 2-AgNPs-SA as an example over a period of 72 h (3 days) in 1% DMSO in PBS (used for PACT studies). There is an increase in ζ (hence increase in stability) when AgNPs and 2 are combined compared to when they are alone. There is not much change of ζ for 2-AgNPs-SA with time over three days, showing the conjugate is stable.

Table 4.4. Zeta potential using **2**, AgNPs and **2**-AgNPs-SA as examples over 72 h.

Complex	Time (h)	Zeta potentials ζ (mV)
2	-	-8.24
AgNPs	-	-21.71
2 -AgNPs-SA	0	-31.07
2 -AgNPs-SA	24	-29.56
2 -AgNPs-SA	48	-30.15
2 -AgNPs-SA	72	-31.63

4.3.4 X-ray diffraction pattern (XRD)

The XRD diffractograms (**Fig. 4.4**) with complex **2**, **2**-AgNPs-SA and AgNPs as examples show peaks characteristic of AgNPs with well-defined crystalline peaks assigned to the 111, 200, 220, 311 and 222 planes corresponding to a face centered cubic crystal of the nanoparticles at $2\theta = 38.1^\circ$, 44.3° , 63.55° , 73.56° and 82.26° respectively [99, 100], ICSD (104391) PDF(01-071-9140). Complex **2** showed a broad peak near $2\theta = 20^\circ$ due its amorphous nature [101]. The conjugate retains the amorphous nature of complex **2** and the crystallinity of AgNPs.

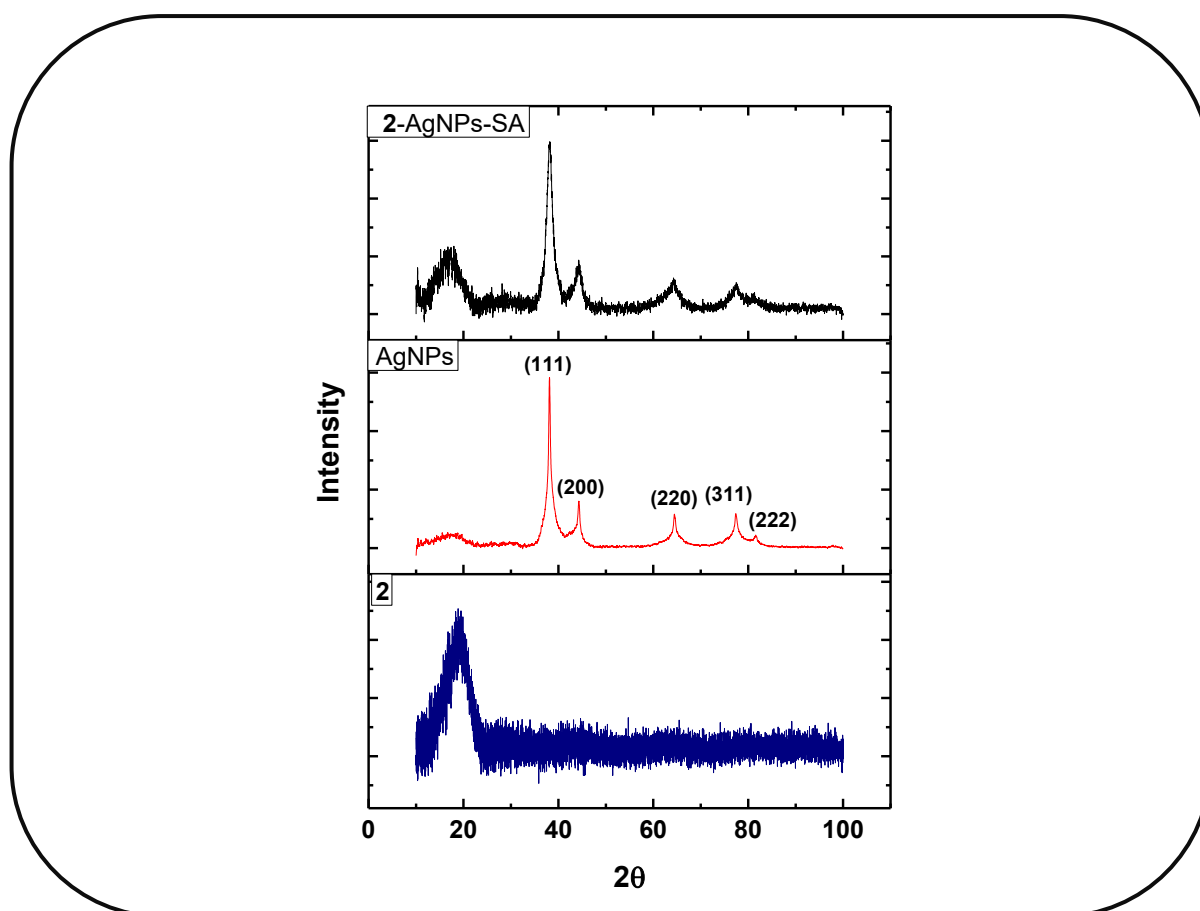


Figure 4.4: Representative XRD diffractograms for AgNPs, **2** and **2-AgNPs**.

4.3.5 Fourier Transform-Infrared Spectroscopy (FT-IR)

FTIR spectra were employed to prove an amide bond formation between the porphyrin complexes and AgNPs, **Fig. 4.5**, using complex **5-AgNPs-amide**, AgNPs and **5** as examples. The porphyrin complexes (**4-6**) and GSH have hydroxyl group terminals from carboxylic acid, shown by broadening from 3019 cm^{-1} to 3034 cm^{-1} . These peaks tend to overlap with NH peaks from GSH as shown by an intense NH peak 3301 cm^{-1} for AgNPs. The shift in the position of NH peak to 3227 cm^{-1} in **5-AgNPs-amide** shows the participation of these groups in the formation of an amide bond. Shifts in the IR confirm structural change [102]. Of note is the appearance of an amide band ($-\text{HN}-\text{C}=\text{O}$) vibration at 1500 cm^{-1} in **5-AgNPs-amide**, which is not present in complex **5** alone or AgNPs, confirming amide bond formation. However, it is still difficult to conclude that the amide vibration band observed in the nanoconjugate could be due to amide bond formation because the GSH ligand also

possessed amide functional moiety in its molecular structure, hence XPS was also employed to prove amide bond formation.

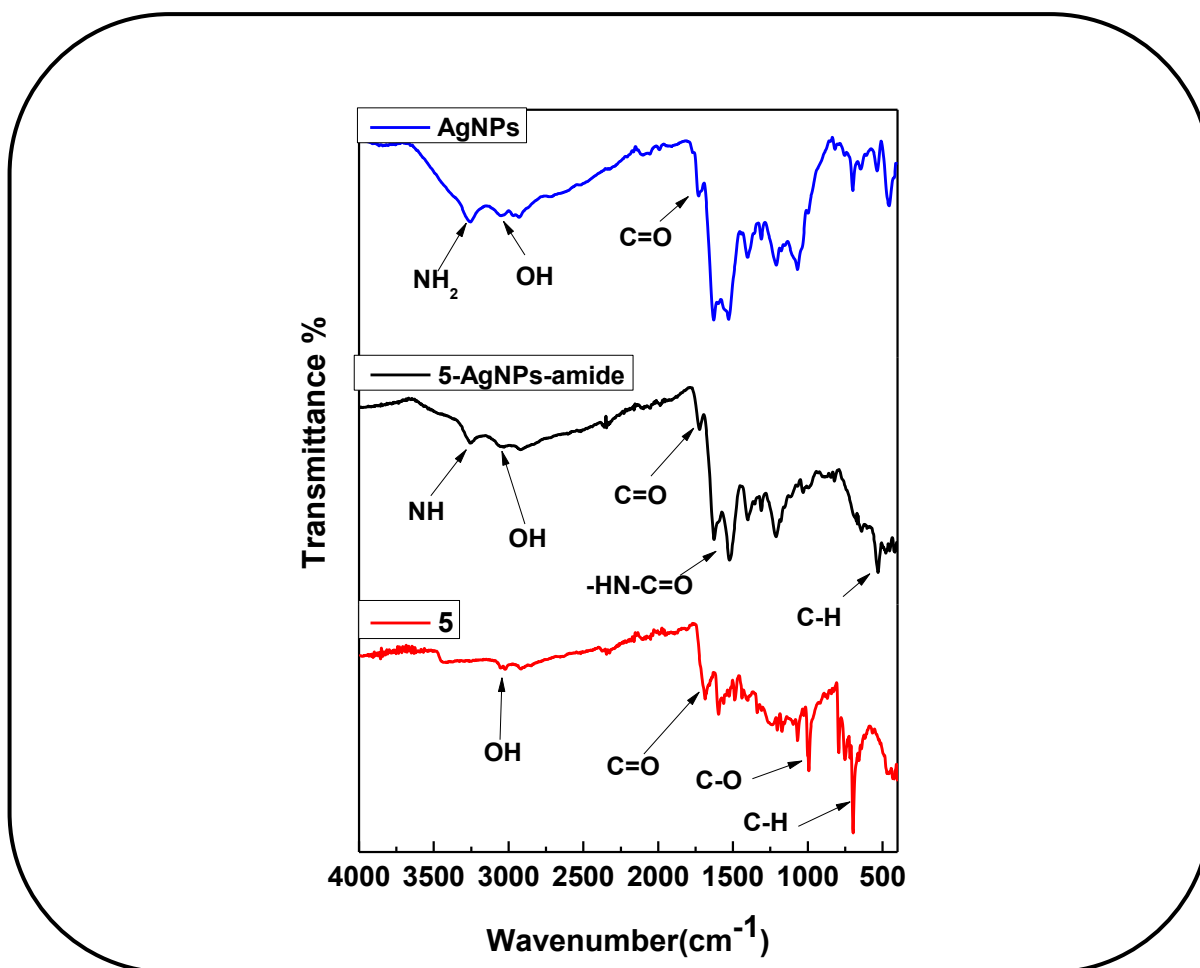


Figure 4.5: FT-IR spectra of GSH capped AgNPs, **5** and **5-AgNPs-amide**.

4.3.6 X-ray photoelectron spectroscopy (XPS)

X-ray photoelectron spectroscopy (XPS) was carried out to confirm immobilization of porphyrin macrocycle on the surface of metallic nanoparticles. XPS high resolution was employed to prove that complexes **1** and **2** (as examples) were linked to silver nanoparticles the latter being through S-Ag affinity the former being N-Ag affinity all of which were interaction by SA. The S 2p peak of complex **2** was deconvoluted and it accounted for two sub peaks which correspond to S-C and S at 161.6 eV and 163 eV, respectively, **Fig 4.6A**. A similar pattern was observed in the conjugate with the appearance of a new subpeak at 162.9 eV (S-Ag) indicating successful linkage of complex **2** onto the surface of AgNPs **Fig. 4.6B**. High resolution N1s XPS was also employed for complex **1** with two subpeaks appearing at 396.2 eV and 397.8 eV

showing N-Zn and N-C respectively **Fig. 4.6C**. The conjugate showed three subpeaks appearing at 395.9, 397.5 and 399.5 eV corresponding to N-Zn, N-C and N-Ag respectively, **Fig. 4.6D**. The new subpeak suggests the formation of N-Ag has taken place.

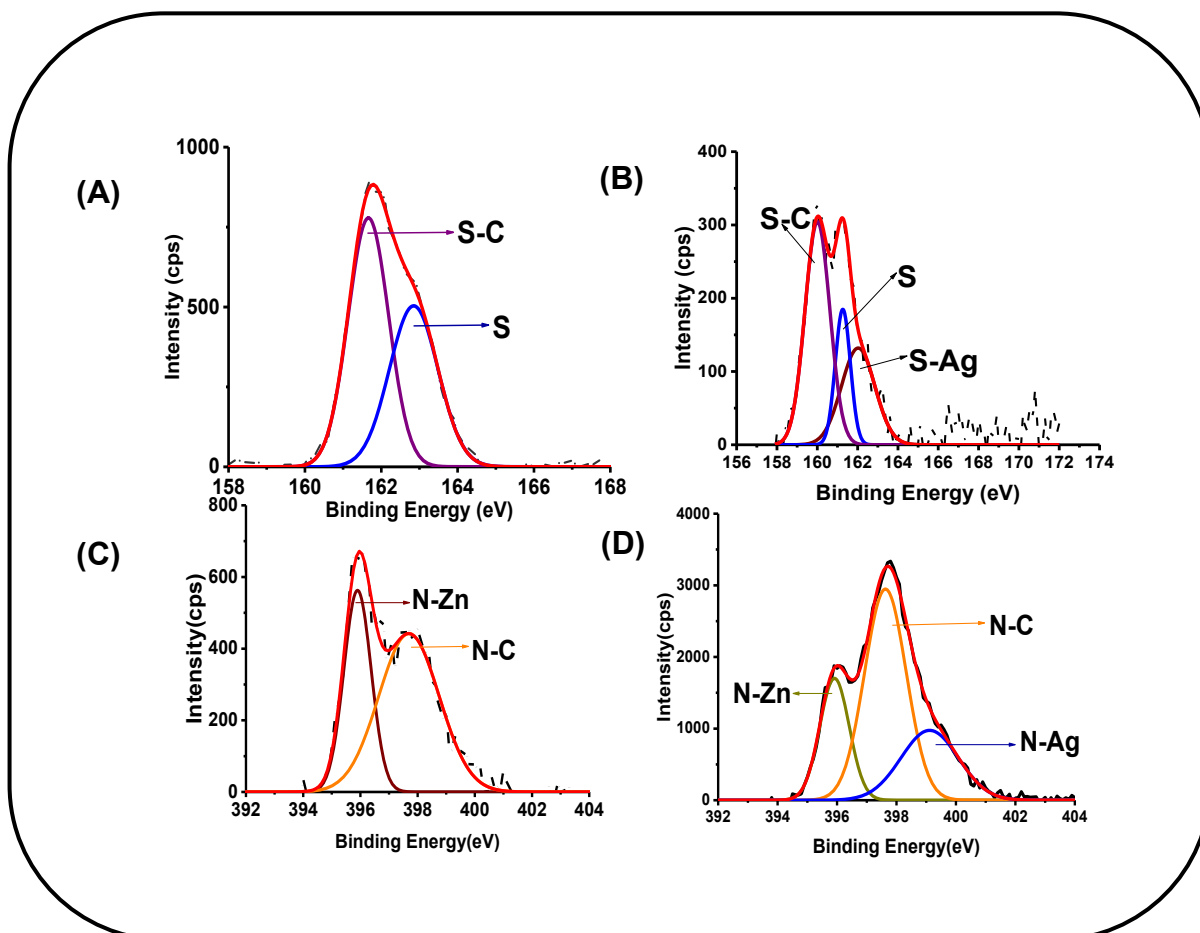


Figure 4.6: High resolution XPS of (A) **2** (B) **2-AgNPs-SA** (C) **1**, (D) **1-AgNPs-SA**.

XPS analysis was further used to confirm amide bond formation using complex **5** as an example. The N1s peak for complex **5** alone (**Fig. 4.7A**) showed two subpeaks at 395.8 eV and 397.6 eV attributed to N-Zn and N-C respectively, while AgNPs displayed three peaks at 395.9, 398.0 and 399.3 eV corresponding to N-C, N-H and N-C=O (amide bond from GSH capping agent), respectively, **Fig. 4.7B**. **Fig. 4.7C** showed the presence of four subpeaks which were attributed to N-Zn, N-C, N-H, and N-C=O at 396.1, 396.9, 398.1 and 399.7 eV (amide linkage to complex **5**) in that

order. The chemical shifts in binding energies thus confirm successful conjugation. The amide bond peak is of higher intensity for complex **5**-AgNPs-amide at 1678 cps as compared to AgNPs at 375 cps due to more amide bonds in the former, thus confirming successful conjugation.

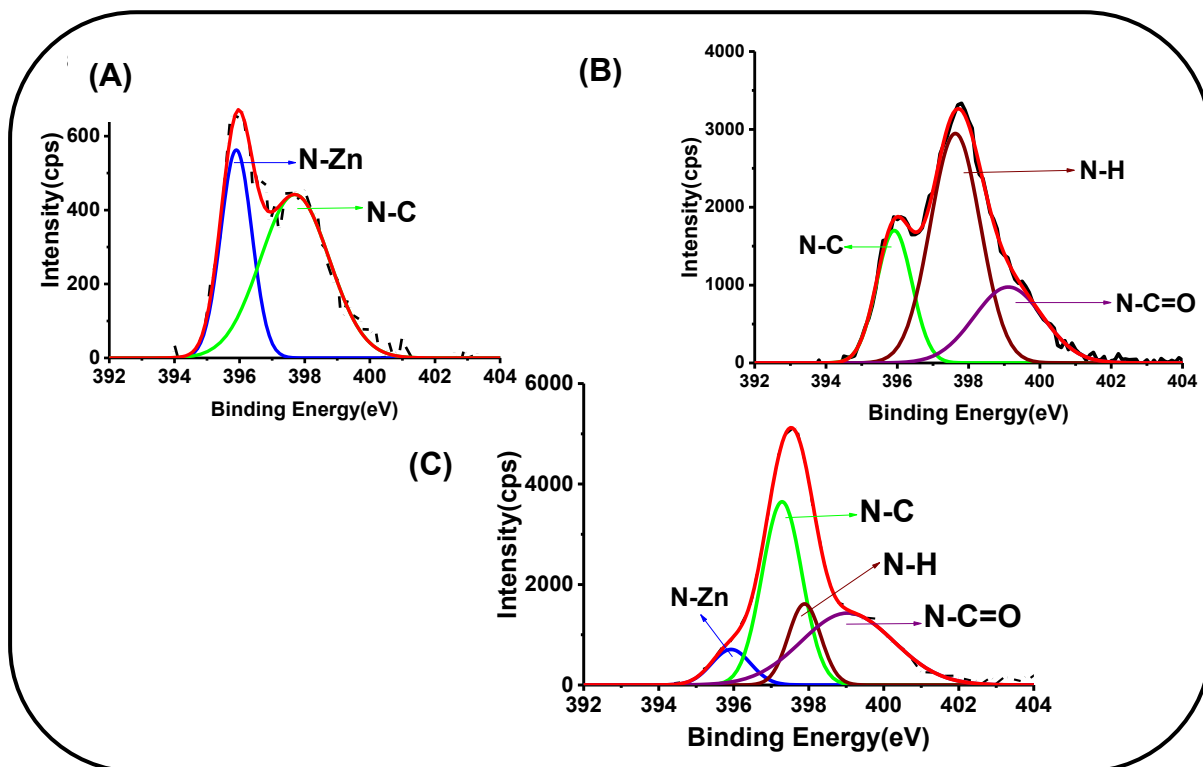


Figure 4.7: High resolution XPS of (A) **5** (B) GSH capped AgNPs (C) **5**-AgNPs-amide.

4.4 Photophysical and photochemical parameters

Fluorescence quantum yields values were determined using the comparative method (eq. 1.1) in accordance with literature procedures [103] using ZnTPP as a standard ($\Phi_F = 0.033$ in DMF) [81].

Singlet oxygen quantum yields (Φ_Δ) were determined in DMF using eq. 1.2 with DMA as the singlet oxygen quencher. The absorbances of DMA were spectroscopically monitored at 425 nm at a predetermined time course.

4.4.1 Fluorescence quantum yields and lifetimes

The Φ_F values before and after conjugation are low $\Phi_F < 0.01$ thus they are not shown in Table 4.5. Metalloporphyrins are reported to exhibit low fluorescence quantum yields [81]. Mono-exponential decay was obtained for all complexes, as seen in Fig. 4.8 below. Fluorescence lifetimes are provided in Table 4.5. The values are low corresponding to low Φ_F values. The lifetimes of the conjugates are less than those for porphyrins alone as expected, due to the external heavy atom effect brought about by incorporation with the nanoparticles [104].

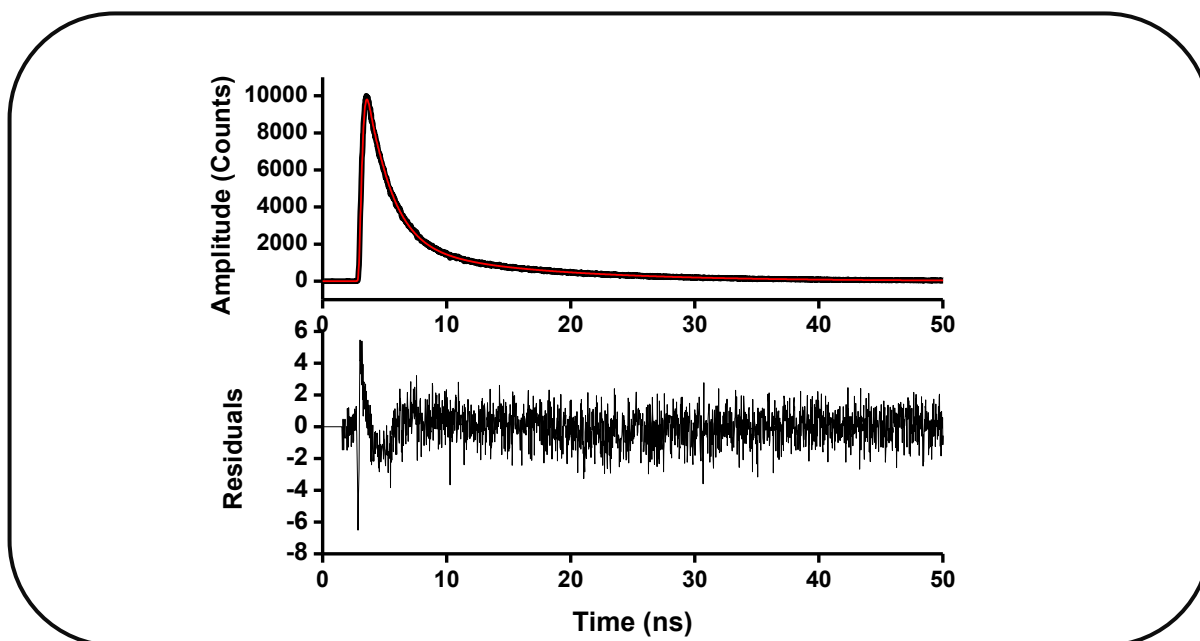


Figure 4.8: Fluorescence decay (black) x^2 fitting (red) and IRF (black) curves for complex **2** in DMF.

Table 4.5. Photophysical parameters of complexes **1-6** and their corresponding conjugates in DMF.

Complex/Conjugate	τ_F , ns (± 0.01)	Φ_Δ
1	0.36	0.38
2	0.49	0.55
3	0.51	0.62
4	0.47	0.49
5	0.38	0.40
6	0.58	0.61
1-AgNPs-SA	0.11	0.47
2-AgNPs-SA	0.19	0.66
3-AgNPs-SA	0.24	0.73
4-AgNPs-amide	0.12	0.57
5-AgNPs-amide	0.10	0.51
6-AgNPs-amide	0.21	0.69
6-AgNPs-SA	0.23	0.71
AgNPs	-	-

4.4.2 Singlet oxygen quantum yields (Φ_Δ)

Table 4.5 lists Φ_Δ values in DMF. In this thesis Φ_Δ values were determined by preparing solutions of the photosensitizer and the standard (rose bengal) in DMF in the dark and irradiated at a crossover wavelength (485 nm) whereby the degradation of DMA peaks was monitored at intervals of 5 min for 30 min, **Fig. 4.9** (using complex **2** as an example). The absence of spectral changes from 450-800 nm region during singlet oxygen measurements suggests that compounds are photostable. Complex **3** gave a high Φ_Δ (0.62), followed by **6** (at 0.61), **2** at 0.55, **4** at 0.49, **5** at 0.40 and lastly complex **1** at 0.38. The high Φ_Δ values for complexes **2**, **3** and **6** may be due to the presence of sulfur atoms on the thienyl rings which enhance the rate of intersystem crossing to the triplet state. For complex **3** and **6**, the high Φ_Δ value is additionally due to asymmetrical structure, which has been

reported to increase singlet oxygen quantum yields in porphyrins [45] when compared to their symmetrical analogue (complex **2**). The Φ_{Δ} values were further enhanced upon conjugation due to an external heavy atom effect that is brought about by incorporation with the nanoparticles.

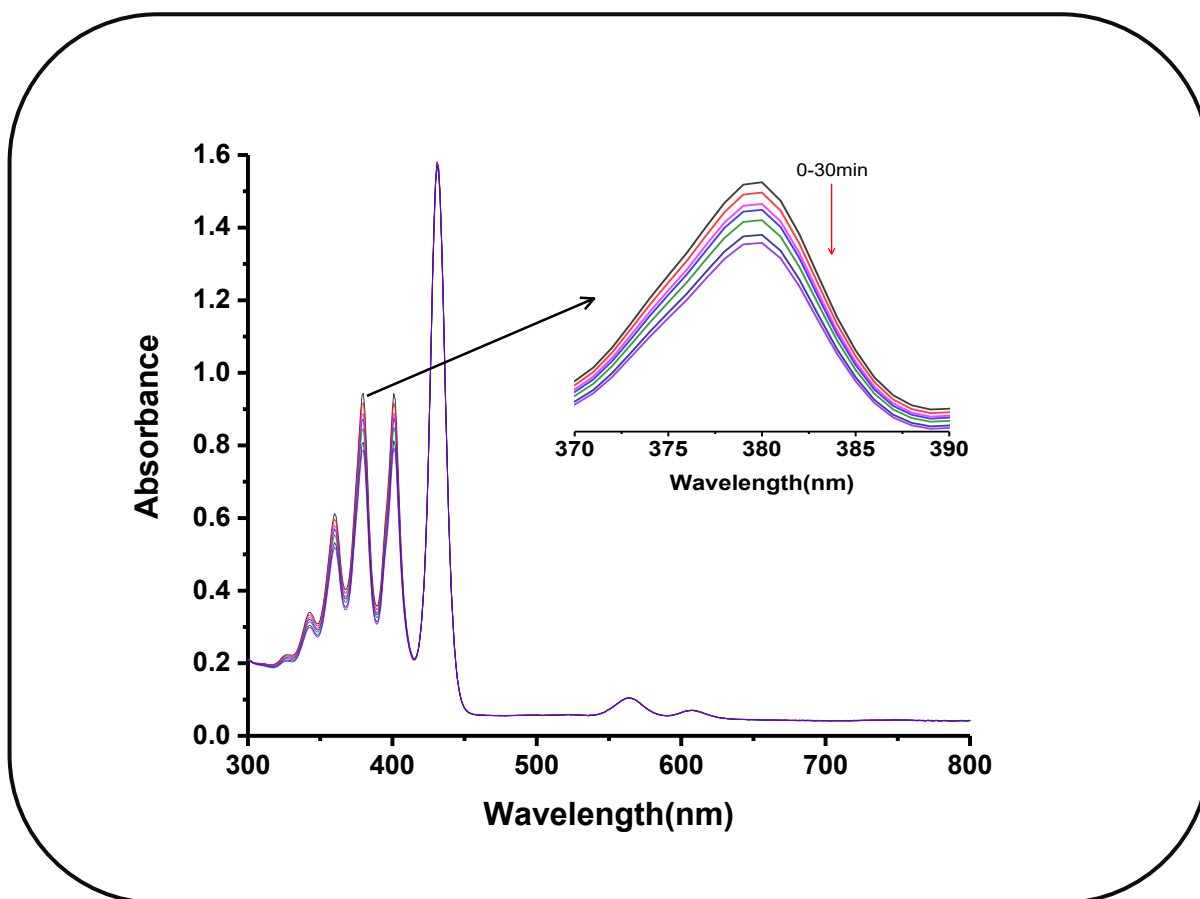


Figure 4.9: Typical degradation of DMA (1.14×10^{-4} M) in the presence of complex **2** (1.42×10^{-7} M).

4.5 Summary of chapter

Complexes **1-6** were synthesised and fully characterised using various techniques to determine structural composition of the porphyrins. The complexes with carboxylic groups were conjugated to nanomaterials that were functionalised with amino functionalised capping agents via amide bond. The conjugates with thienyl and pyridyl substituents were linked to OLA/OLM capped AgNPs via chemisorption onto the surface of the nanoparticles. The photophysical properties of asymmetrical porphyrin **3, 4, 5, 6** and symmetrical **1** and **2** were studied alone and

when conjugated to AgNPs. All the conjugates show an enhancement in the singlet oxygen quantum yield, which was found to be more pronounced in asymmetric porphyrins.

Chapter 5

Antimicrobial experiments

This chapter discusses the biological activity of AgNPs, bare porphyrin complexes and their conjugates for photoinactivation of *S. aureus*

5.1 PACT Studies of *S. aureus*

In this thesis, complexes **1-6** and their corresponding conjugates were employed for photoinactivation of *S. aureus* and the results are displayed in **Fig. 5.1-5.5**. There are two most widely used methods for quantitative determination of bacterial populations. These methods are the standard (viable, plate count) and spectrophotometric (turbidimetric) analysis [105]. In this thesis the spectrophotometric analysis was employed. A 595 nm light source was employed since wavelength in this region have been used for PACT using porphyrins [106, 107]. With real life applications in mind such as deeply seated infections, irradiation was done at the Q bands which is within the red region and has been reported to be effective in penetrating as deep as 3 mm as compared to 1.5 mm for blue region irradiation (Soret band) [108]. At first a concentration dependant study was carried out. **Fig. 5.1A** and **B** show typical concentration dependant studies done at 75 min irradiation. Complexes **1-3** and **4-6** were done at different concentration ranges. A concentration of 0.36 µg/mL was chosen for **4-6** since there was only a small change in viability with increasing concentration. A large concentration range was used for subsequent studies for **1-3**, for more effective PACT activity. Complexes **1-3** were done at a chosen concentration of 2.0 µg/mL since at larger concentrations the PACT activity was too high to see changes, **Fig. 5.1A**. 1% DMSO had no effect on bacteria, **Fig. 5.1-5.5**. PACT activity was found to increase with increasing time of irradiation.

For statistical analysis, the data obtained from the three independent triplicate experiments were analysed with a 3-way factorial ANOVA Anova (analysis of variance) to determine the statistical differences. TukeyHSD posthoc test was used to determine the mean differences *in vitro* photodynamic antimicrobial chemotherapy effect of the photosensitizers on *S. aureus*, p-value of <0.05 was considered statistically significant.

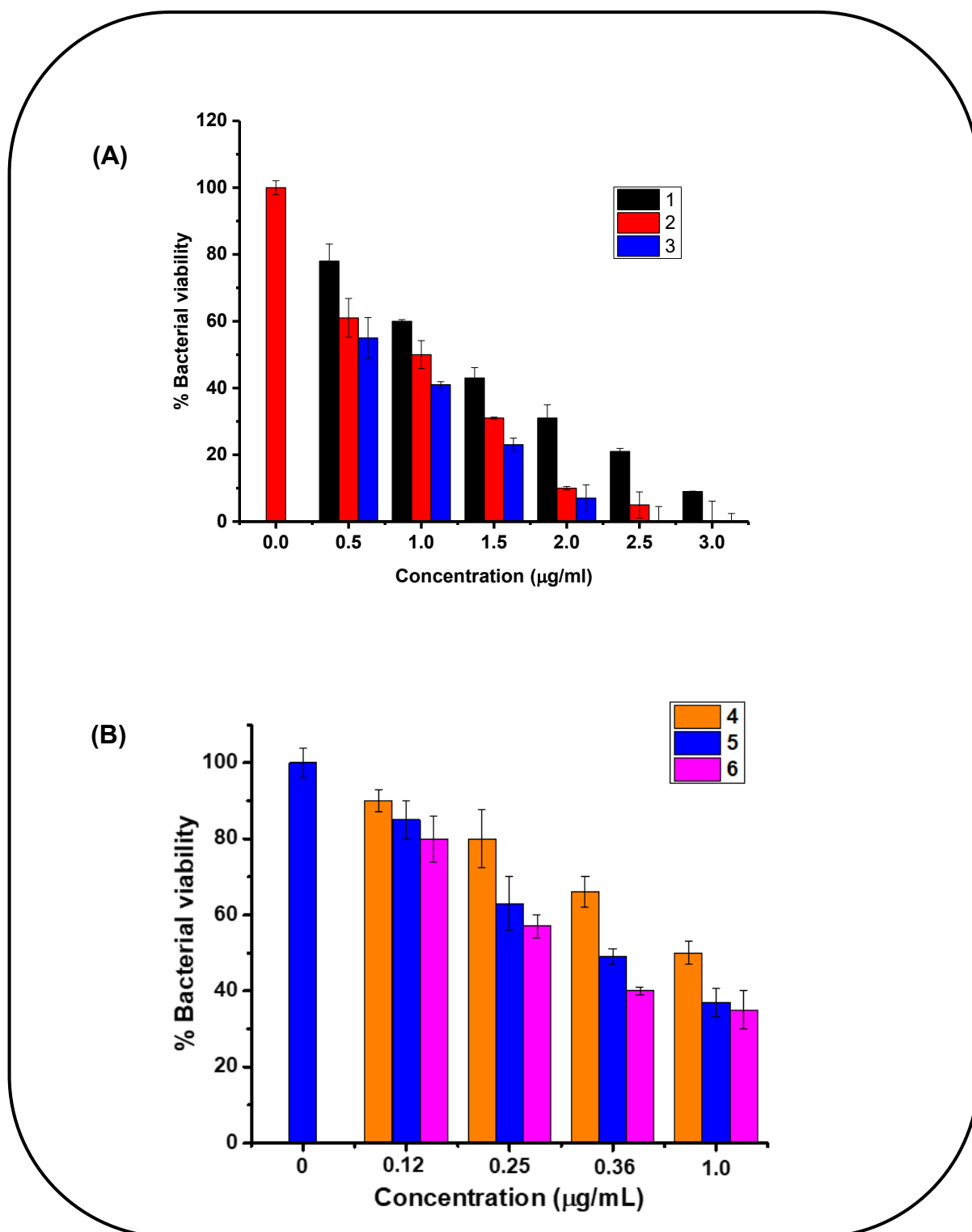


Figure 5.1: Concentration dependent study using complexes (A) 1-3 and (B) 4-6 as examples in 1% DMSO/PBS over 75 min irradiation against *S. aureus*.

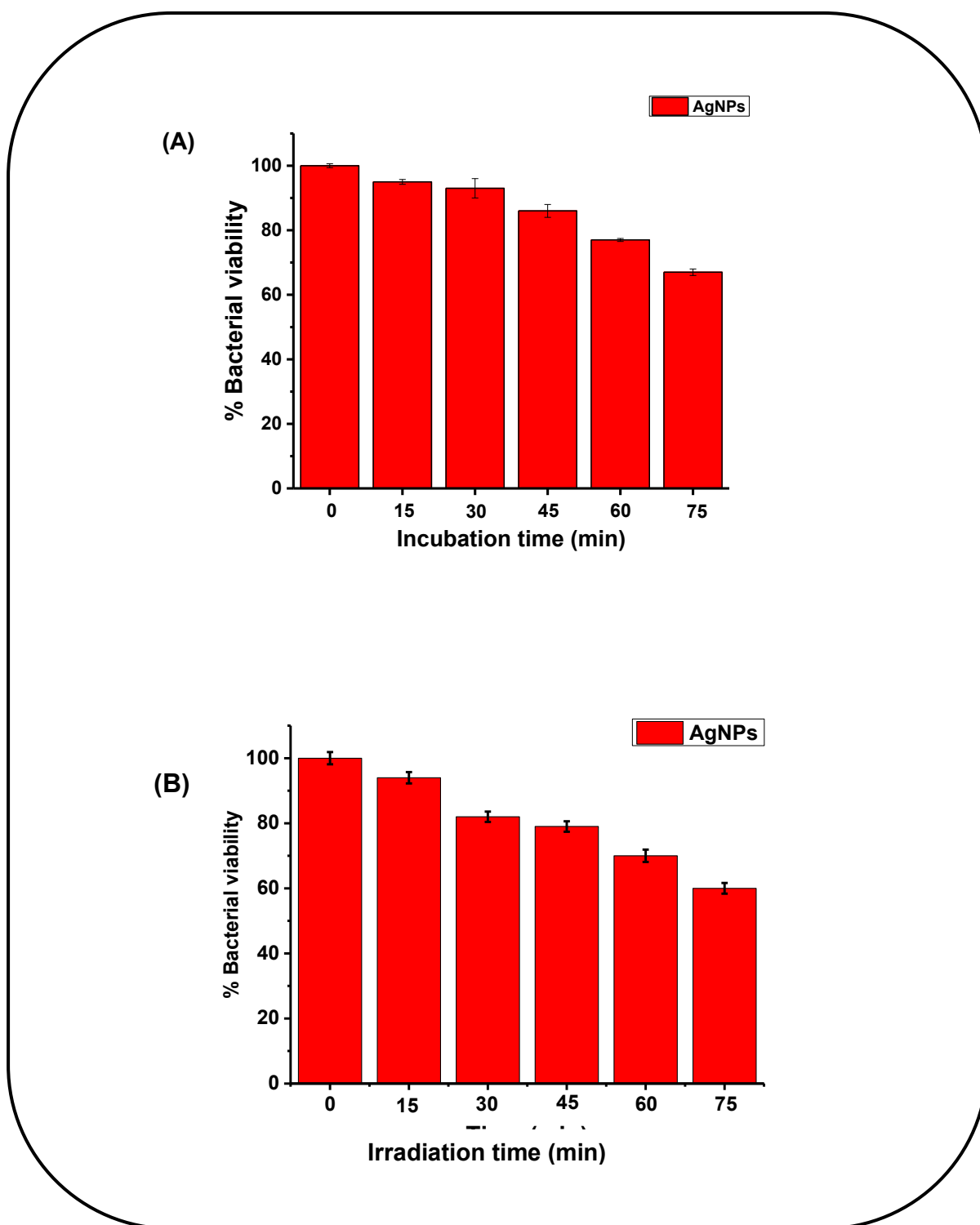


Figure 5.2: Bacterial viability due to (A) dark toxicity of AgNPs and (B) photodynamic effect of AgNPs at 0.36 $\mu\text{g/mL}$ against *S. aureus* in 1% DMSO/PBS.

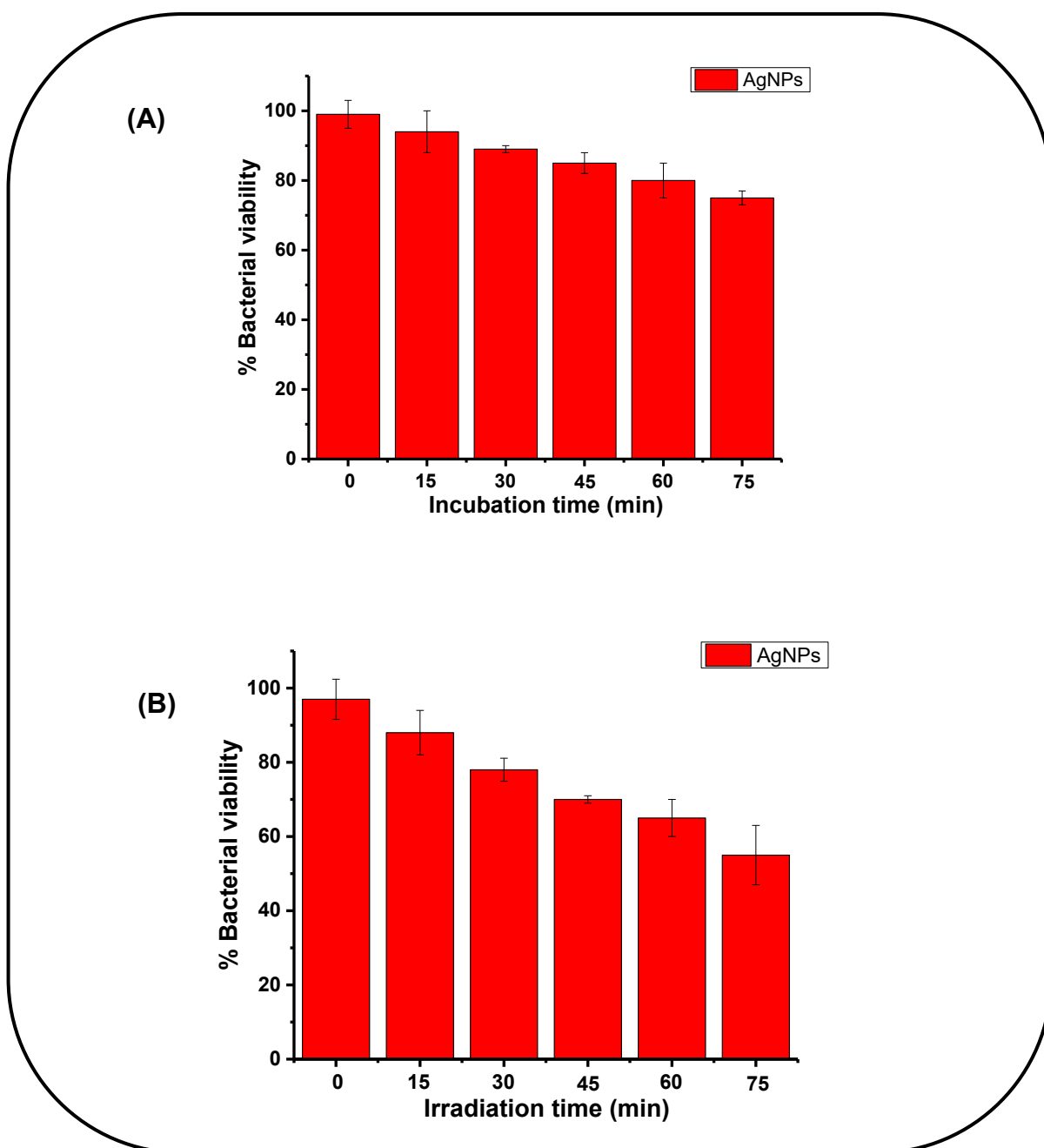


Figure 5.3: Bacterial viability due to **(A)** dark toxicity of AgNPs and **(B)** photodynamic effect of AgNPs at 2.0 $\mu\text{g/mL}$ against *S. aureus* in 1% DMSO/PBS.

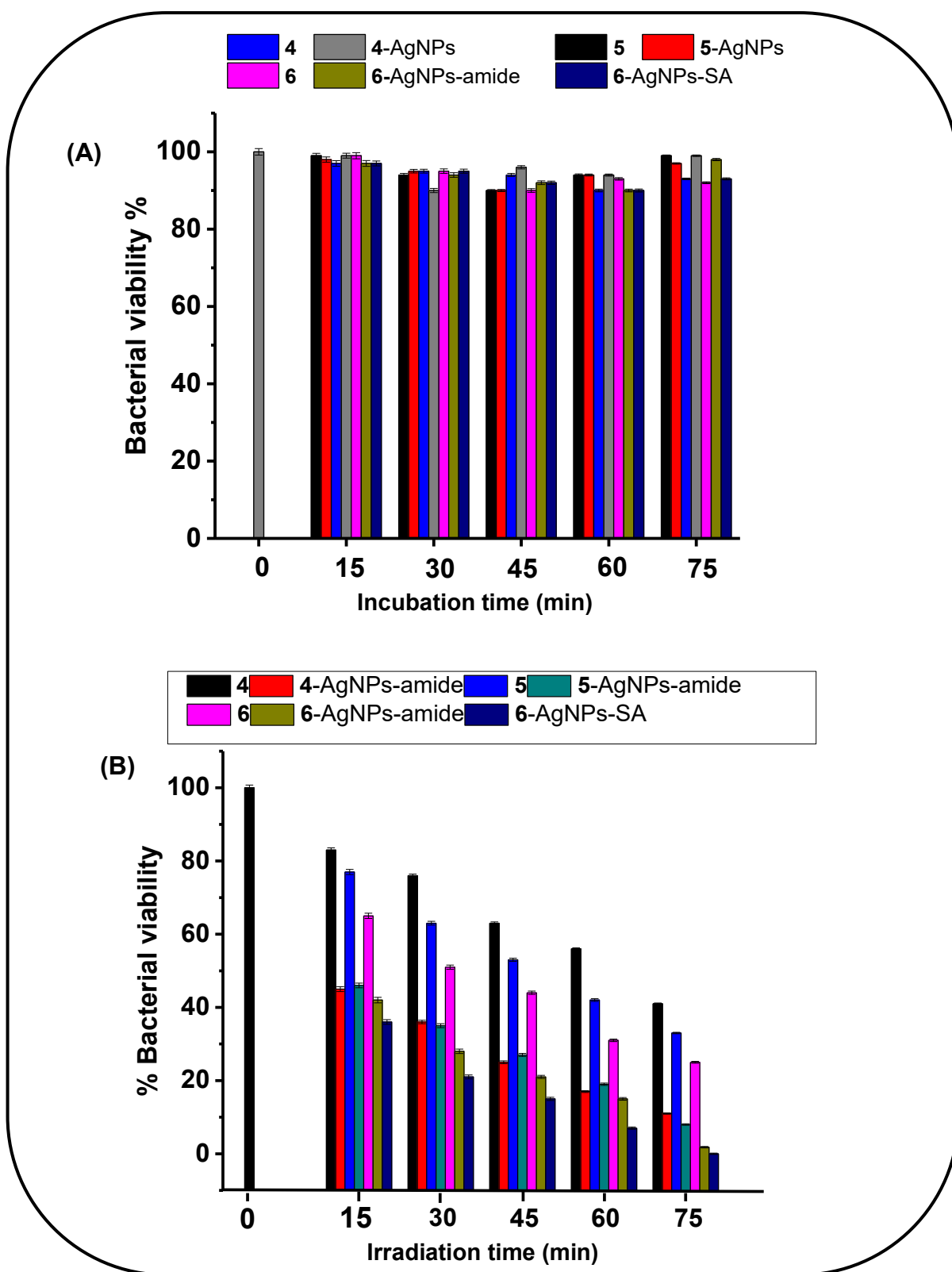


Figure 5.4: Bacterial viability due to (A) dark toxicity of 4-6 and their conjugates and (B) photodynamic activity of 4-6 and their conjugates against *S. aureus* in 1% DMSO/PBS. Concentration = 0.36 µg/mL.

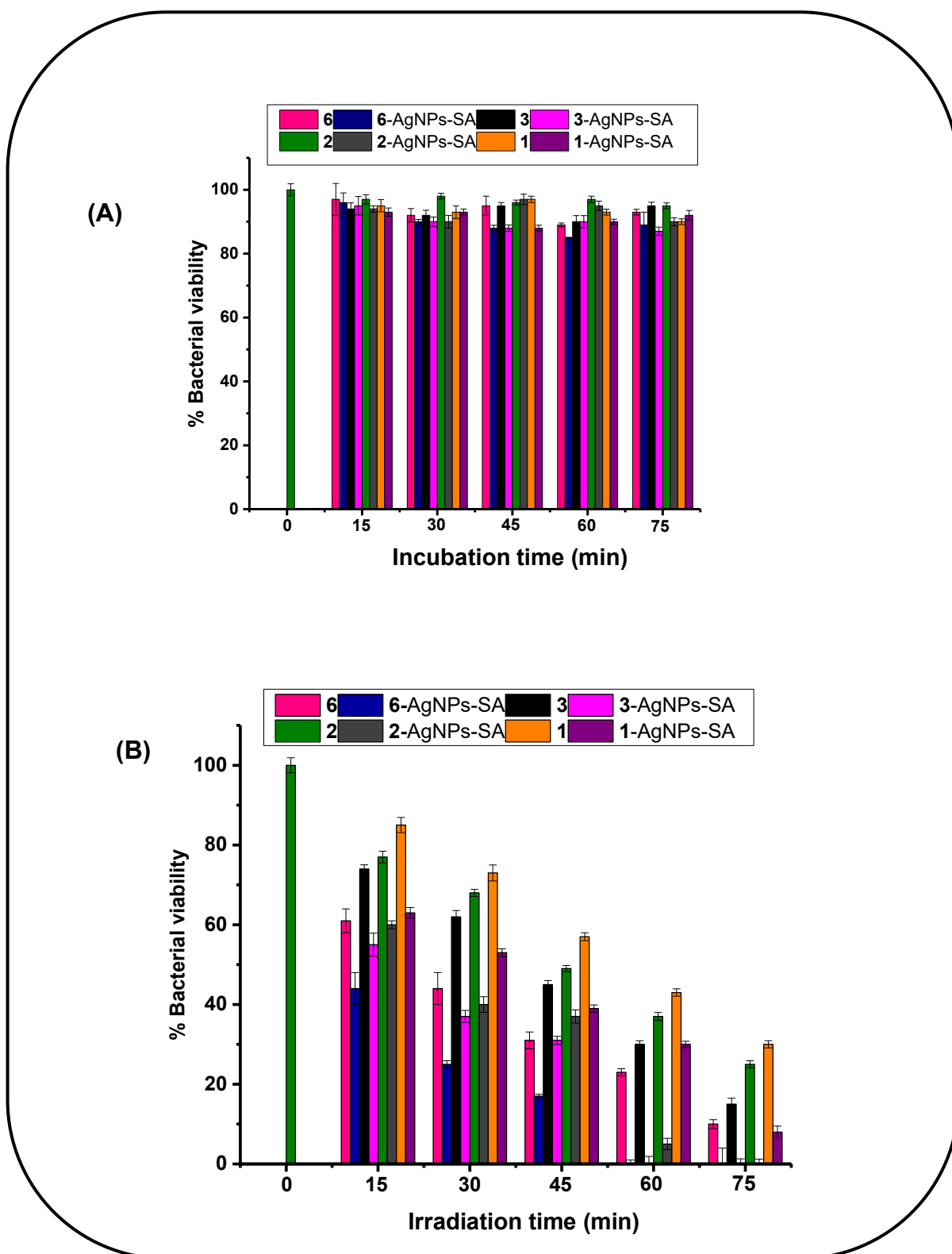


Figure 5.5: Bacterial viability due to (A) dark toxicity of 1-3 and 6 and their conjugates and (B) photodynamic activity of 1-3 and 6 and their conjugates against *S. aureus* in 1% DMSO/PBS. Concentration = 2.0 $\mu\text{g/mL}$.

The biocidal property of AgNPs is mainly due to Ag ions released from AgNPs. Silver ions are firmly adsorbed on the cell membrane leading to protein coagulation [108], which may be enhanced by light hence the decrease in bacterial viability with incubation and irradiation time, **Fig. 5.2B** and **5.3B**. The dark toxicity effect and PACT activities were evaluated for 75 min at 15 min intervals (**Fig. 5.4A** and **Fig. 5.5A**) whereby at all incubation times, all complexes and their conjugates had the bacterial viability were all above 90% in the dark, hence showing no dark toxicity. There were significant decrease in survival rate in the presence of light for the conjugates as compared to porphyrins alone, **Fig. 5.4B** and **Fig. 5.5B**. This may be due to the synergy that exists between the porphyrins and nanoparticles. Conjugate **6**-AgNPs-SA showed more activity than **6**-AgNPs-amide at the same concentration, this is due to the enhanced singlet oxygen generating ability of the former. This shows the advantage of self-assembly over amide bond formation. Self-assembly also has advantage in that it eliminates the extra steps involved in chemical conjugations [109]. Log reduction values in **Table 5.1A** and **B** were used to quantify the results. It is important that studied photosensitizers cross the border of 3-log reduction, which is recommended by FDA (Food and Drug Administration) regulations [110-112]. The degree to which the photosensitizers were able to successfully kill pathogens was compared with the control that had no photosensitization. Porphyrins alone had log reductions with ($p > 0.05$) showing statistical insignificance. The conjugates gave better log reduction values that were found to be statistically significant ($p < 0.05$). Thus, the nanoparticles enhance the photoinactivation process due to improved singlet oxygen quantum yield. Conjugate **6**-AgNPs-SA gave the largest log reduction of 8.91 log unit at 2.0 $\mu\text{g/mL}$ and 6.46 log unit at 0.36 $\mu\text{g/mL}$, the second-best performing conjugate was **3**-AgNPs-SA with log reduction of 8.22 log unit, this shows the importance of self-assembly over amide linkage. Effect of asymmetry was also evident as the asymmetric thienyl derivatives (**3**, **6**) and the corresponding conjugates gave better activity over their corresponding symmetric derivatives, as seen in **Fig. 5.5**. **Fig 5.6** was used to justify the photodynamic effect observed using conjugate **3**-AgNPs-SA as an example over 75 min illumination. By the 75th minute, the colony count was zero, further supporting the results observed in **Fig. 5.5B** that 2-thienyl substituents were very effective because these groups have been found to contain antioxidants and to exhibit antifungal,

antibacterial and anticancer activity [113-115], hence they gave better photodynamic effect as compared to phenyl derived groups (**1**, **4-5**).

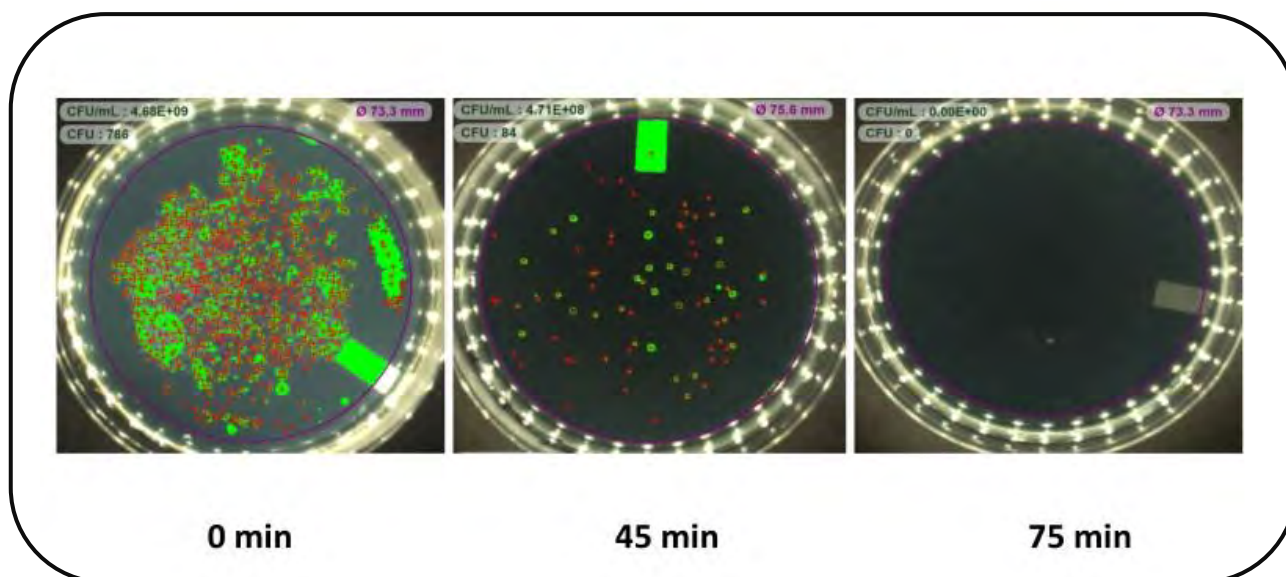


Figure 5.6: Micrograph showing effect photodynamic activity using complex **3**-AgNPs-SA as an example at varying irradiation times.

Table 5.1A: Log reduction values for photodynamic effect on *S. aureus* at 0.36 $\mu\text{g/mL}$ at 75 min irradiation.

Complex/Conjugates	Log reduction
4	0.41 ($p>0.05$)
5	0.32 ($p>0.05$)
6	0.57 ($p>0.05$)
4 - AgNPs-amide	1.72 ($p=0.02$)
5 - AgNPs-amide	1.31 ($p=0.03$)
6 - AgNPs-amide	2.45 ($p=0.002$)
6 - AgNPs-SA	6.46 ($p=0.001$)

Table 5.1B: Log reduction values for photodynamic effect on *S. aureus* at 2.0 µg/mL at 75 min irradiation.

Complex/Conjugates	Log reduction
1	0.35 ($p>0.05$)
2	0.49 ($p>0.05$)
3	0.53 ($p>0.05$)
6	0.64 ($p>0.05$)
1-AgNPs-SA	4.21 ($p=0.002$)
2-AgNPs-SA	8.05 ($p=0.001$)
3-AgNPs-SA	8.22 ($p=0.001$)
6- AgNPs-SA	8.91 ($p=0.001$)

5.2 Synergy studies

To further explore the synergetic effect of porphyrin-AgNPs for PACT, combination index (CI) was employed as a parameter via the Chou-Talalay method [116] using **1-AgNPs-SA**, **2-AgNPs-SA** and **3-AgNPs-SA** as examples. The CI values reflect the interaction brought about by dual functional mechanism of porphyrin-AgNPs whereby less values indicate more efficient synergy ($0.3 < CI < 0.7$) [117] as shown in **Fig. 5.7**. The point of effect was monitored at 15 min intervals over a period of 75 min. The results indicate a strong synergistic effect of PACT with more drug-drug interaction over increase in illumination time (point of effect), this further corresponds to the decrease in % bacterial viability by porphyrin-AgNPs as observed in **Fig. 5.5B** over a period of 75 min with **3-AgNPs-SA** showing pronounced dual interaction as compared to symmetric conjugates of **1-AgNPs-SA** and **2-AgNPs-SA**.

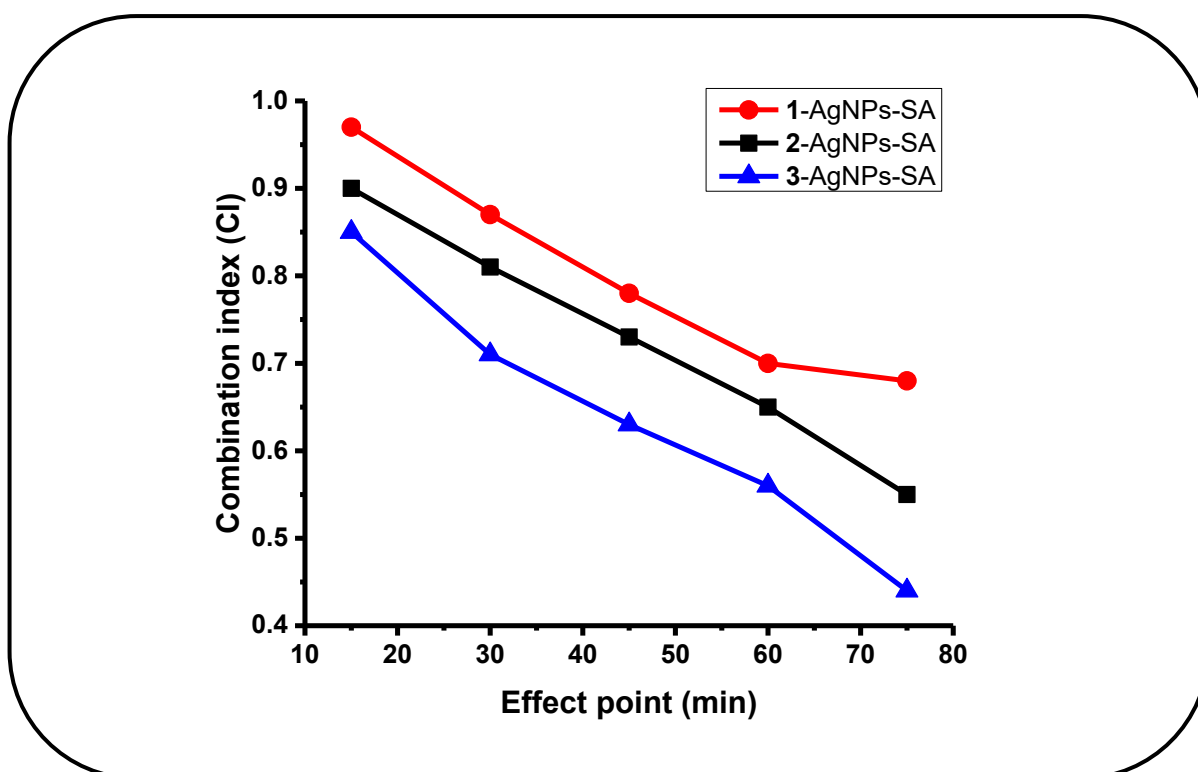


Figure 5.7. Synergy studies by combination index of 1-AgNPs-SA, 2-AgNPs-SA and 3-AgNPs-SA.

5.3 Summary to this chapter

Complex 6-AgNPs-SA gave better photoinactivation activity as compared to the rest. This is primarily due to thienyl substituents on the *meso*-position of the porphyrins along with antimicrobial activity of AgNPs along with asymmetry, this further highlights the effect of thienyl rings over phenyl ring structures. The susceptibility of *S. aureus* is more pronounced for self-assembly interaction as compared to amide linkage with more notable log reductions in the former at the same concentration.

Chapter 6

Conclusion and recommendations

This chapter gives conclusive remarks and suggestions regarding the work presented in this thesis

6.1 General conclusions

This thesis reports for the first time on the effect of thienyl derived porphyrins in comparison to some phenyl derivatives through covalent or non-covalent linkage to AgNPs for PACT. Complex **6** was conjugated to spherical AgNPs via SA and covalent linkage. The singlet oxygen quantum yields of the conjugates were higher when compared to the bare complexes, with complex **6**-AgNPs-SA the highest. The porphyrins and conjugates were used in PACT studies and **6**-AgNPs-SA showed more antibacterial activity against *S. aureus* as the log reduction unit obtained was 6.46 log unit at a lower concentration (0.36 µg/mL) and 8.91 log at a concentration of 2.0 µg/mL (which indicates 99.99% of the bacteria have been killed). The log reductions for *S. aureus* were 8.91 and 6.46 log units for **6**-AgNPs-SA at 2.0 µg/mL and 0.36 µg/mL respectively, and 8.22 log units for **3**-AgNPs-SA, 8.05 log units for **2**-AgNPs-SA and 4.21 log units for **1**-AgNPs-SA all at 2.0 µg/mL, which were all above the standard log of 3, and this is an indication that 99.99% of the bacteria have been killed. The conjugates by SA were shown to generate efficient singlet oxygen and PACT activity as compared to those linked via amide bond. This again cements the importance of SA over amide bond. Of all complexes reported in this thesis, the most effective were thienyl substituted porphyrins. The properties of thienyl groups were evident as efficient generation of singlet oxygen was observed in asymmetric thienyl substituted porphyrins. Effect of asymmetry proved beneficial since it was observed asymmetric porphyrins gave enhanced PACT activity over their symmetric analogues throughout. Antimicrobial studies revealed an additive effect of photodynamic activity of the thienyl substituted porphyrins and cytotoxicity of AgNPs in the conjugate as it showed high antimicrobial activity towards *S. aureus*. All conjugates are potential antimicrobial agents with thienyl derivatives more effective under illumination.

6.2 Recommendations

Towards the end of 2019, a drug resistant bacterium that broke out at Tembisa Hospital, in South Africa claimed the lives of 10 babies in two months. There was a *Carbapenem-Resistant-Enterobacterales* (CRE) breakout (November 1 to December 31 2019) at the hospital's neonatal unit, which affected 17 babies. The number of

deaths caused by multidrug resistant bacteria is alarming. Consequently, it has been suggested that rising global temperatures leads to antibiotic drug resistance becoming more prevalent amongst vulnerable communities. This makes the search for alternative drugs more prominent. This thesis has provided insight into possible laser-based treatments, which have little or no chance of developing resistance to bacteria. Not only can this treatment target skin infections but it also has the possibility of tackling deeply seated infections because of absorption in the far-red region of the therapeutic window. The results reported in this thesis support the idea that bacteria are more prone to porphyrin-AgNPs than conventional antibiotics.

References

1. J. O'Neil. Tackling drug-resistant infections globally: Final report and recommendations, London, United Kingdom: 2016, p. 1-84.
2. WHO: Antimicrobial Resistance? In: Global Report on surveillance. Edited by WHO. Geneva, Switzerland, 2014.
3. Y.Y. Liu, Y. Wang, T.R. Walsh, L.X. Yi, R. Zhang, J. Spencer, Y. Doi, G. Tian, B. Dong, X. Huang, *Lancet Infect. Dis.* 16 (2016) 161-168.
4. B.B. Xavier, C. Lammens, R. Ruhai, S. Kumar-Singh, P. Butaye, H. Goossens, S. Malhotra-Kumar. *Euro Surveill.* 21 (2016) 8-13.
5. O. Raab, *Biol.* 39 (1900) 524-546.
6. T. Maisch, *Laser. Med. Sci.* 22 (2007) 83-91.
7. L. Ryskova, V. Buchta, R. Slezak, *Cent. Eur. J. Biol.* 5 (2010) 400-406.
8. H. Von Tappeiner, A. Jodblauer, *Deutsch. Arch. Klin. Med.* 80 (1904) 427-487.
9. M. Wainwright, *J. Antimicrob. Chemother.* 42 (1998) 13-28.
10. J. Chen, N. Chen, Y. Zhang, S. Zhou, J. Wang, N. Chen, J. Huang, F. Yan, M. Huang. *J. Porphyr. Pthalocya.* 15 (2011) 293-299.
11. B. N. Green, C. D. Johnson, J. T. Egan, M. Rosenthal, E.A. Griffith, M. W. Evans, *J. Chiropr. Med.* 11 (2012) 64-76.
12. <https://www.redbubble.com/people/stanleyillust/works/21341791-gram-positive-vs-gram-negative-bacteria> accessed: 16/12/2019.
13. A.R. Battersby, C.J.R. Fookes, G.W.J. Matcham, E. McDonald, *Nature* 285 (1980) 17-21.
14. B. Krautler, *Chimia.* 41 (1987) 277-292.
15. J.E. Falk, *Porphyrins and Metalloporphyrins*, Elsevier, Amsterdam, 1964.
16. P. Rothmund, *J. Am. Chem. Soc.* 57 (1935) 2010-2011.
17. P. Rothmund, *J. Am. Chem. Soc.* 58 (1936) 625-627.
18. P.S. Traylor, D. Dolphin, T.G. Traylor, *J. Chem. Soc. Chem. Comm.* 5 (1984) 279-280.
19. A.D. Adler, W. Shergali, F.R.I. Longo, *J. Am. Chem. Soc.* 86 (1964) 3145-3149.
20. A.D. Adler, F.R. Longo, J.D. Finarell, J. Goldmach, J. Assour, L. Korsakof, *J. Org. Chem.* 32 (1967) 476.
21. J.A.S. Cavaleiro, M. Defatima, P.N. Condesso, M.M. Olmstead, D.E. Oram, K.M. Snow, K.M. Smith, *J. Org. Chem.* 53 (1988) 5847-5849.

22. M.C. Berenbaum, S.L. Akande, R. Bonnett, H. Kaur, S. Ioannou, R.D. White, U.J. Winfield, *Br. J. Cancer* 54 (1986) 717-725.
23. J.S. Lindsey, I.C. Schreiman, H. C. Hsu, P. C. Kearney, A. M. Margueretta, *J. Org. Chem.* 52 (1987) 827-836.
24. J.S. Lindsey, *Acc. Chem. Res.* 43 (2010) 300-311.
25. G.R. Geier, J.S. Lindsey, *J. Chem. Soc. Perkin Trans. 2.* 5 (2001) 677-686.
26. J. Mack, M. Stillman, *Coord. Chem. Rev.* 993 (2001) 219-221.
27. M. Gouterman, *In the Porphyrins*, (Ed. D. Dolphin), Part A. Physical Chemistry, Academic Press, New York. 1978.
28. A. J. McHugh, M. Gouterman, C. Weiss, *Theoret. Chim. Acta* 24 (1972) 346-370.
29. A. M. Schaffer, M. Gouterman, E. R. Davidson, *Theoret. Chim. Acta* 30 (1973) 9-30.
30. M. J. Stillman, T. Nyokong, *In Phthalocyanines: Properties and Applications*, Eds. C. C. Leznoff, A. B. P. Lever, VCH, New York. 1989.
31. K. M. Smith, *In Porphyrins and Metalloporphyrins*, Elsevier, Amsterdam, 1975.
32. J.L. Soret, *Compt. Rend.* 97 (1883) 1269-1273.
33. R. Bonnett, *Chemical Aspects of Photodynamic Therapy*, Gordon and Breach Science Publishers, Amsterdam, 2000.
34. P. J. Spellane, M. Gouterman, A. Antipas, S. Kim, Y. C. Liu, *Inorg. Chem.* 19 (1980) 386-391.
35. M. Gouterman, *J. Mol. Spectrosc.* 6 (1961) 138-163.
36. Y. Nitzan, H. Ashkenazi, *Curr. Microbiol.* 42 (2001) 408-414.
37. M. Merchat, G. Bertolini, P. Giacomini, A. Villanueva, G. Jori, *J. Photochem. Photobiol. B.* 32 (1996) 153-157.
38. M. R. Hamblin, T. Hasan, *Photochem. Photobiol. Sci.* 43 (2004) 436-450.
39. W. N. Burda, K. B. Fields, J. B. Gill, R. Burt, M. Shepherd, X. P. Zhang, L. N. Shaw, *Eur. J. Clin. Microbiol. Infect. Dis.* 31 (2012) 327-335.
40. S. Meng, Z. Xu, G. Hong, L. Zhao, Z. Zhao, J. Guo, *Eur. J. Med. Chem.* 4 (2015) 35-92.
41. M. Managa, E. Antunes, T. Nyokong, *Polyhedron* 76 (2014) 94-101.
42. M.C. Gomes, S.M. Woranovicz-Barreira, M.A.F. Faustino, R. Fernandes, M. G. P. M. S. Neves, A.C. Tome, N.C.M. Gomes, A. Almeida, J.A.S. Cavaleiro, A. Cunha, J.P.C. Tome, *Photochem. Photobiol. Sci.* 10 (2011) 1735-1743.

43. R. Soman, D. Raghav, S. Sujatha, K. Rathinasamy, C. Arunkumar, RSC Adv. 5 (2015) 61103-61117.
44. S. Banfi, E. Caruso, L. Buccarfuni, V. Battini, S. Zazzaron, P. Barbieri, V. Orlandi, J. Photochem. Photobiol. B. 85 (2006) 28-38.
45. A.S. Oliveira, D. Licsandru, R. Boscencu, R. Socoteanu, V. Nacea, L. F. V. Ferreira, Int. J. Photoenergy. 41 (2009) 10. <http://dx.doi.org/10.1155/2009/413915>
46. R. Bonnett, Metal complexes for photodynamic therapy, in Comprehensive coordination chemistry II: from biology to nanotechnology, J.A. McCleverty, T.J. Meyer, eds., Elsevier, Amsterdam, 2004.
47. B.C. Simone, G. Mazzone, N. Russo, E. Sicilia, M. Toscano, Molecules. 22, (2017), 1093. <https://doi.org/10.3390/molecules22071093>.
48. L. Zhai, K.W. Yang, Dyes Pigm. 120 (2015) 228-238.
49. Z. Chen, S. Zhou, J. Chen, L. Li, P. Hu, S. Chen, M. Huang, J. Lumin. 152 (2014) 103-107.
50. M.Q. Mesquita, C.J. Dias, P. M. S. Neves, G. Maria, A. Almeida, F. Faustino, M. Amparo, Molecules 23 (2018) 2424-2470.
51. A. Ghosh, S.M. Mobin, R. Frohlich, R.J. Butcher, D.K. Maity, M. Ravikanth, Inorg. Chem. 49 (2010) 8287-8297.
52. S. Muratsugu, A. Yamaguchi, G-I. Yokota, T. Maeno, M. Tada. Chem. Commun. 54 (2018) 4842-4845.
53. Y. Zhou, F. Liu, H. Wu, B. Qu, L. Duan, Asian J. Chem. 27 (2015) 616-620.
54. P.R. Kumar, N.J. Britto, A. Kathiravan, A. Neels, M. Jaccob, E.M. Mothi, New J. Chem. 43 (2019) 1569-1580.
55. R. L. Milot, G.F. Moore, R.H. Crabtree, G.W. Brudvig, C.A. Schmuttenmaer, J. Phys. Chem. C. 117 (2013) 21662-21670.
56. R. Chouikrat, A. Champion, R. Vanderesse, C. Frochot, A. Moussaron, J. Porphyr Phthalocya. 19 (2015) 596-600.
57. R. Ambre, K-B. Chen, C-F. Yao, L. Luo, E. Wei-Guang Diao, C-H. Hung., J. Phys. Chem. C. 116 (2012) 11907-11916.
58. H. Sakurai, M. Haruta, Appl. Catal. A. 127 (1995) 93-105.
59. M.C. Daniel, D. Astruc, Chem. Rev. 104 (2004) 293-346.
60. M. Burghard, K. Balasubramanian, Small 1 (2005) 180-192.
61. A.D. Yoffe, Adv. Phys. 50 (2001) 208.

62. H. Mader, X. Li, S. Saleh, M. Link, P. Kele, O.S. Wolfbeis, *Ann. N.Y. Acad. Sci.* 1130 (2008) 218-223.
63. J.L. Vivero-Escoto, R.C. Huxford-Phillips, W. Lin, *Chem. Soc. Rev.* 41 (2012) 2673-2685.
64. S.C. Feifel, F. Lisdat, *J. Nanobiotechnol.* 9 (2011) 59-70.
65. S. Gurunathan, J.H. Park, J.W. Han, J.H Kim, *Int. J. Nanomed.* 10 (2015) 4203-4222.
66. K.M. Abou El-Nour, A. Eftaiha, A. Al-Warthan, R.A. Ammar, *Arab. J. Chem.* 3 (2010) 135-140.
67. A. Tao, P. Sinsermsuksakul, P. Yang, *Angew. Chem. Int. Ed.* 45 (2006) 4597-4601.
68. B. Wiley, Y. Sun, B. Mayers, Y. Xia, *Chemistry* 11 (2005) 454-463.
69. V. Deepak, P.S. Umamaheshwaran, K. Guhan, R.A. Nanthini, B. Krithiga, N.M. Jaithoon, S. Gurunathan, *S. Colloid Surface B.* 86 (2011) 353-358.
70. A. Amulyavichus, A. Daugvila, R. Davidonis, C. Sipavichus, *Fiz. Met. Metalloved.* 85 (1998) 111-117.
71. K. Mallick, M.J. Witcomb, M.S. Scurrrell, *J. Mater. Sci.* 39 (2004) 4459-4463.
72. M. De, S. Rana, H. Akpınar, O.R. Miranda, R.R. Arvizo, U.H. Bunz, V.M. Rotello, *Nat. Chem.* 1 (2009) 461-46.
73. Y. Lu, Y. Yin, B.T. Mayers, Y. Xia, *Nano Lett.* 2 (2002) 183-186.
74. E. Boisselier, D. Astruc, *Chem. Soc. Rev.* 38 (2009) 1759-1782.
75. S. Çınar, G. Gündüz1, B. Mavis, Ü. Çolak, *J. Nanosci Nanotechnol.* 11 (2011) 3669-3679.
76. A. Taglietti, Y. A. D. Fernandez, E. Amato, L. Cucca, G. Dacarro, P. Grisoli, V. Necchi, P. Pallavicini, L. Pasotti, M. Patrini, *Langmuir.* 28 (2012) 8140-8148.
77. D.F. Moyano, V.M. Rotello, *Langmuir* 27 (2011) 1037-1038.
78. R. Mout, D.F. Moyano, S. Rana, V.M. Rotello, *Chem. Soc. Rev.* 41 (2012) 2539-2544.
79. A.-H. Lu, E.L. Salabas, F. Schuth, *Angew. Chem. Int. Ed.* 46 (2007) 122-124.
80. J. Chen, L. Yang, J. Chen, W. Liu, D. Zhang, P. Xu, T. Dai, L. Shang, Y. Yang, S. Tang, Y. Zhang, H. Lin, Z. Chen, M. Huang, *Chem. Eng. J.* 374 (2019) 1373-1381.

81. R. L. Brookfield, H. Ellul, A. Harriman, G. Porter, *Chem. Soc. Faraday Trans.* 82 (1986) 219-233.
82. S. Dhimi, A.J. De Mello, G. Rumbles, S.M. Bishop, D. Phillips, A. Beeby, J. *Photochem. Photobiol.* 61 (1995) 341-346.
83. S.E. Maree, D. Phillips, T. Nyokong, *J. Porphyr. Phthalocya.* 6 (2002) 17-25.
84. J.C. Swarts, M.D Maree, *J. Porphyr. Phthalocya.* 11 (2007) 613-617.
85. A.T. Rhys Williams, S.A. Winfield, J.N. Miller, *Analyst* 108 (1983) 1067-1071.
86. N. Gandra, A.T. Frank, O. Le Gendre, N. Sawwan, D. Aebisher, J.F. Liebman, K.N. Houk, A. Greer, R. Gao, *Tetrahedron* 62 (2006) 1071-1077.
87. H. Hiramatsu, F.E. Osterloh. *Chem. Mater.* 16 (2004) 2509-2511.
88. K. Sanusi, J.M. Stone and T. Nyokong. *New J. Chem.* 39 (2015) 1665-1677.
89. M. Onaka, T. Shinoda, Y. Izumi and E. Nolen., *Chem. Lett.* 22 (1993), 117-120.
90. M.W. Eason, *Syntheses of Trimethylamine- and Phosphonatesubstituted Carboranylporphyrins for Application in Boron Neutron Cancer Therapy.* Louisiana state university, Baton Rouge, 2008.
91. E.A. Amuhaya, *Synthesis, biological and photophysical studies of novel compounds for cancer therapy.* PhD thesis, Louisiana state university, Baton Rouge, 2011.
92. S.-J. Wang, Y.-L. Peng, C.-G. Zhang, Y.-B. Li, C. Liu. *Bull. Korean Chem. Soc.* 36 (2015) 2693–2702.
93. A. Ghosh, S.M. Mobin, R. Frohlich, R.J. Butcher, D.K. Maity, M. Ravikanth, *Inorg. Chem.* 49 (2010) 8287-8297.
94. I. Gupta, C.-H. Hung, M. Ravikanth, *Eur. J. Org. Chem.* 22 (2003) 4392-4400.
95. K.J. Reimer, M.M. Reimer, M.J. Stillman, *Can. J. Chem.* 59 (1981) 1388-1394.
96. M. Tsuji, S. Gomi, Y. Maeda, M. Matsunaga, S. Hikino, K. Uto, T. Tsuji, H. Kawazumi, *Langmuir* 28 (2012) 8845-8861.
97. L. Li, J.-F. Zhao, N. Won, H. Jin, S. Kim, J.-Y. Chen, *Nanoscale Research Lett.* 7 (2012) 386-394.
98. I. Ostolska, M. Wisniewska, *Colloid Polym. Sci.* 292 (2014) 2453-2464.
99. M.H Majles Ara, Z. Dehghani, R. Sahraei, A. Daneshfar, Z. Javadi, F. Divsar, J. *Quant. Spectrosc. Radiat. Transfer* 113 (2012) 366-372.
100. M.A. Majeed Khan, S. Kumar, M. Ahamed Salman, A. Alrokayan, M.S. Alsalhi, M. Alhoshan, A.S. Aldwayyan. *Appl. Surf. Sci.* 257 (2011) 10607-10612.

-
101. M. Morisue, I. Ueno, T. Nakanishi, T. Matsui, S. Sasaki, M. Shimizu, J. Matsui, Y. Hasegawa. *RSC Adv.* 7 (2017) 22679-22683.
102. B.C. Smith, *Infrared Spectra Interpretation: A System Approach*, CRC Press, New York, (1998).
103. S. Fery-Forgues, D. Lavabre. *J. Chem. Educ.* 76 (1999) 1260-1264.
104. Y. Shimizu, T. Azumi. *J. Phys. Chem.* 86 (1982) 22-26.
105. A.L. Koch. *Anal. Biochem.* 38 (1970) 252-259.
106. M.M. Gois, C. Kurachi, E.J.B. Santana, E.G.O. Mima, D.M.P. Spolidorio. *Lasers Med. Sci.* 25 (2010) 391-395.
107. B.M. Amos-Tautua, S.P. Songca, O.S. Oluwafemi. *Molecules* 24, 2456 (2019); [doi:10.3390/molecules24132456](https://doi.org/10.3390/molecules24132456).
108. W.K. Jung, H.C. Koo, K.W. Kim, S. Shin, S.H. Kim, Y.H. Park. *Appl. Environ. Microbiol.* 74 (2008) 2171-2178.
109. W. Zhuang, Y. Wang, P. Cui, L. Xing, J. Lee, D. Kim, H. Jiang, Y. Oh. *J. Control Release* 294 (2019) 311-326.
110. L. Sobotta, P. Skupin-Mrugalska, J. Piskorz, J. Mielcarek. *Dyes Pigm.* 163 (2019) 337-355.
111. E. Alves, M.A. Faustino, M.G. Neves, A. Cunha, J. Tome, A. Almeida. *Future Med. Chem.* 6 (2014) 141-164.
112. A. Spaeth, A. Graeler, T. Maisch, K. Plaetzer. *Eur. J. Med. Chem.* 159 (2017) 423-440.
113. M. Ashok, B.S. Holla, N.S. Kumari. *Eur. J. Med. Chem.* 42 (2007) 380-385.
114. L. Lan, W. Qin, X. Zhan, Z. Liu, Z. Mao. *Med. Chem.* 14 (2014) 994-1002.
115. S.S. El-Nakkady, S.E. Abbas, H.M. Roaiah, I.H. Ali. *Global J. Pharm.* 6 (2012) 166-177.
116. Y. Zhu, C. Xu, N. Zhang, X. Ding, B. Yu, F.-J. Xu, *Adv. Funct. Mater.* 28 (2018) 1706709.

117. F. Xiao, B. Ciao, C. Wang, X. Guo, M. Li, D. Xing, X. Hu, ACS Nano. 13 (2019) 1511-1525.

Appendix

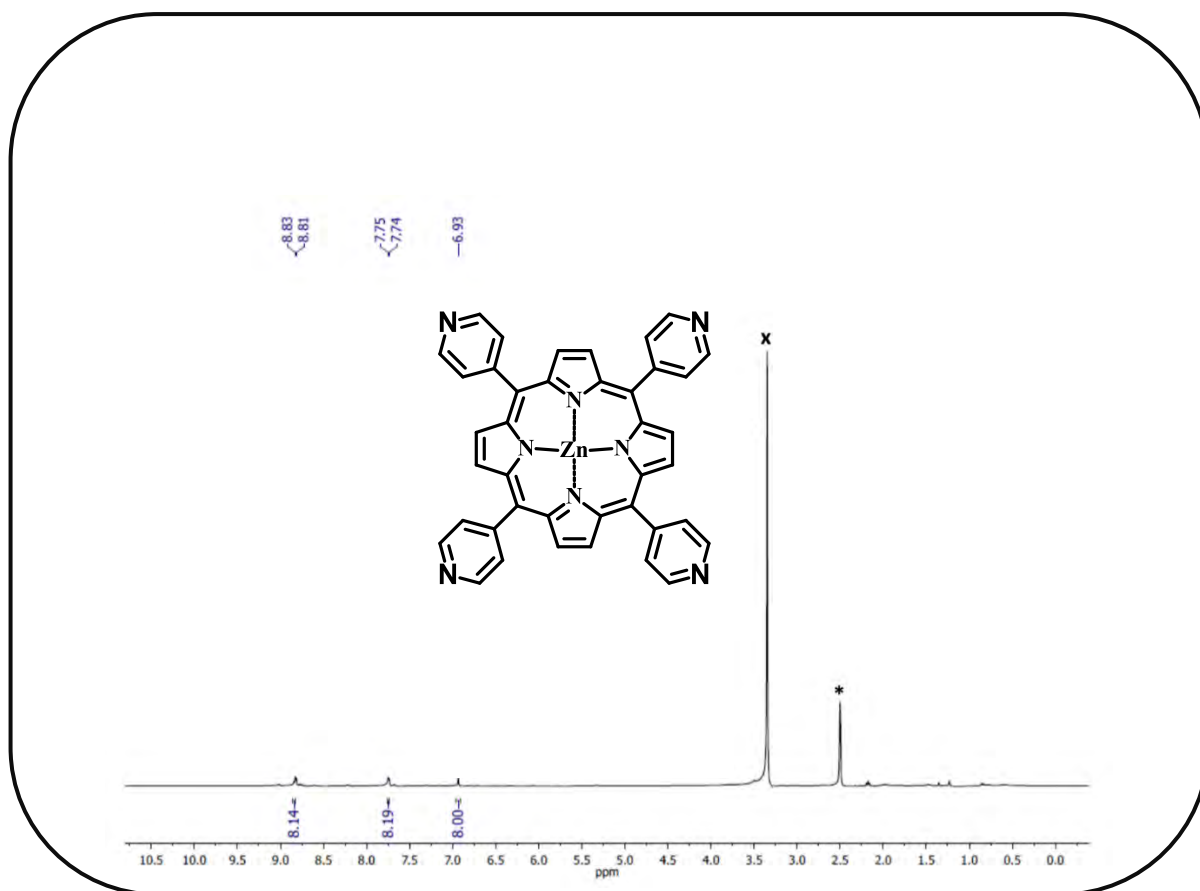


Figure A.1: ^1H NMR (400MHz) of **1** (*-DMSO- d_6 , x-water).

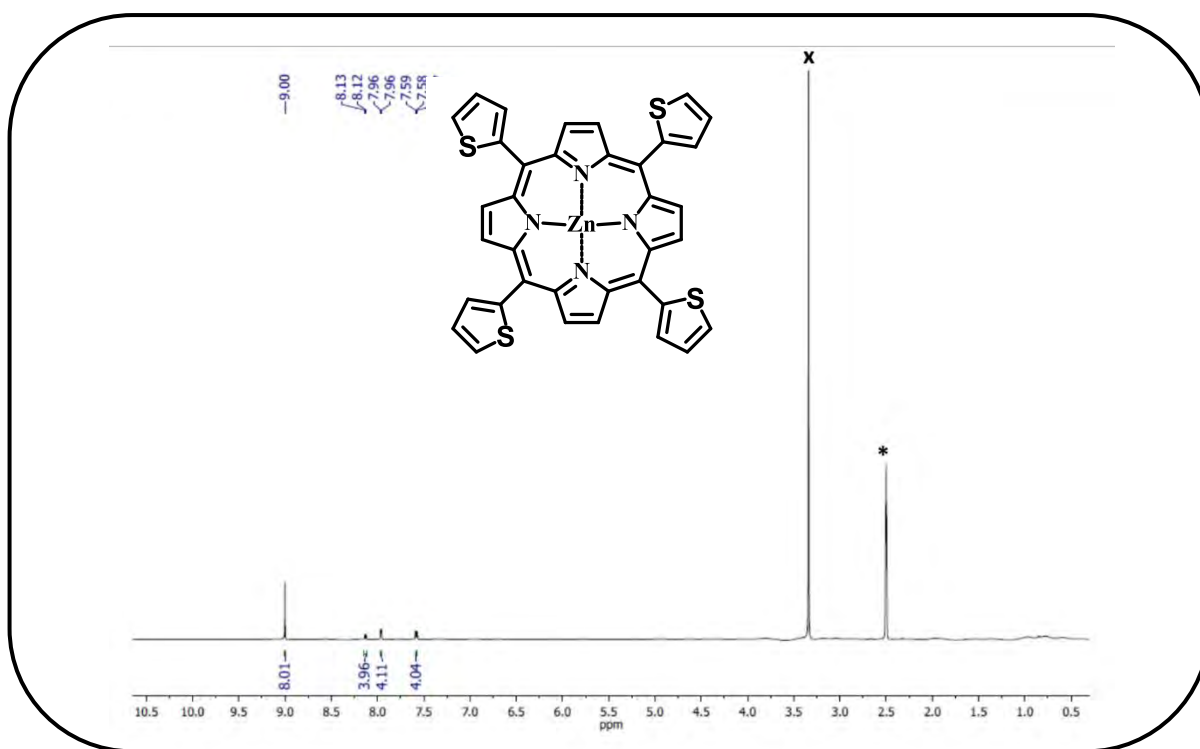


Figure A.2: ¹H NMR (400MHz) of 2 (*-DMSO-d₆, x-water).

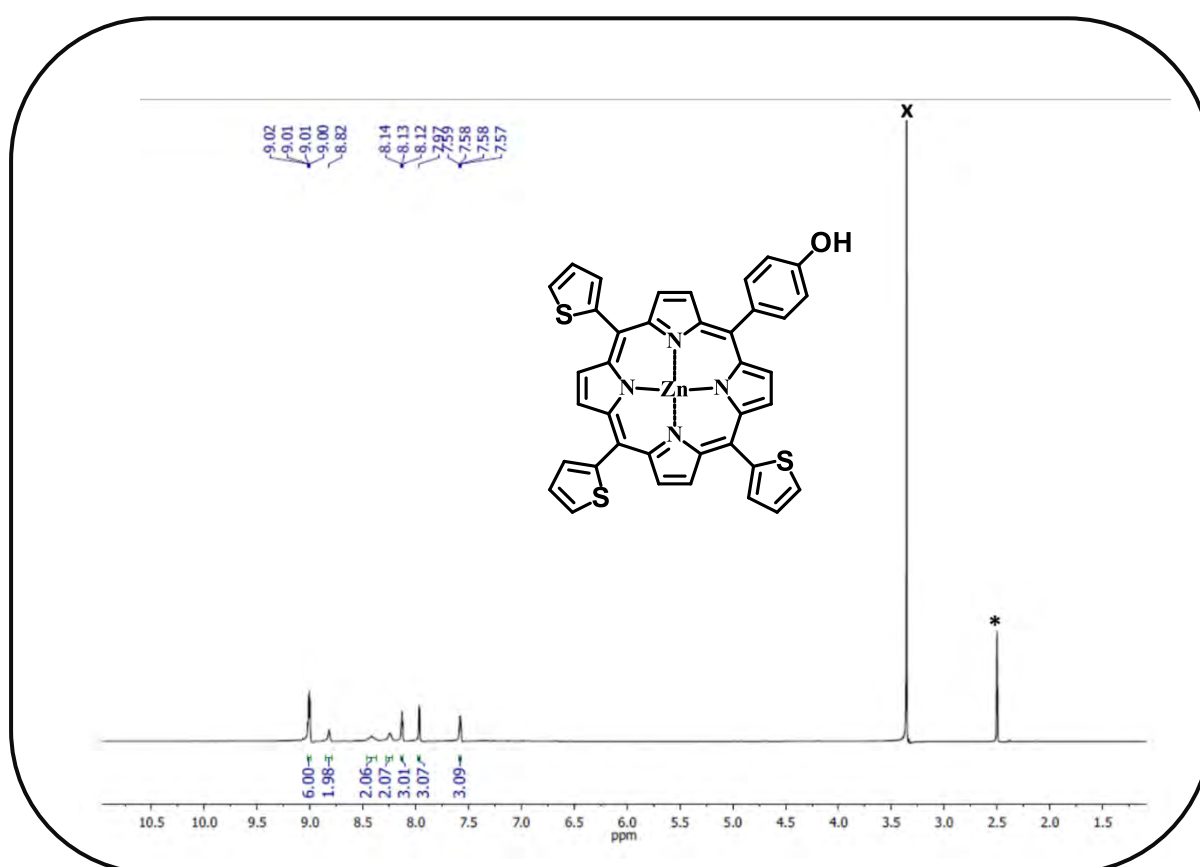


Figure A.3: ¹H NMR (400MHz) of 3 (*-DMSO-d₆, x-water).

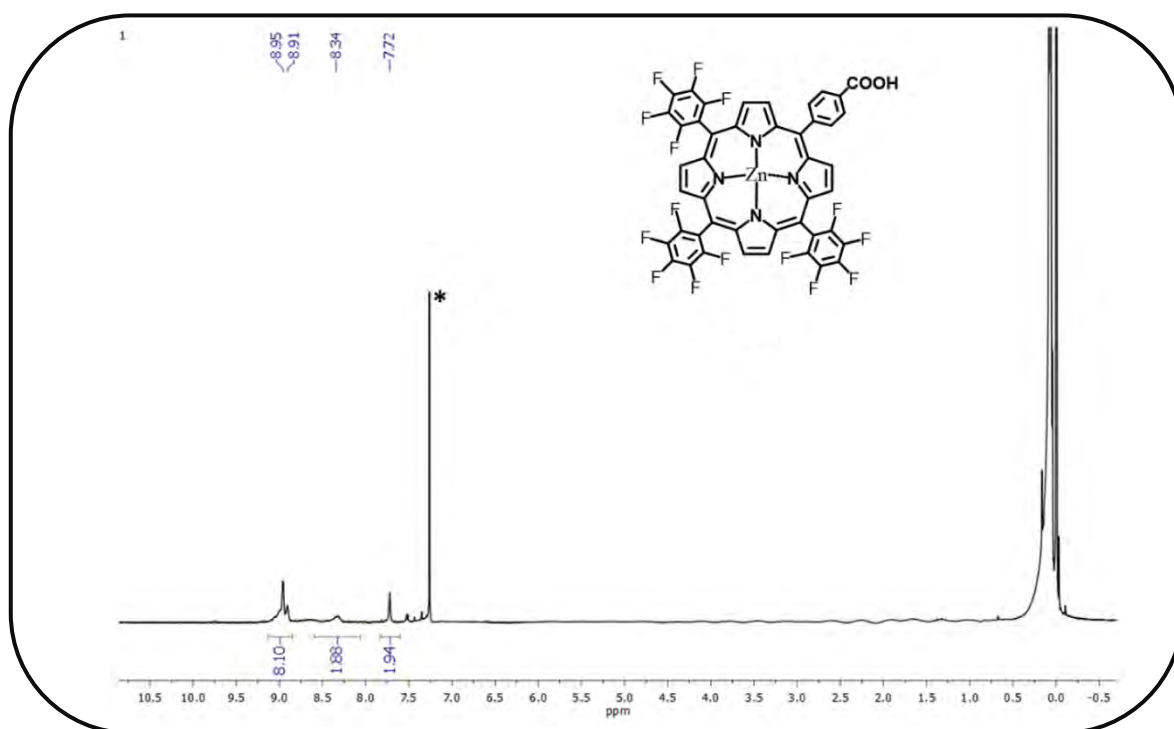


Figure A.4: ^1H NMR (600MHz) of **4** ($^*\text{-CDCl}_3$).

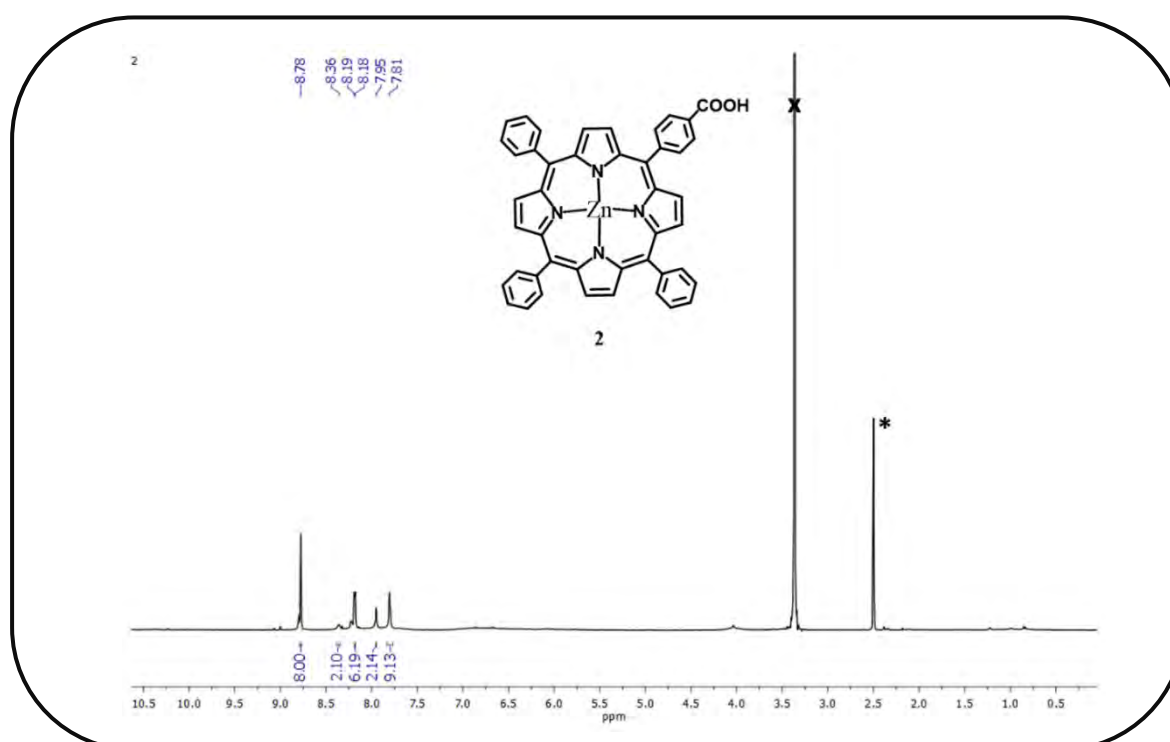


Figure A.5: ^1H NMR (600MHz) of **5** ($^*\text{-DMSO-d}_6$, x-water).

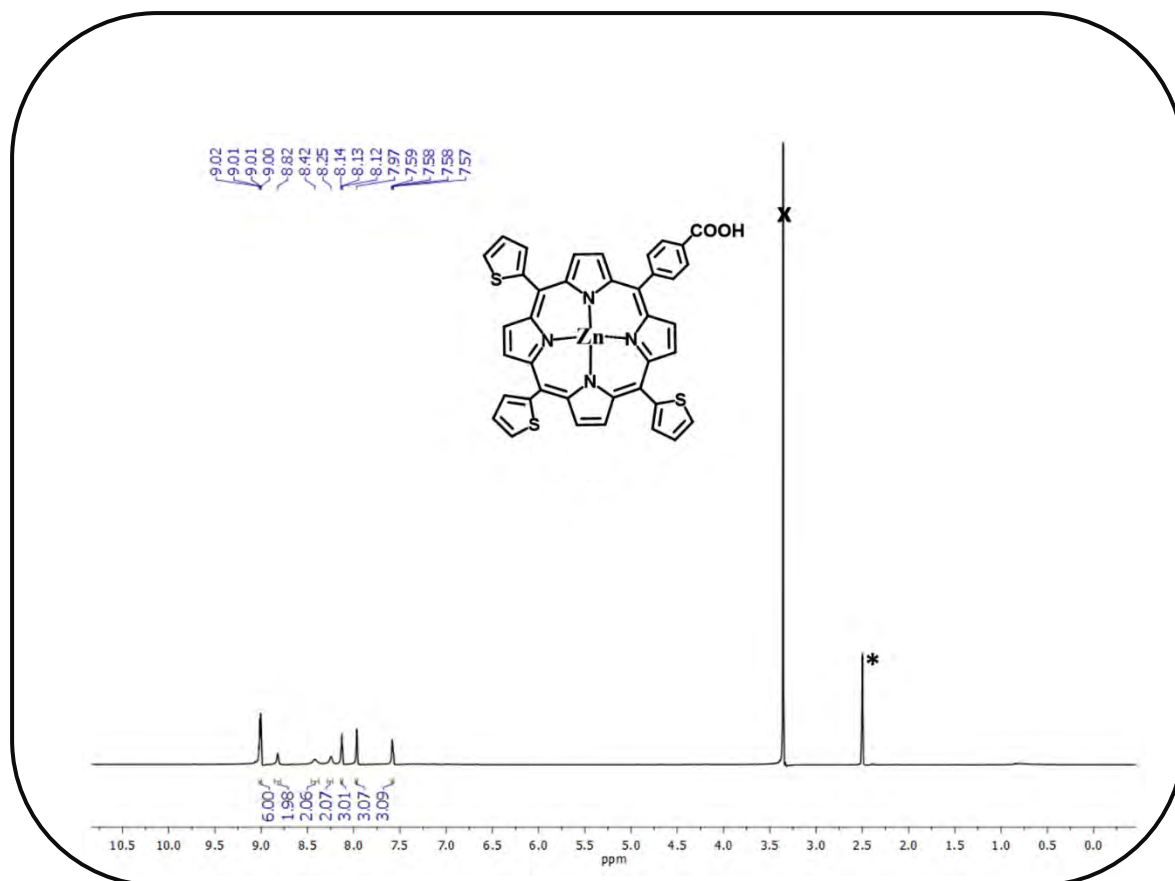


Figure A.6: ^1H NMR (600MHz) of **6** (*- DMSO-d_6 , x-water).